2020-01-01

A Cellulose-Based Biological Sensor For The Quantitative Determination Of Glucose And Glycated Hemoglobin (HbA1C)

Gilberto Henao-Pabon
University of Texas at El Paso

A CELLULOSE-BASED BIOLOGICAL SENSOR FOR THE QUANTITATIVE DETERMINATION OF GLUCOSE AND GLYCATED HEMOGLOBIN (HbA_{1c})

GILBERTO HENAO-PABON

Doctoral Program in Biomedical Engineering

APPROVED:

Thomas Boland, Ph.D., Chair

Taslim Al-Hilal, Ph.D.

Daniel Terreros, MD., Ph.D FCAP

Robert Moreno, MD.

Stephen L. Crites, Jr., Ph.D.
Dean of the Graduate School

DEDICATION

I dedicate this dissertation to my friend, advisor, and partner Sylvia Marquez, who on daily bases traveled with me through difficulties, and achievements on daily basis.

A CELLULOSE-BASED BIOLOGICAL SENSOR FOR THE QUANTITATIVE DETERMINATION OF GLUCOSE AND GLYCATED HEMOGLOBIN (HbA_{1c})

by

GILBERTO HENAO-PABON, Dr. Med.

DISSERTATION

Presented to the Faculty of the Graduate School of

The University of Texas at El Paso

in Partial Fulfillment

of the Requirements

for the Degree

DOCTOR OF PHILOSOPHY

Department of Metallurgical, Materials and Biomedical Engineering

THE UNIVERSITY OF TEXAS AT EL PASO

May 2020

ACKNOWLEDGEMENTS

I would like to give special acknowledgements to the members of my academic committee, teachers, administrative faculty and classmates.

I especially grateful to:

1. Dr. Thomas Boland, UTEP Professor and BME Director, for permitting me to be a research student in the UTEP graduate bioengineering program and for his kind advice and strong support on this stage of the staircase of biomedical knowledge.
2. Dr. James Li, UTEP Associate Professor, for allowing the use the laboratory space and generous sharing of reagents and supplies, and for bench guidance including from his postgraduate and graduate teams.
3. Dr. Taslim Al-Hilal, UTEP Assistant Professor, who kindly evaluated and analyzed my progress and guided thorough difficult moments.
4. Dr. Sudhakara Prasad, Associate Professor, for sharing his knowledge with me and so becoming a role model and adviser; I appreciate his friendship as well.
5. Dr. Jorge Lopez, UTEP Professor, for giving me his support on technically and theoretically complex physicochemical methodologies and for his friendship.
6. Dr. Robert Moreno MD, Board Certified in Internal Medicine, for being my guiding light on patient care particularly of patients with metabolic diseases.
7. Dr. Daniel Terreros MD, TTUHSC Tenured Professor, for his sustained concerns about the development of the project, his suggestions and constant constructive criticism, that gave my project additional balance regarding the interactions between engineering and medicine.

I am also grateful to Larry Peterson, VP of sales, and Carmen Peterson, for their unconditional support and above all, for their assistance with the manuscript.

I acknowledge support for my graduate studies from:

1. NIH/NIAID under award number R21AI107415.
2. NIH/NIGMS award number SC2GM105584.
3. NIH/NIMHD/RCMI under award number 5G12MD007593-22.
4. The Medical Center of the Americas (MCA) Foundation.
5. The U.S. NSF-PREM program (DMR 1205302), the NIH BUILD program.
6. The UTEP Biomedical Program and the UTEP Office of the Dean of Graduate Studies,
7. The Texas Tech Health Sciences Center at El Paso, Research Center Laboratory, Daniel Terreros MD PhD, Director.
8. The University of Texas System STARS Award, and
9. The IDR Program at the University of Texas at El Paso.

ABSTRACT

Importance: Diabetes is a common world-wide disease characterized by insulin resistance and as result there is an increased risk of cardiovascular disease and other metabolic abnormalities, that contribute to irreversible end-organ damage. The cause of diabetes is multifactorial and includes genetic, inflammatory and environmental factors plus lifestyle issues. Because in diabetes there are high levels of glucose and glycated hemoglobin, these molecules are used in clinical settings for the acute and chronic management of diabetic patients.

Objectives*: a.* To design and build an electrochemical biological sensor using the enzyme Glucose Oxidase (GOX) to detect glucose in biological fluids.
b. To design and build an electrochemical biological sensor using amino-phenyl-boronic acid (APBA) to detect glycated hemoglobin (HbA_{1c}) in blood.

Methodology: The two types of electrodes were built using a similar carbon-coated cellulose matrix followed by a surface pretreatment (Pre-Anodization), and by the addition of cross-linking molecules in order to generate specific covalent bonds. Theses cross-linkers attach to anodized cellulose fibers by specific functional groups as carboxyl's, generating avid binding sites for either GOX or APBA. The GOX transfers electrons to the matrix through its flavin adenine nucleotide (FAD) subunits as its oxidase's glucose; the number of electrons transferred is proportional to the glucose concentration in the test solution. Due to the presence of catalase activity in the APBA-HbA_{1c} complexes, and in the presence of H_2O_2, a proportional number of electrons to the number of bound glycated hemoglobin is transferred to the matrix.

Results: The specific covalent immobilization of GOX and cofactor APBA, was successfully achieved on carbon precoated cellulose matrix. The proposed use of zero-length cross-linkers create the indispensable molecular bindings sites for the functionality of theses disposable paper-carbon electrodes. The GOX-based sensor showed a high sensitivity (60.8723 $\mu A.\ mM^{-1}cm^{-2}$) and specificity for the detection of glucose. This APBA-based sensor also showed in laboratory settings high specificity and sensitivity (208.9461 $\mu A\ mM^{-1}cm^{-2}$).

Conclusions and Relevance: These new laboratories tested electrodes to detect glucose and HbA1c met FDA requirements and have a great potential to be used as new biosensors for the management of diabetes in clinical settings. Furthermore, these electrodes have the potential for clinical acceptance due to their manufacturing friendliness of portability, high sensitivity, high specificity and low costs.

TABLE OF CONTENTS

LIST OF FIGURES

LIST OF EQUATIONS

CHAPTER 1. INTRODUCTION AND BACKGROUND

Diabetes is quickly growing to be an epidemic disease, due to the fact that in the last three decades (*CDC, 2011*). About 30.3 million children and adults in the U.S. have diabetes, (9.4% of the population), according to the CDC (*ADA, 2015; CDC, 2017*). Of those, 23.1 million people were diagnosed with diabetes and 7.2 million were undiagnosed (*CDC, 2015; CDC, 2017*). In addition, 84.1 million people are classified as a pre-diabetes (*CDC, 2014; CDC, 2017*). Diabetes is more prevalent in the elderly population, where it affects 1 in 4 people over the age of 65 or 23.1 million adults (*CDC Newsroom, 2019*). However, it also affects the younger population, with one in five adolescents and one in four young adults having pre-diabetes with an adverse cardiometabolic risk (*Andes et al, 2019*).

An estimated of 1.3 million new cases of diabetes were diagnosed among US adults aged 18 years or older in 2017 (*CDC Newsroom, 2019*).

The organization for economic cooperation and development (OECD) countries, (comprising 34 countries; including United States, Canada, Australia, Japan, Korea, Mexico, Chile and several European countries), reports 85 million people have diabetes representing around 7% of the population aged 20-79 years. By 2030, this number will be projected to reach 108 million people in OECD countries (*Wise, J, 2015*), and 439 million of the world's adult population (7.7%). In developed and developing countries, the projected increase in the numbers of adult with diabetes is 20% and 69% respectively (*Shaw et al, 2014*). According the World health organization (WHO) in 2014, 422 million adults had diabetes (*Shaw et al, 2010*), (*WHO Web-assessed in May 2019*).

In the U.S., based on race and ethnicity, diabetes affects 15.1% of American Indians/Alaskan Natives, 12.7% Non-Hispanic black, 12.1% of Hispanics, 8.0% of Asian Americans and 7.4%

Non-Hispanic whites (*CDC, 2017*). Diabetes was the seventh leading cause of death in the United States in 2015 (*CDC, 2017*).

Diabetes can be classified as:

1. Type 1 diabetes, (T1D): In T1D the body produces no insulin, due to the failure of the beta cells of the islets of Langerhans in the pancreas, which can affect adults and children, and represents 5% of people with diabetes (WHO/IDF, 2006; *ADA, 2008*).

2. Type 2 diabetes, (T2D): T2D is characterized by an insufficient production of insulin by the pancreas by beta cells, from insulin resistance by the cells specifically in the liver, muscles and fat tissue, even when there is a normal level of insulin, and represents approximately 95% people with diabetes (*WHO/IDF, 2006; ADA, 2008; Vijan, S., 2010*).

3. Gestational diabetes (GDM): GDM is a condition when expecting women exhibit high blood glucose levels, especially during the second and third trimester of pregnancy (*Moore & Griffing, 2014*).

4. Specific types of diabetes: Examples of this class are diseases of exocrine pancreatic function, such as monogenic diabetes (MODY) and chemical/drug induced diabetes (*ADA, 2019, WHO, 2019*).

The screening for diabetes and pre-diabetes is the primary objective for determining the diabetes care *(US. PSTF, 2008).* Hypertension and dyslipidemia are clear risk factors for cardiovascular disease (CVD) and diabetes (*Lopez-Jaramillo et al, 2014*) with CVD is being a major cause of morbidity and mortality for individuals with diabetes.

Glucose is the parameter key for diabetes control. Diabetes can be diagnosed by the measurement of insulin secretion and response to glucose levels. The two most frequently used tests are:

1. Fasting plasma glucose (FPG) level at or above ≥126 mg/dL (7.0 mmol/L), OR

2. **Glycate hemoglobin (HbA1c) at or above 6.5 % (48 mmol/mol), OR**

3. 2-h plasma glucose (PG) ≥200 mg/dL (11.1 mmol/L during an oral glucose tolerance test (OGTT). (*ADA, 2008; WHO/IDF, 2006, ADA, 2019***).**

Pre-diabetes is defined as a condition in which individuals have fasting plasma glucose (FPG) of 100 mg/dL to 125 mg/dL (5.6 mmol/L – 6.9 mmol/L) or HbA_{1c} > 5.7 % to <6.5% (39 – 47 mmol/mol) or 2-h plasma glucose (PG) during 75 g oral glucose tolerance test (OGTT) of 140 mg/dL to 199 mg/dL (7.8 mmol/mol – 11.0 mmol/mol) levels higher than normal, but no higher, to be classified as diabetes (*Vijan, S. 2010; CDC, 2012; ADA, 2019*). This metabolic state is generally not characterized by a decreased blood insulin level. *(See Appendix 1.1, 1.2 & 1.3 for more details to diagnostic diabetes and Pre-diabetes).*

Glycated Hemoglobin (HbA_{1c}), may be considered as the most important biomarker for assessing long-term glycemic status due the presence and severity of hyperglycemia, implying diabetes (≥6.5%) or pre-diabetes state (≥5.7% - <6.5%), and can be considered as risk factor (*Lyons & Basu, 2012*). Individuals with HbA_{1c} values between 6.0% - 6.5%, have a 25% to 50% risk of developing diabetes over the next 5 years, that is 20 times higher compared to individuals having HbA_{1c} concentrations of 5.0% *(Zhang, et al 2010*). *(See Appendix 2. 1. $HgbA_{1c}$ discovery and medical clinic utility).*

There is a direct correlation between insulin resistance and HbA_{1c}, showing a strong relationship with the sensitivity of insulin in healthy subjects with normal glucose tolerance (NGT), low levels of insulin sensitivity correspond a high levels of insulin resistance (*Lin, et al, 2014).* HbA_{1c} is a reliable biomarker and an excellent indicator of insulin resistance for testing individuals for diabetes, prediabetes and poor glycemic control in children having higher levels of cholesterol, and triglycerides (*Borai, et al, 2011; Onal et al, 2014*). Patients with obesity and any other component of metabolic syndrome [glucose metabolism disorders or glucose intolerance, high blood pressure (HTN), dyslipidemia] and are related to insulin resistance as a common pathway for them, and HbA_{1c} can identify persons at increased risk for cardiovascular disease (CVD), Stroke, and death (*Selvin et al, 2010*).

HbA_{1c} is a more predictable measurement of chronic glucose levels, expressing the degree of glucose exposure over a long period of time. $HgbA_{1c,}$ due to this factor, has a more intimate relationship with the of complications, more a than a single measurements or continuous episodic measurements in glucose values. HbA_{1c} value shows the effectiveness of the therapy by monitoring long-term serum glucose regulation (*ADA, 2010*), the implementation of HbA_{1c} control method, soon after the diagnosis of diabetes, is also associated with long-term reduction in micro-vascular disease (nephropathy, neuropathy and retinopathy) (*UKPDS, 1998*; *Carnethon et al, 2010; WHO, 2011; Stokes & Metha, 2013*). Measuring HbA_{1c} levels is not recommended as frequently as measuring glucose levels, but has advantages, because it can be done even in the non-fasting state, has a higher repeatability, and lower costs. HbA_{1c} testing has an important role in the diagnosis of diabetes or pre-diabetes; it assess the effectiveness and safety for a management plan to control the hyperglycemic or hypoglycemic levels, in patients with type 2 diabetes and type 1 diabetes; and as preventive assessment identifying patients with high risk, who can developed major

complications. “American diabetes association (ADA) proposed optimal targets, but each target must be individualized to the needs of each patient and his or her disease factors” (*ADA, 2018*). In pregnant women HgA_{1c} levels exhibited high sensitivity and low specificity for diagnosing gestational diabetes, and values of HbA_{1c} levels between 5.7 – 6.4% are an appropriate and effective indicator for identifying patients at highest risk of developing gestational diabetes (GDM) and a predictor of potential postpartum death (*Fong et al, 2014; Kwon et al, 2015*).

The formation of HbA_{1c} is mainly dependent on the interaction between blood glucose concentration and the life span of red blood cells (RBC). The amount of HbA_{1c} is directly proportional to a time-averaged concentration of glucose within the red blood cell, and the fact that HbA_{1c} accumulates through the red cell’s life-span explains why young red cells have lower amounts of HbA_{1c} than old red cells (*Bunn et al, 1976*). Thus, the amount of HbA_{1c} reflects the average of blood glucose levels for the last 2-3 months, the average lifespan of red blood cells; the daily fluctuations of the glucose level cannot affect the HbA_{1c} levels and are therefore used as a more accurate index for diagnosis and long-term monitoring and control for the Diabetes (*Pundir & Chawla, 2014*). According the international HbA1c derived average glucose (ADAG) study, HbA_{1c} has a strong and significant correlation between the HbA1c levels and the estimated average glucose (eAG) or mean blood glucose (MBG), suggesting that both result (HbA_{1c} levels and eAG result) must be reporting to clinicians to have a better evaluation profiles of the patients (*ADA, 2018*), (*See Appendix 2. 2).*

Glucose is a primary source of energy for cells, essential for metabolism and homeostasis. Glucose transporters allow the movement of glucose through the plasma membrane of the cells. The

facilitated diffusion glucose transports (GLUT) type, a facilitated diffusion mechanisms, from the extracellular space to the intracellular space but driven through a chemical gradient either into the cells or out the cells; and the sodium-glucose linked transporters (SGLT) type, which must work with the sodium concentration gradient; are the main glucose transports. Basically, this kind of family's transporters are known to facilitate the entry of glucose into the cells and each one has many different members, which are directly related to the distribution, substrate specificity, the organ involved, and regulatory mechanism, due to specialized expression. Glucose transporters the sodium (Na^+) coupled glucose transporters (SGLT) with 14 members, is an active glucose process transport which needs to work against a glucose concentration gradient from the lumen of intestine or the nephron against glucose concentration gradient by coupling glucose uptake with the Na^+ gradient, which is being transported down its concentration gradient, maintained by the active transport of Na^+ across the basolateral surface cells by membrane-bound sodium-potassium ATPase (Na^+-K^+-ATPase), as a source of chemical potential. The SGLT1 is primarily expressed in intestine; SGLT2 is highly expressed in the cortex of the kidney; SGLT3 functions as glucose sensor in the cholinergic neurons, skeletal muscle, kidney, intestine, brain and the liver, controlling glucose levels. The second family is known as the glucose facilitative transporters (GLUT), protein involved in glucose translocation across the cell membrane, with 14 members, working basically for a diffusion process, due to the gradient of concentration. One of the most important transporters is known as GLUT1 found in the erythrocyte membrane, known as Erythrocyte-type transporter GLUT1, and in the blood-brain barrier. GLUT3 confined only to tissues with a high glucose demand, brain and nerve. GLUT4, high-affinity insulin responsive GLUT4, occurs basically only in skeletal muscles and adipose tissues. Understanding the working mechanisms of glucose transport; its expression in different and specific tissues, its acute and chronic regulation through

circulating hormones, and their defects or damages to this transportation system, all together or independent can be the basis for diseases such as diabetes, obesity, nonalcoholic fatty liver, hypertension. Allowing physicians and researchs to have a better approaches for prevention and management of diabetes, with new antidiabetic drugs, new methods for non-invasive diagnosis and close monitoring blood sugar levels (*Gould & Holman, 1993; Cholkar, et al, 2013; Ward, C., 2015; Navale & Paranjape, 2016; Deng & Yan, 2016; Litwack, Gerald, 2018*).

1.1. Introduction of the Glucose Biosensor (PA-PPE-GOX-Glucose).

All glucose measurements are based on interactions with one of the three enzymes: hexokinase (HK), beta D-glucose: oxygen-1-oxidoreductase (GOX), and glucose-1-dehydrogenase (GDH) (*Yoo & Lee, 2010; Price, C, 2003; D'Costa et al, 1986).*

GOX is a glycoprotein, with a molecular weight of about 150-180kDa (*Gao et al, 2014*). It is the enzyme most widely used in glucose sensors, consisting of two identical 80-kDa subunits with two flavin adenine dinucleotide (FAD) coenzymes, bounded as a redox cofactor. The active site is a flavin adenine nucleotide (FAD) which exist in two forms: oxidized (FAD) or reduced ($FADH_2$) (*Bolt, A, 1998).* (See figure 1.1)

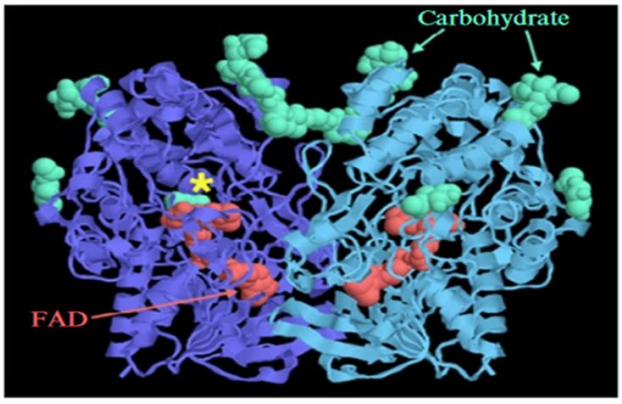

Figure 1.1. Crystal (X-ray) structure of glucose oxidase. Viswanathan, Sowmya; Li, Pingzuo; Choi, Wonbong et al. Protein–carbon nanotube sensors: Single platform integrated micro clinical lab for monitoring blood analytes. Methods in Enzymology. 2012. Vol. 509. Chapter 9: 165-194. Permission received to publish figure.

Immobilized GOX-FAD, oxidizes β-D-glucose to β–D-gluconolactone and gluconic acid as final product, and the $FADH_2$ generated by this reaction can be oxidized to FAD by oxygen with hydrogen peroxide the byproduct of this reaction, and using as a glucose as an electron donor, according the follow equation: (*Wilson & Turner, 1992*) (See figure 1.2).

Equation 1:

$$GOX(FAD) + \beta\text{-}D\text{-}Glucose \rightarrow GOX(FAD)\ Glucose \rightarrow GOX(FADH_2)\ glucono\text{-}d\text{-}lactone$$

$$GOX(FADH_2) + O_2 \rightarrow GOX(FAD) + H_2O_2 \rightarrow 2H^+ + O_2 + 2e^-$$

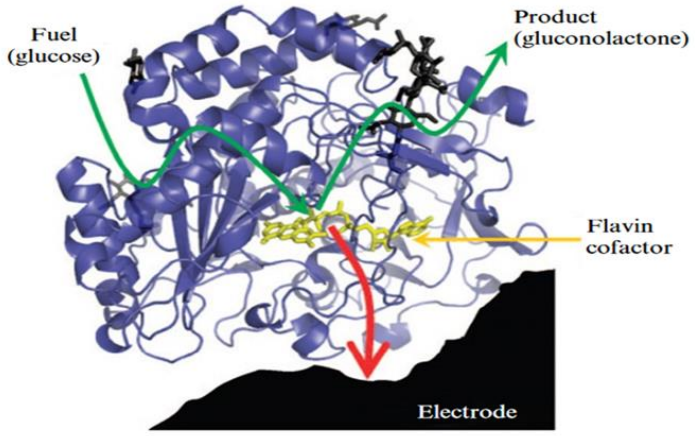

Figure 1.2 Glucose oxidase catalyzes glucose oxidation releasing electrons. Viswanathan, Sowmya; Li, Pingzuo; Choi, Wonbong et al. Protein–carbon nanotube sensors: Single platform integrated micro clinical lab for monitoring blood analytes. Methods in Enzymology. 2012. Vol. 509. Chapter 9: 165-194. Permission received to publish figure.

The GOX is immobilized on the surface of an electrode, is covered by a membrane, which provides more stability to the enzyme and prevents interference from other substances that can react with the enzyme (*Gao et al, 2014; Harper & Anderson, 2010*). Glucose oxidase activity must be converted into an analytical signal (*Bolt, 1998*), and the formation of hydrogen peroxides can be used as a signal, too (*Yoo & Lee, 2010*). The decrease in the oxygen concentration due to the

reactant consumption or the increase in the hydrogen peroxide reaction product, can both be determined electrochemically (*Yoo & Lee, 2010*). Oxidation of hydrogen peroxide at a platinum electrode generates a number of electron transfers, and this electron flow is directly proportional to the number of glucose molecules present in the blood (*Guilbaut & Lubrano, 1973*), thus this method is an example of indirect glucose detection.

The newest generation of glucose biosensors are reagent less, such as amperometric glucose biosensor, based on direct electron transfer (DET) between the cofactor FAD of GOX and the electrode surface without mediators (*Wang, J. 2008*). GOX immobilized onto the heterogeneous surface has an electrochemical response due to a redox reaction of $FAD/FADH_2$, and FAD undergoes a redox reaction where two-electron are coupled with two-protons according to the following equation:

Equation 2: $\boldsymbol{GOX/FAD + 2e^- + 2H^+ = GOX/FADH_2}$.

Two electrons act in the electrochemical process of $FAD/FADH_2$, with two-proton redox reactions. GOX has an isoelectric point of -0.40V to -0.48V and can carry charges showing a pair of weak redox peaks in the cyclic voltammetry diagram, with an anodic peak at E_{pa} = -0.445 V, a cathodic peak at E_{pc} = -0.483 V, a differential electric point of ΔE_p = 0.038 V and a midpoint potential of $E_{1/2}$ = 0.464 V. Together, this proves that the redox center of GOX, FAD, is reduced to $FADH_2$ and reversibly, is re-oxidized to FAD in the redox process (*Cai & Chen, 2004*).

GOX based, glucose biosensors, have attracted much attention due to their simplicity in fabrication, reagent-less nature, portability, low operational costs, the fact that they do not require an electron transport mediator between the enzyme substrate complex and the electrode, and there

has high sensitivity and specificity. (*Wang et al, 2009, 97.18 $\mu A\ mM^{-1}cm^{-2}$; Salimi et al, 2009, 826.3 nA $\mu M^{-1}cm^{-2}$; Zhang et al, 2011; 16.6 $\mu A\ mM^{-1}cm^{-2}$; Sehat et al, 2014; 278.4 $\mu A\ mM^{-1}cm^{-2}$).*

The main limitation is that the commercially available GOX, GDH, FAD and GDH-pyrroloquinoline quinone (GDH-PQQ) based glucometers have a narrow range of operation (20 mg/dL- 600 mg/dL) and only two met the ISO-2013 criteria for the international standards for blood glucose monitoring systems, which requires that 95% of measured glucose values to fall within ± 15 mg/dL (at <100 mg/dL) or ± 15 % (at ≥ 100 mg/dL) (*Freckmann et al, 2012 and Ekhlaspour et al, 2016*). Such bottlenecks arise in part due to limitations in DET, and the inaccessibility of actives sites of GOX. In fact, for most glucose biosensors, the active redox center of GOX: FAD/ $FADH_2$ is deeply embedded within a protein shell at approximately a 13 Å depth which limits electron-transfer rate between the active site of GOX and the electron surface (*Wilson & Turner, 1992; Ivnitski et al, 2008; Guo & Li, 2010*).

Attempts at increasing the DET of GOX using functionalized carbon nanotubes-composites of carbon nanotubes and graphene have been reported, however due to structural deformability and non-ohmic contacts this approach suffers from low electrical conductivity (*Chen et al, 2012; Mani et al, 2013; Palanisamy et al, 2014; Terse-Thakoor et al, 2015*). *Yang et al, 2008,* reported improved DET from GOX using pre-anodized screen-printed carbon electrodes, treated with a sulfonated perfluorocarbon polymer dispersion (Nafion®).

To achieve the covalent immobilization of GOX, on a pre-anodized paper-carbon electrode (PA-PPE), we propose here to use a zero-length cross linking agent. Cross linkers are molecules with more than one reactive end, that can attach to specific functional groups, like carboxyl, amines,

sulfhydryl and others generating covalent bonds with proteins like enzymes. The crosslinker 1-ethyl-3-3-dimethylaminopropyl carbodiimide hydrochloride (EDC) is a carbodiimide joining carboxylates with primary amines at zero-length. By adding a N-hydrosuccinimide (NHS), an ester group is formed as a reactive group when EDC is activated. NHS ester-activated crosslinkers, known as 1-Hydroxy-2,5-pyrrolidinedione or N-hydroxysuccinimide, which react with primary amines in slightly alkaline conditions of pH 7.2 – 8.5, to yield stable amide bonds (*Prasad et al, 2007*).

Pre-anodization

A pre-anodization (PA) procedure of the printed paper carbon electrode is the first step of generating a more sensitive electrode. This step is followed by EDC/NHS modification and the covalent immobilization of GOX. PA occurs without mediator; it causes the carbon atoms at the surface of the electrode to reorient, by increasing roughness porosity, and generating new edge-plane sites, as well as, generating new functional carbonyl groups at the surface of the edge-planes and this modification is thought to increase the amount of enzyme at the surface improving DET. It has been shown that the oxidation on pre-anodized substrates occurs at a much higher potential with significant shifts in peak potentials reflecting a faster electron transfer reaction. The increased electrocatalytic activity has been related a reorientation of the surface bound carbon-oxygen functional groups, and a generation of the new edge planes sites, through atomic reorientation. In addition, this techniques introduces surface carbonyl groups which appear at the more reactive edge-plane sites, which in turn paves the way for much improved crosslinking as well as electrochemical conductivity (*Prasad et al, 2007; Prasad et al, 2008; Yang et al, 2014; Thiyagarajan et al, 2014*).

By utilizing EDC and NHS (*Janegitz, et al 2011; Prasad et al, 2015*), we proposed to bind GOX to PA-PPE, and to study this modified electrode for its ability to detect glucose. As one will see at the conclusion of this dissertation, these modifications improved the electrodes, to the point of reliable glucose concentrations detection in the range from 18 mg/dL and 900 mg/dL, covering the entire range of hypoglycemic and hyperglycemic states, while maintaining low cost and portability required for a point-care testing device.

1.2. Introduction to glycated hemoglobin biosensor (PA-PPE-APBA-HbA_{1c}).

The formation of HbA_{1c} is mainly dependent on the interaction between blood glucose and red blood cells (RBC). HbA_{1c} should be directly proportional to a time-averaged concentration of glucose within the red blood cell, and the fact that HbA1c accumulates through the red cell's life-span, which explains why young red cells have lower amounts of HbA_{1c} than old red cells (*Bunn et al, 1976*). According to Bunn et al, 1976, the time-averaged rate calculated for synthesis of HbA_{1c} was 7.1 nM/mL per day. The extremely slow conversion of HbA_0 to HbA_{1c} suggests a non-enzymatic process (*Bunn et al, 1978*). As a consequence, turnover of red blood cells and the concentration of glucose: 50% of HbA_{1c} value is the result of the glucose exposure during the previous 30 days period, 40% of HbA_{1c} value is the result of the glucose exposure during the 30-90 days period and 10% value formed by glucose exposure during the previous 91-120 days period (*Henrichs, H., 2009*). Thus, the amount of HbA_{1c} is proportional to the average of blood glucose level over 2-3 months and is largely independent of hourly and daily glucose levels fluctuations. Therefore, its value is generally seen as a more accurate index for diagnosis and an important indicator during long-term monitoring and control of diabetes (*Pundir & Chawla, 2014*).

The hematocrit (HCT), plasma viscosity (1.34 mPa-s) and the aggregation and deformability of RBC regulate the blood viscosity (3×10^{-3} to 4×10^{-3} Pa-s). An increased blood viscosity decreases the diffusion of blood components, and therefore decreases the current in amperometric sensors. The intravascular viscosity of the diabetic erythrocyte has been shown to be increased due to increased HbA_{1c} levels in patients with poor diabetic control. The glycosylation process may alter the interaction between the hemoglobin and the RBC membrane, modify the flexibility and deformability of the RBCs (viscoelastic properties of the erythrocyte membrane), altering their internal viscosity, with consequently impairment of blood rheology. These alterations in the hemoglobin molecule, RBC membrane, advanced glycation end products, associated with a hyperglycemic state, oxidative stress by reactive oxygen species (ROS), increased levels of markers of inflammation [C-reactive protein (CRP), interleukin (IL)-6, plasminogen activator inhibitor-1(PAI-1), tumor necrosis factor-alpha (TNFα)], increase the trend towards aggregation, deformability of RBC, hypoxia with subsequent vascular vasodilatory adaptations, and contribute to the development of diabetic micro and macrovascular diseases and diabetic microangiopathy (*Watala et al, 1992; Paneni et al, 2013; Martin-Timon et al, 2014; Chawla et al, 2016; Sherwani et al, 2016*). Hyperglycemia in both T1D and T2D, represents the main risk key factor for microvascular complications, has the same risk for cardiovascular diseases (CVD) and mortality, with a higher risk ratio over CVD mortality per unit change of HbA_{1c} 1% increase in T1D (50%) than in T2D (7%) (*Juutilainen et al, 2008; Tandon et al, 2012).*

HbA_{1c} is formed by condensation of glucose molecule with the N-terminal amino group of valine of the β–chains of HbA_0 ($\alpha_2\beta_2$) undergoing an Amadori rearrangement, to form a more stable ketoamine linkage, a post-translational modification of $HbA_{0.}$ as shown in Figure1. 3.. In order of prevalence, the main sites of hemoglobin glycosylation, are β-Val-1, β-Lys-66 and α-Lys-61.

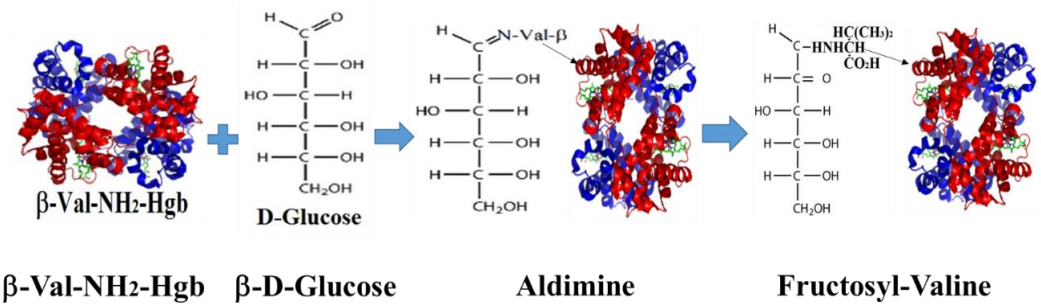

Fig.1.3 The condensation of HgA0-(α_2-β_2) -(β-Val-NH_2) with β-D-Glucose.

The HbA_{1c} level can be defined as the ratio between the HbA_{1c} concentration and total hemoglobin concentration Hb T (*Pundir & Chawla, 2014*).

In healthy people, hemoglobin (Hb) consists of approximately 97% adult hemoglobin (HbA), 2.5% HbA_2 and 0.5% fetal hemoglobin (HbF). Approximately 94% of HbA is non-glycated, and 6% is glycated hemoglobin (*Lenters-Westra et al, 2013*). Glycated hemoglobin consists of HbA_{1a} and HbA_{1b} called minor components which make up ~1% and HbA_{1c} also called main component, the remaining ~5% of the total 6% glycated hemoglobin *(Fitzgibbons et al, 1976; Bunn et al, 1978; Bunn et al, 1976)*. The HbA_{1c} levels found in clinical investigations range from 5% to 20% with values from 4% to ≤5.5% considered normal. A 1% change in the HbA_{1c} level reflects a fluctuation of mean blood glucose (MBG) concentration in plasma of approximately ~2.0 mM/L or 35.64 mg/dL, based on the following equation:

Equation 3: [MBG (mmol/L) = (1.98 x HbA_{1c}) - 4.29], ~35.64 mg/dL (*Pundir & Chawla, 2014*).

The national glycohemoglobin standardization program (NGSP) expresses the values of HbA_{1c} as a proportion of the total hemoglobin (HbA_{1c}%), and the international federation of clinical chemistry and laboratory medicine (IFCC) expresses the value of $HgbA_{1c}$ as millimoles of HbA_{1c} per mole of total hemoglobin (mmol/mol) (*Ang et al, 2014; Jia, W., 2016*). Since 2007 the globally accepted consensus HbA_{1c} should be presented in both NGSP and IFCC units.

The A_{1c}-derived average glucose (ADAG) study supports the notion of a close relationship between A_{1c} levels and average glucose (AG), for both type of diabetes, and express HbA_{1c} as:

Equation 4: eAG (mg/dL) = (28.7 x HbA1c %) – 46.7,

and the relationship between the NGSP network (%HbA_{1c}) and the IFCC network (mmol/mol) could be express as:

Equation 5: NGSP = [0.09148 * IFCC] + 2.152)

(*Nathan et al, 2008; Hanas & John, 2010; Hanas & John, 2013*).

In the U.S. physicians use the NGSP units. (*See Appendix 2.2 for more details of the relationships*). Amperometric methods to detect HbA_{1c}, are based on the recognition of amino-phenyl-boronic acid (APBA), which interact with the sugars and has the ability to bind glucose and glycated proteins through a boronic acid-diol bond. Boronic acid could covalently bind to either 1, 2 or 1, 3-diol group and the cis-diol group, of the surface sugar from glycated proteins, under weak alkaline conditions, to form reversible cyclic boronic esters (Figure 1. 4). With the bound sugar, boronic acid-modified electrode surface have been shown to be more negatively charged (*Song & Yoon, 2009*). The catalytic reduction of H_2O_2 by HbA_{1c} can be monitored as an analytical signal in sensor, due to Hgb having four iron heme groups that catalyze the reduction reaction of H_2O_2 (*Kim & Shim, 2013, Sheikholeslam et al, 2011*). Reduction of hydrogen peroxide at a platinum electrode generates a number of electrons transfers, and this electron flow is directly proportional to the numbers of HbA_{1c} molecules present in blood (*Kim & Shim, 2013*). Since the reduction of H_2O_2 is specifically catalyzed by HbA_{1c} (*Bunn et al, 1978*). Amperometric assays based on HbA_{1c} do not require any enzymes. These types of HbA_{1c} biosensors are reagent less, based on DET between the cofactor APBA and HbA_{1c} and the electrode surface without mediators (*Song & Yoon, 2009*). The APBA serves 2 functions:

a. selective binding to HbA_{1c} over the other immobilized hemoglobins (using boronic acid part), ***b.*** Participation in the electrochemical reaction for HbA_{1c} measurement through its ferrocene part (*Park et al,2008; Chuang et al, 2012*).

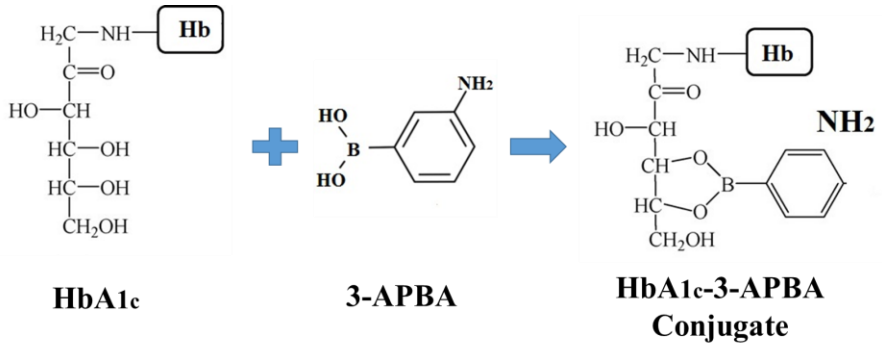

Figure 1.4. The conjugation of HbA_{1c} and 3-aminophenyl-boronic acid (3-APBA)

Since only APBA and the immobilized HbA_{1c} are needed for continuous and efficient electron transfer (*Park et al, 2008; Chuang, et al, 2012*), the use the pre-anodization procedure, to increase surface carboxylic and carbonyls groups functionalities on the edge planes, may also enhance the signals of APBA-HbA_{1c} anode and shifts the redox potential to a more positive potential range than the redox potential of conventional APBA systems (*Sheikloleslam et al, 2011; Prasad et al, 2012*).

1.3. Environmental concerns.

Before developing a universal biosensor device for glucose and HbA_{1c}, as a word of caution, researchers need to consider different variables and limitations.

The limitations are related to the environmental conditions of blood, human physiological and pathological conditions such as, hematocrit (HCT), blood osmolarity, partial pressure of oxygen (PaO_2), pH, Temperature (T), altitude, and Humidity (*Yoo et al, 2010; Erbach et al, 2016*). High HCT and high osmolarity slows the diffusion, and reduces the current, as well as reducing the glucose readings. A high PaO_2 can decrease glucose readings (*Tang et al, 2001*), and oxygen as competes with the mediator for the electrons from the enzyme. Extreme conditions such as high and low temperature, humidity, altitude, and pH, can influence the kinetics of the biochemical reaction, altering the stability of the enzyme and the reliability of glucometers (*Lam et al, 2014; Tang et al, 2000*).

The interferents substances or electrochemical interferents substances as: uric acid, creatinine, acetaminophen, cholesterol, triglycerides, salicylic acid, ascorbic acid, oxygen, dopamine, mannitol, methyldopa, are all known as electroactive species of molecules that can interfere within the operative potential of amperometric sensors, causing false high blood glucose readings, due to more free electrons from non-glucose molecules (*Yoo et al, 2010; Erbach et al, 2016; FDA, 2016*).

The performance accuracy of blood glucometers (GM) needs to be "matched appropriately to the clinical requirements for the setting in which they are used" (*Walsh, 2012*). These clinical accuracy requirements would be equivalent to analytic standards that would permit appropriate treatment decisions to be made directly from GM results as accuracy and precision. "Patients in these professional healthcare settings may be seriously ill, and clinically fragile, and are more likely than lay users, to present physiological and pathological factors that could interfere with glucose measurements" (*FDA, 2018*), therefore, GMs to be used at these POC of prescription drugs in professional healthcare settings must have a highly accuracy.

In October, 2016 The Food and Drug Administration (FDA), issued the guidance for blood glucose monitoring systems (BGMS) intended to use in diverse professional healthcare, such as general hospital wards, intensive care units, acute and chronic care facilities, assisted living facilities, nursing homes and physicians 'offices, on subjects in different states of health. "BGMSs intended for prescription-use in the hospital setting should be able to measure blood glucose accurately down to 10 mg/dL and up to 500 mg/dL, or a clinical justification should be provided for alternate measuring ranges and BGMSs intended for use outside a hospital setting and which will not reasonably be used to test neonatal samples should be able to measure blood glucose accurately down to 20 mg/dL". "The term lay-user encompasses a group of individuals with wide ranges in age, dexterity, vision, training received on performing testing, and other factors that can be critical to the patient's ability to accurately use the device and interpret test results".

In *2018, FDA* released a draft guidance document for the industry on self-monitoring blood glucose (SMBG) test system for over-the-counter use, intended for self-monitoring blood glucose by lay-users at home. "To meet the clinical needs of the user population, SMBGs should minimally be able to measure blood glucose accurately between 50 mg/dL and 400 mg/dL, or a clinical justification should be provided for alternate measuring ranges". Generating a distinction between two basic glucometers according to the intention of use:

a. BGMSs intended for use in point-of-care professional healthcare settings and

***b*.** SMBGs intended for home use for self-monitoring by lay-users,

"the FDA believes that by making this distinction, SMBGs can be better designed to meet the needs of their intended use populations, thereby providing greater safety and efficacy" (*FDA, 2016 & 2018*). *(See Appendix 1.4 for more details).*

SMBG has been established as a valuable tool for the management of diabetes (*Poolsup et al, 2009; ADA, 2013; Czupryniak et al, 2014*). The goal of SMBG is to help the patient to achieve and maintain normal glucose concentration in order to delay or prevent the progression of micro-vascular (retinopathy, nephropathy, & neuropathy) and macro-vascular (stroke, coronary artery disease) complications (*Adler et al, 2000; Ali et al, 2013*). The American diabetes association (ADA), recommends that SMBG be an integral part of treatment for patients with type 1 and type 2 diabetes. When SMBG was incorporated in the management for diabetes, due to the fact that the diabetic population was correctly identified, and that the population that where on the edge, (prediabetic state patients), could be recognized, and grouped with this classification and separated from diabetics, with greater acuity.

SMBG had a maximum market share in 2016, but due to implementation of SMBG as a therapy and the rise in the prevalence of diabetes worldwide has a major influence in this market segment to grow rapidly in the forthcoming years. “One of the major growth drivers of the market segment is the preference for early diagnosis, which helps in enabling appropriate and prompt intervention and reducing overall disease burden and promoting health”. The global market for blood glucose monitoring devices (BGMs) is expected to grow at a moderate rate and record a compound annual growth rate (CAGR) of close to 12% during the forecast period. Educators of the American diabetes association have a released procedure for primary care practice, which states that the costs of medical services incurred by diabetic patients can be reimbursed through medicare. Due to the availability of theses reimbursement options, this can be considered as one of the growth drivers for the global BMG devices market, because it positively influences the increases in sales. “Vendors are increased their online marketing and promotional activities, that means the demand

for online purchase of glucose meters, blood glucose strips and lancets are growing, and all these factors intensify the level of market competition in the forthcoming years". There exists a competitive scenario (approx. 200 companies) between the company manufacture's, to have a good product due to sensitivity, technology, differentiation and operative service (*see de Global BGM devices market by Technavio, 2017*).

By 2030, according to the organization for economic cooperation and development (OECD), the prevalent cases are going to reach about 47,973,000 in Europe, 66,812,000 in the Americas and 18,234,00 in Africa, which means that the market related to diabetes and the coo-morbidities increase to faster.

The global market size of blood glucose monitoring devices is expected to reach US$17.8 billion by 2026, according to a new research report from Grand View, Inc., which registers 7.1% of CAGR during the forecast period (*Web-Assessed in Nov 2019*).

In reference to the HbA_{1c}, in 1996, following the recommendations of the American association of clinical chemistry (AACC) the National glycohemoglobin standardization program (NGSP)-HbA_{1c} was implemented to standardize HbA_{1c} results obtained in the diabetes control and complications trial (DCCT), epidemiology of intervention and diabetes complications (EDIC) and the United Kingdom prospective diabetes study (UKPDS), which used the high-performance liquid chromatography (HPLC) technique as the gold standard assay, due to HbA_{1c}'s emphasis as a control marker diabetes (*Goldstein et al, 1987; Lenters-Westra, W.B. 2011; Little et al, 2011; NGSP-Web assessed in Nov. 2019*).

The college of American pathologists (CAP) conducts surveys of NGSP-certified techniques using reference standards as part of the NGSP protocol in the reference laboratory network, the survey

does not describe any criteria for acceptance of precision and accuracy but "recommend a mean bias of <0.2 % and a coefficient of variance (CV) ≤ 3.5% (preferably <2%) while noting that less acceptable assay methods are those with a mean bias of >0.3 % and CV >4%". The NGSP requires that the average differences between an individual network laboratory and the central primary reference laboratory (CPRL) not exceed 0.35%, and a (CV) ± 3.5%, as the exclusive criterion for CAP HbA_{1c} surveys, adopted and updated in 2019, as an acceptable limit for the accuracy-based grading will be ± 5%. The 95% of confidence interval (CI) of the differences between the certifying method and the secondary reference laboratory (SRL) must fall within ± 0.75% HbA_{1c} for manufacturer certification (*Goodall et al, 2007*; *Little et al, 2011; Withley et al, 2015; Paknikar et al, 2016; FDA, 2016; Little et al, 2019; NGSP-Web assessed in Nov. 2019).* International federation of clinical chemistry and laboratory medicine (IFCC) methods are more time consuming and comparatively higher in cost and are not meant for routine clinical usage.

FDA has a second regulation for HbA_{1c} diagnostic test systems, which defines "HbA_{1c} test system as a device used to measure the percentage concentration of hemoglobin A_{1c} in blood. Measurement of hemoglobin A_{1c} is used as an aid in the diagnosis of diabetes mellitus and as an aid in the identification of patients at risk for developing diabetes mellitus" (*FDA, 2016*). "The ADA encourages physicians to evaluate both HbA_{1c} concentrations and self-measured blood glucose meter results, when assessing a patient's level of glycemic control". The ADA recommends that HbA_{1c}-point of care, (POC), methods not be used to diagnose diabetes, and suggest that the results obtained from the HbA_{1c}-POC devise can be used to monitor diabetes in some situations (*FDA, 2016; ADA, 2018 & 2019*). (*See Appendix 2.3. for $HgbA_{1c}$).*

The FDA imposes restrictions on HbA_{1C}-POC test devices and has classified these devices into class II category because they have a moderate risk associated with use. Class II devices are limited by device-specific regulations that include performance standards, labeling requirements associated with the device use, pre-market data requirements, post-market surveillance. The labelling on these devices should have a list of contraindications, precautions, warnings, adverse reactions, and other instructions for use and handling before the equipment is released on the market (*FDA, 2019*).

Multiple studies have shown that HbA_{1c}-POC testing offers substantial benefits to patients by making testing more accessible, allows immediate feedback for the patient and for the doctor at the time of a clinical visit, laboratory results provided avoiding repeated visits for review and therefore providing an opportunity for more timely treatment changes, with greater satisfaction and motivation of the patient, to achieve better control of their diabetes (*Crocker et al, 2013; Paknikar et al, 2016*). Many reviews have been done, to know the different methods based on electrochemistry biosensors to detect HbA_{1c} through POC, see the follow excellent reviews references (*Pundir et al, 2014; Ang et al, 2015; Wang et al, 2015; Yazdanpanah et al, 2015; Lin & Yi, 2017). (See Appendix 3 for HbA_{1c}).*

Leca et al, 2012 and Lenters-Westra & Slingerland, 2014 propose that HbA_{1c}-POC measurements at least once a year should be confirmed by a laboratory method and call for mandatory proficiency testing for HbA_{1c}-POC test users to ensure continuous quality, and for the physicians basically not to rely on the quality control for glucose for a long term on HbA_{1c}-POC devices *(Leca et al, 2012; Lenters-Westra & Slingerland, 2014*).

Lenters-Westra & Slingerland, in 2009 evaluated 8 different glycated hemoglobin POC devices and 6 of them did not meet the generally accepted analytical performance criteria of a CV < 3.0%

and a NGSP manufacturer certification, and, also they evaluated in 2014, 3 of the 7 POC devices did not meet the criteria due to a high CV and low CI *(Lenters-Westra & Slingerland, 2010 and 2014*).

According to *Lenters-Westra et al, 2013*, the main problem for the HbA_{1c}-POC devices lies in a poor analytical performance, due to a high analytical variation (CVa) of the HbA_{1c} laboratory assay bias as reference methods, and the lot numbers of dependency (*Lenters-Westra & Slingerland, 2010; Lenters-Westra, E, 2011; Lenters-Westra, et al, 2013; NGSP-Web. Assessed Nov. 2019*). *See Appendix 2.4. for all the prerequisites for the introduction of an HbA_{1c}-POC.*

"The global point of care (POC) hemoglobin (Hb) A_{1C} testing market was valued at about $0.41 billion in 2018 and is expected to grow to $0.53 billion at a compound annual growth rate (CAGR) of 6.4% through 2022" (*Gale online, assessed on Dec.4, 2019*).

1.4. Paper and Carbon electrodes

Paper, is a thin material produced by pressing wet fibers, typically pulp of cellulose, derived from wood or herbs that have been dried on flexible sheets, and has microstructures in three dimensions. Paper is a biodegradable material and due to its' capillary effect can transport liquids, forming hydrophobic barriers, all in one hydrophilic paper-based matrix to immobilization analyte and reagents. Paper can be characterized by its' weight, and the thickness of the paper is often measured by the clamp, which is typically given in thousandths of an inch. The density of paper ranges from 250 Kg/m^3 (16 $lb./ft^3$) for tissue paper to 1,500 Kg/m^3 (94 $lb./ft^3$) for some specialty paper. Special paper is a porous blotting paper which has a thickness of 0.07 mm to 2 mm. This special paper includes a chromatography paper which has a thickness of 0.05 mm to 0.25 mm and the porous

have a diameter of 5 μm to 15 μm. High-quality chromatography paper can be modified to allow electrical pathways and electrical conductivity, and also provide coupling with other moieties through its functionalization. Papers which are electrically conductive and/or magnetically sensitive, may have conductive carbon or fibers of metal, and papers which have biodegradable polymers may be biocompatible with μPADs. One of the largest contributions to microfluidic technology was made by the Whiteside' group with the use of paper as a basis for bioassays, due to its' low cost (*Martinez et al, 2010; Nie et al, 2010*).

Carbon-based inks have been used extensively as conductors and found their way into devices such as printed circuits and electrodes for sensors. A carbon-based ink is an ink containing a carbon particulate such as graphite, amorphous carbon, or a fullerene, suspended in a binder and a solvent. These inks are applied on a surface via several deposition techniques, including painting on with a brush, syringe application, and screen printing. The ink is allowed to dry, and the resulting carbon coated surface is subjected to a treatment at temperatures ranging from 50°C to several hundred degrees Celsius. This high temperature treatment, or curing, is necessary to attain high conductivity in the resulting composite conductors, because the carbon particles are coated with surfactants to prevent aggregation in the ink and stabilize it. In some cases, the conductive ink undergoes a new treatment to modify the structural properties of carbon, as in our case with the pre-anodizing technique. Carbon electrodes based on carbon inks, show a very rich chemical surface, making this surface suitable for building a matrix with multiple applications to sensing and detect analytes. Because "all common carbon electrode materials retain the basic structure of six-member aromatic ring and sp2 bonding" *(Wang, J., 2006),* and due to the physic structure variability, the carbon electrodes on their surfaces differ in relative density from basal planes and

edge planes, making this edge orientation more reactive for better adsorption and more effective electron transfer. The proven presence of the functional groups on the surface of carbon electrodes show increased electrochemical reactivity. The quality and quantity of functional groups depends greatly on the material of the carbon and the pre-treatment used to make it more efficient and suitable. Carbon has a low or no ability to react and it is stable and unreactive under specific conditions. It has a wide potential window, as related to its' mechanical properties, and with a very low current in the background for these applications. One the more important aspects is the low cost for use in sensor applications (*McCreery, R.L, 1991; Wang, J., 2006*).

1. 5. Proposal (Research Strategy).

We propose to make a biological sensor platform, referred to as matrix, for covalent immobilization of GOX onto a pre-anodized paper carbon electrode (PA-PPE), by means of the zero-length cross-linker agent EDC and NHS. We will test the following which would later enables the use of materials as glucose sensors:

a. the activity of the GOX, which has the redox cofactor FAD/$FADH_2$ and catalyzes the oxidation of β-D-glucose by molecular oxygen producing gluconic acid and hydrogen peroxide.

b. the effect of surface pretreatments such as treating the carbon electrode at a high potential in a various solvents or electrolytes to generate surface functional groups, carboxyl, carboxylic, phenol, hydroxyl, epoxy.

We also propose to use the matrix platform for immobilization of APBA and HbA_{1c}, and study the following effects:

a. Use pre-anodized paper printed electrode for electrochemical detection of HbA_{1c}.

b. Employ surface pretreatments and study the effect on the electrode function.

c. Study the interactions of surface immobilized APBA with sugars, it's binding glucose, and ability to capture glycated proteins, such as HbA_{1c}.

d. Study the catalytic activity of captured HbA_{1c} to reduce H_2O_2, and the relation of the electrochemical current with respect HbA_{1c} concentration.

1. 6. General Objectives

a. Design and build an amperometric electrochemical biological sensor and matrix platform electrode transducer using glucose oxidase as an enzyme, to detect glucose.

b. Design and build an amperometric electrochemical biological sensor and matrix platform electrode transducer using amino-phenyl-boronic acid to detect HbA_{1c}.

c. The long-term objective is to build a combined kit that permits to measure both parameters using the corresponding electrodes.

1. 7. Specific Objectives

a. Design and fabricate a printer paper electrode (PPE) using a conductive carbon and Ag/AgCl ink, to develop a carbon-based working electrode (WE), counter electrode (CE), and silver pseudo reference electrode (RE).

b. Create a pre-anodized (PA)-PPE applying an electrical potential to the PPE to increase the carbon and oxygen functionalities.

c. Design and build a glucose oxidase pre-anodized printer paper electrode (PA-PPE-GOX) transducer material for use as a glucose biosensor.

d. Design and build an amino-phenyl-boronic acid pre-anodized printer paper electrode (PA-PPE-APBA) to detect HbA_{1c}.

e. Analyze the surface characterization of the biosensor PA-PPE-GOX and PA-PPE-GOX-Glucose.

f. Analyze the surface characterization of the biosensor PA-PPE-APBA and PA-PPE-APBA-HbA_{1c}.

g. Analyze the PA-PPE-GOX to detect glucose through different electrochemical techniques such as cyclic voltammetry, square wave voltammetry and chronoamperometry.

h. Analyze the PA-PPE-APBA-HA1c through different electrochemical techniques as cyclic voltammetry and chronoamperometry.

CHAPTER 2. METHODOLOGY REVIEW

2. 1. Pre-anodization Technique.

The pre-anodization technique, without mediator, causes a surface reorientation to generate more edge plane sites and facilitate direct electron transfer (DET). The oxidation could be taking place at a much higher potential with a significantly negative shift peak potential, which reflects a faster electron transfer process at the pre-anodized electrode; and this faster electron transfer occurs due to a new generation of carbon-oxygen functional groups (-C=O, -C-OH, -COOH-) on the surface of the electrode *(Kavan, L., 1997; Ilangovan et al, 1997; Lakshmirayanan et al, 2004*).

Electrochemical carbon denotes "synthetic solids consisting mainly of atoms of the element carbon", which can be prepared electrochemically from suitable precursors through the anodic oxidation and /or cathodic reduction *(Kavan, L., 1997*). Carbon is produced in various forms, which may exhibit different heterogeneity of its surface structure and properties. "Electrochemical carbons' often shows a very peculiar carbyne-like structure which is based on linear sp-bonded carbon chains" (*Kavan, L., 1997*). There is a wide variety of carbon-graphite products that have been used as working electrodes; such as black carbon, glassy carbon (GC), carbon-nanotubes (CNTs) glassy-carbon electrodes modifies (CNT-GCE), carbon fibers, graphite powder, graphite pyrolytic (PG), highly ordered pyrolytic graphite (HOPG), edge-plane pyrolytic graphite electrode, multi-walled carbon nanotubes (MWCNT) modified electrode, pre-anodized screen-printed carbon electrode (designed SPCE*), each one shows different physical and chemical properties (*Banks et al, 2005, Prasad et al, 2007*). The structure of graphite layers in a modified carbon electrode surface show two types of graphite planes: the basal plane, consist of graphite layers which runs parallel to the surface and contains all the atoms of a graphite layer, having specific physicochemical properties which can retard the transfer of electrons; and the edge-plane,

as defects in the surface known as steps, which runs perpendicular to the basal plane, and they expose all the edges that are in the graphite layers and promote more charge-transfer mechanisms, (modified electrons with a major proportion of edge-plane defects have higher electron transfer). The basal plane and the edge-plane show, at the carbon electrode surface, different electrochemical properties due to the nature of its chemical links in the graphite and are considered as a heterogeneous electrode electrochemically. Redox reactions show that the kinetic of the electrodes in the basal plane are slower than the electrode kinetic that occurs in the edge-plane, and these differences are a result of the greater reactivity in the edge-plane compared with the basal plane (*Kneton et al, 1992; Banks et al, 2005; Banks & Compton, 2005*).

Variations in Raman spectroscopy with respect to the intensity ratio of the D and E_{2g} Raman bands across the carbon surface, shows varying carbon microstructures and disorders in graphitic materials (*Bowling et al, 1989*), and its magnitude correlates inversely with the micro-crystallite size determined from X-ray diffraction (*Ray et al, 1997*). The D band at ~1360 cm^{-1} arises from the breakdown of the k-vector selection rule, concerning the reduced symmetry at graphitic edges, and mechanical treatment generated structural defects on the surface of modified carbon which gives rise to smaller graphitic, having more and new edge carbon atoms with high reactivity (*Nakamizo et al, 1984*); and the D/E_{2g} ratio increases with higher edge plane density (*Ray et al, 1997). Prasad et al, in 2007* was able to show, significative changes in the Raman Spectroscopy of the SPCE* (after pre-anodization), in reference to the intensity of D (disorder) band at ~1,360 cm^{-1} and a broadening in the ~1,582 cm^{-1} band, as well as the ratio between the $D/E_{2}g$ which was higher; also through the X-Ray photoelectron spectroscopy confirm the presence of more carbonyl groups (-C-OH, -C(=O)-OH, -C=O); and *Bowling et al, in 1989* found that the large improvement in the electron transfer kinetics with higher K^0, had a meaningful relationship with the increase in

~1,360 cm^{-1} band intensity, which is couple with edge-plane graphite, with higher edge-plane density (*Prasad et al, 2007; Bowling et al, 1989*).

Studies and analyses with different classes of modified carbon electrodes were made to show how the surface structure can affect the reactivity of the electrode. The anodic oxidation and defects in HOPG compared to an unmodified basal plane, shows modified HOPG to be more reactive towards the adsorption and the transfer of electrons with extreme variation in their properties due the exposure of a large quantity of new edge-planes at the electrode surface (*Bowling et al, 1989; Rice et al, 1989*). Glassy carbon (GC) that has any disturbance in the ordered baseline plane (nearby defects) significantly increased electron transfer rates and adsorption, consequently, GC exhibited an increase in the electrochemical activity, rapid kinetics and strong adsorption. The disorder in defects of GC increases the density of the states and makes the carbon behave more like a metal (*McCreery et al, 1994; Dekanski et al, 2001*). The contribution of the diffusion convergent to the voltammetry, increases in such a way that achieves a faster transport of the mast per unit of area of the electrode, resulting in larger and voltammograms current densities that appear increasingly distorted from the well-documented macro electrode shape *(Eklund et al, 1999*).

The electrocatalytic activity increases due to stimulation on the carbo-oxygen functional groups bounds at the new edge-planes sites, generated through the surface reorientation, at the surface of the carbon electrode (*Kavan, L., 1997; McCreery et al, 1994*). During pre-anodization, the modified carbon electrode (CE) tends to be more porous, due to its superficial reorientation which generates new edge-plane sites, as well, it generates new functional carbonyl groups at the surface of the edge-planes (*Prasad et al, 2007*). *Zen et al, in 2000*, working with pre-anodized glassy carbon electrodes (GCE), found that the increase in the forward step at the voltammogram in redox

reaction was due to the surface functional groups, and the associated Faradic process for the redox system (difference between the forward and reversed intercepts), for GCE electrodes working with Pb(II)/Pb(III) redox system solution, was under a diffusion-controlled mechanism. *Prasad et al, in 2008*, working with SPCE* found that the rise in the background current in the cyclic voltammogram is a proof of the formation of redox active groups (carbonyl groups functionalities). The peak currents for oxidation exhibit a linear relationship with the square root of scan rate and suggest that the electron transfer is a process controlled by diffusion *(Prasad et al, 2008*). The new formed carboxy-oxygen functionalities or carbonyl functionalities post pre-anodization raises the kinetics for electron transfer and therefore shows a remarkable electrocatalytic activity in relationship with the analytes, promoting a means for binding the absorbing materials (*Banks et al, 2005*).

There are many different pre-treatment techniques to prepare and activate carbon modified electrodes, known as a pre-anodization process, with subsequent modification of the surface electrode area through thermal, mechanical, chemical and electrochemical methods. Some other relevant references include: Heat treatment procedures (*Stutts et al, 1983; Hu et al, 1986*); mechanical treatment for fresh and well-defined electrodes, as abrasion and ultraclean polishing techniques (*Hu et al, 1985*); irradiation with ultrasound of GC electrodes show increased density of electroactive surface oxides (*Zhang et al, 1993*); activation of GC using carbon arc treatment, with a fresh increased surface electrode area (*Upadhyay, P., 1989*); direct electrochemical oxidation activation (*Prasad et al, 2007; Engstrom et al, 1984; Kepley et al, 1988*); intense laser pulse treatment showing that the electron transfer activation is consistent with a high density of edge-planes (*Bowling et al, 1989*); and the formation of carbon–oxygen surface groups, C=O, O-C-O, O-C=O functionalities, during the oxygen plasma treatment in modified carbon black

surfaces (*Evans et al, 1979; Takada et al, 1996; Notsu et al, 1999*). Activation of carbon electrodes, using large anodic currents and polishing procedures result in cleavage and reformation of carbon-oxygen bonds at the surface at the electrode, (induce the formation of edge planes as well surface functional carbonyl groups on the graphite edge-planes) (*Stutts et al, 1983; Ray et al, 1997*).

The surface of the carbon is modified radically, depending on its original carbon components and the pre-treatment selected, consequently, the structural characterization becomes more difficult to identified. It becomes possible to prepare reproducibly active carbon surfaces, particularly from based-carbon substrates, due to ***i.*** the surface of the electrode area expands through the surface, which becomes rougher and increases the transport rate of the mass. ***ii.*** The new surface carbon functional groups, (that can act as mediators with faster electron transfer), are formed in the new edge-planes, defects or microstructure of carbon materials, which becomes new sites for a faster transfer of electrons with low overpotentials and are determinants for the reactivity of the electrode (*Hu et al, 1985; Zhang et al, 1993; Chen et al, 1996*). They function as mediators or hotspots for the covalent binding of biological molecules to speed up the electron transfer rate, to enhance the sensitivity and reproducibility of the electrode.

Electrochemical pre-treatment methods have proved to be effective. Pre-treatment introduces or modifies the nature of the functional groups and these groups can serve as electron mediators between the electrode and the electroactive species on the electrode surface: Long-duration pre-anodization followed by short-duration cathodization, *Engstrom et al, in 1984*, found that the relationship between oxygen and carbon ratio (O/C ratio) increases, due that because the surface of the electrode is oxygenated, compatible with the idea of new functional groups containing oxygen are formed through the pre-anodization; application of square-wave pulses several times between two extreme potentials as electrochemical treatment of graphite-epoxy electrode carbon

electrode and microcylinder electrode of carbon fibers (*Falat et al, 1983; Kovach et al, 1986*); electrochemical pretreatment method by cycling the potential several times over a wide potential range between two pre-stated voltages in GC electrodes give well-defined peaks at the electrode surface due to the immobilization of the functional groups (*Kepley et al, 1988, Barbero et al, 1988*); working with coke-based activated carbons modified through reduction with H_2 and oxidation with HNO_3, *Xie et al, in 2010* shows that the generation of carbonyl groups (groups with oxygen in the surface of the electrode) through a Faradaic process cause modification of the capacitance and increase the relationship between the electrode-electrolyte interface (wettability). During the anodic polarization of GC electrodes, in an acidic media, which begins with the oxidation of a minimum surface of the active sites. These active sites are likely to be considered defects in the structure of the CNO graphitic, such as discontinuities in the basal plane with different functional groups formed, such as carbonyl, carboxyl, and phenolic bonded to the carbon shown in the recorded XPS technique analysis. If all surface-active sites are oxidized, the penetration of electrolytes becomes more intense through the domains of graphitic structure of GC and begins the growth of a layer of graphite-oxide, which subsequent increases in the real electrode surface. At that point, with high positive potentials, may cause the oxidation of carbon to CO and/or CO_2, which increase the electrochemical activity (*Dekanski et al, 2001*).

Pre-anodization of a carbon modified electrode has a great influence on electron transfer through greater geometric surface area. The surface area can be estimated by the Brunauer-Emmett-Teller (BET) method, which uses isotherms. Using the BET method *Lakshminarayaran et al, 2004,* found an increase on surface area due to the generation of carbon-functional groups (-C=O, -C-OH, -COOH) on the electrode surface (*Gregg et al, 1982; Lakshminarayaran et al, 2004)*.

2. 2. Zero-Length Crosslinkers.

There are two kinds of cross-linkers: ***a.*** the zero-length cross-linkers (UV light, tetranitromethane, carbodiimides, etc.) which induce a covalent link directly between macromolecules without interposition of a bridge and ***b.*** the contact-site cross-linking agents, known as one-atom bridge cross-linkers, a covalent bridge consisting of one atom (usually carbon) from the cross-linking agent (*Kunkel et al, 1981*).

The zero-length crosslinkers technique, achieves chemical crosslinking or the chemical process to join two or more molecules through a covalent bond, and forms protein conjugates, without the introduction of extra arm atom or a spacer molecule to the product, two conjugated crosslinked peptides. This action is also called bioconjugation, which is referred to in the use in biomolecules especially with proteins. "The key to forming a successful bioconjugate is to select the appropriate crosslinking reagent, which in turn contains the chemical features available in the molecules, that link them together" (*Hermanson, G. 2013*). These modifications are involved in the attaching or cleaving of chemical groups, to improve the solubility, keep the native structure of the protein, optimize and retain the enzyme protein biological activity with low to moderate grades of conjugation. Crosslinking reagents are molecules with more than one reactive end that are capable of attaching to specific functional groups like carboxyl (-COOH), primary amines ($-NH_2$), sulfhydryl (-SH), carbonyls (-CH)), and interact with specific amino acid side chains to generate a covalent bond (amide linkage) between a pair of proximal residues of proteins (*Fasol et al, 1971; Grabarek & Gergely, 1990; Conde et al, 2012*). The crosslinking of proteins and covalent modification rely on availability of the crosslinker reagents capable to react with existing specific structural and functional groups inside the proteins. Zero-length cross-linking agents: abolish the potential for cross-reactivity by mediating a direct linkage between two substances; efficient in

forming conjugates between a carbohydrate and a protein, a peptide and a protein, and two protein molecules. Carbodiimides are the more useful zero-length cross-linkers for the formation of amide-bond between a carboxylic acid and a primary amine. For bioconjugation methods, there are small functional groups of proteins as selectable targets. Four protein chemical targets account for most crosslinking and chemical modification techniques:

Primary amines (–NH2): This group exists at the N-terminus of each polypeptide chain called the alpha-amine (α-amine), and in the side chain of lysine (Lys, K) residues called the epsilon-amine (ε–amine). Because of its positive charge at physiologic conditions, primary amines are usually outward facing (i.e., on the outer surface) at the proteins; thus, they are usually accessible for conjugation without denaturing the protein structure.

Carboxyls (–COOH): This group exists at the C-terminus of each polypeptide chain and in the side chains of aspartic acid (Asp, D) and glutamic acid (Glu, E). Like primary amines, carboxyl is usually on the surface of the protein structure.

Sulfhydryls (–SH): This group exists in the side chain of cysteine (Cys, C). Often, as part of a protein's secondary or tertiary structure, cysteines are joined together between their side chains via disulfide bonds (–S–S–). These must be reduced to sulfhydryl's to make them available for crosslinking, by most types of reactive groups.

Carbonyls (–CHO): Ketone or aldehyde groups can be created in glycoproteins by oxidizing the polysaccharide post-translational modifications (glycosylation) with sodium meta-periodate.

Zero-length cross-linkers as carbodiimides which can form three different kinds of bonds: amide bond between a primary amine and a carboxylic acid; a phosphoramidate bond between the

reaction of an organic phosphate group and an amine group; and a secondary and tertiary amine bond between the reductive amination of the primary or secondary amine and aldehyde group.

The more useful carbodiimides are:

i. 1-ethyl-3-(3-dimethylaminopropyl) carbodiimide hydrochloride (EDC), more common and useful when working with water-soluble coupling conditions and the formation of a water-soluble byproduct, urea. The ideal conjugation of biological molecules which contain amines and carboxylates.

ii. 1-cyclohexyl-3-(2-morpholinoethyl) carbodiimide (CMC) is a water-soluble compound, commonly used for biological conjugations, but has potential side reactions, such as allergenic properties.

iii. Dicyclohexyl carbodiimide (DCC) insoluble in water, the applications are more common for the organic synthesis.

iv. Diisopropyl carbodiimide (DIC) insoluble in water, also, for common use in organic reactions, but has side reactions, such as undergo.

v. EDC plus N-hydroxysulfosuccinimide (Sulfo-NHS) reaction raises the solubility and produces more stability, to the active intermediate, which at the end reacts with the primary amine. Sulfo-NHS combines quickly with the primary amines, due to the hydrophilic reactive group. According to *Barre et al, in 2017* he wrote reviews about the use for standard coupling reactions, for conjugated biological molecules, which relied on the use of one carbodiimide reagent as EDC and active ester formed from NHS, and *Staros, in 1986* he reported that the reactions coupled with EDC plus sulfo-NHS show more efficiently and increase the yield of conjugation, compared with EDC alone (*Staros,J. 1986; Hermanson, G., 2013; Barre et al, 2017*).

Crosslinker reactive groups are selected, based in chemical reactivities, specificity for functional groups and water solubility. EDC is a zero-length crosslinking reagent for protein studies. EDC activates carboxyl groups and causes a direct formation of peptide bond or amide-bond between carboxylate (-COOH) groups from carboxylic acids, glutamate (Glu or E), aspartate (Asp or D) or the protein C-terminal to primary amines (-NH_2) of lysine or the N-terminal of the protein. EDC couple phosphate groups to primary amines and does not become part of the crosslinked. EDC is a water-soluble reagent, for reactions in aqueous and physiological buffers (*Staros, J. 1986; Grabarek & Gergely, 1990; Sriswasdi, S., 2013*).

Sulfo-NHS esters have the same reactivity and specificity as NHS esters due to hydrophilic active groups, they combine faster with the primary amines in the target molecules. The reaction between the carboxylate with NHS in the presence of a carbodiimide form the NHS ester. In bioconjugation of protein molecules "the NHS esters crosslinking reagents couple principally with the α-amines at the N-terminals and the ε-amines of lysine side chains" (*Staros, J.1982; Hermanson, G. 2013*). NHS is a water-soluble analog of sulfo-NHS and improves the efficacy of EDC. It enables control and modification of carbodiimide crosslinking reactions that involve the activation of carboxylates groups, to be conjugate with the primary amines, and can create stable amino reactive intermediates allowing an efficient conjugation to the primary amines, at physiologic pH (*Anderson et al, 1964; Staros, J. 1986; Barre et al, 2017*).

The crosslinking mechanism with EDC plus NHS has an initial phase, the reaction of a carboxylic acid group with a water-soluble carbodiimide to form O-acylisourea; the next phase can include three different options: ***i.*** a nucleophilic substitution with an amino group, C-NH_2 of lysine to form the amide bond; ***ii.*** Hydrolysis by water which occurs if there are no primary amino groups to

conjugate, regenerating the carboxylic acid and forming an Iso-urea form by product; (*Hoare & Koshland, 1967*) and ***iii.*** adding NHS (N-hydroxysuccinimide), the uncharged analog of sulfo-NHS, to an EDC coupling, (EDC couples NHS to carboxyls) this increases the stability and improves the efficiency by capturing the transient 0-acylisourea intermediate as a stable amino-reactive sulfo-NHS ester. This process can react with the primary amine to form the amide bond, increasing the efficacy of EDC-mediated coupling reactions as well with the two-stage process. EDC plus sulfo-NHS reaction together is highly efficient and increases the conjugation yield compared with that obtained only with EDC. Esters sulfo-NHS are active hydrophilic groups that react quickly with primary amines in the target molecules. See figure 2. 2. 1 (*Mansson et al, 1978; Staros, J., 1986; Hermanson, G., 2013*).

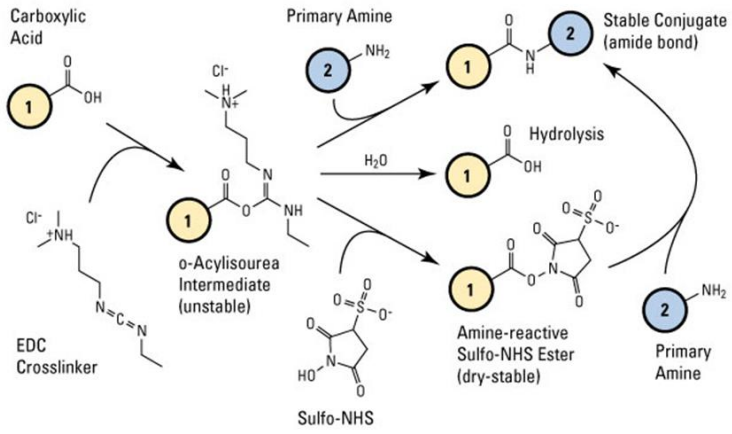

Figure 2.2.1. Sulfo-NHS plus EDC (carbodiimide) crosslinking reaction scheme. Carboxyl-to-amine crosslinking using the carbodiimide EDC and sulfo-NHS. Addition of NHS or sulfo-NHS to EDC reactions increases efficiency and enables molecule (1) to be activated and conjugate with another amino group from a protein. ThermoFisher scientific Web. Assessed Dec. 2017.

2. 3. Direct Electron Transfer (DET).

DET is a process in which one or more electrons, and equally one or more protons, are transferred in electrochemistry reactions in a redox system. DET has a transfer energy given by the displacement of the electron from a high energy level, to a low energy level (Shell), but can also force the electronic transfer by adding energy to the electron. Works by *Marcus, Sutin, Albery* on direct electron transfer detail with accuracy, eloquence and academic beauty, the evolution in knowledge about DET from the physical and biochemical point of view.

The Marcus microscopic model developed for homogeneous electron transfer processes in the outer-spheres (terminology used to describe electron-transfer reactions of coordination compounds, "outer-sphere denotes a reaction between two species in which the original coordination spheres which are maintained in the activated complex, an electron transfer from one primary bond system to another") in a single electron transfer from an electrode to species O (oxidized form), to form the product R (reduced form) $\boldsymbol{O_I + R_{II} \rightarrow R_I + O_{II}}$. It is a heterogenous process but "are radiation-less electronic rearrangements of reacting species, (the electron must move from an initial state, on the electrode or in the reductant R, to a receiving state, in species O or on the electrode, of the same energy)". "As in any reaction, the system as a whole, proceeds from configurations (coordinates) in the vicinity of the equilibrium ones, for the reactants to those for the products. These coordinates involve vibrational coordinates of the reactants, when their equilibrium values differ before and after electron transfer, as well as the orientational coordinates of the surrounding solvent molecules: averaged equilibrium orientations of those solvent molecules differ for reactants and products because each reactant undergoes a change of charge. The potential energy of the reactants and surrounding medium is a function of all of these nuclear coordinates (thousands of them) and defines a many-dimensional potential-energy surface, and the

transfer will occur only at or near nuclear configurations (represent the totality of translational, rotational and vibrational coordinates of all the molecules) for which the total potential energy of the reactants and surrounding medium is equal to that of the products and surrounding medium". The Marcus model also establishes that "the reactants and products do not change their configurations during the actual act of transfer", based in the Franck-Condon principle which says, "the nuclear momenta and positions do not change on the time scale of electronic transitions", which means in this particular case "the reactant and product, O and R, share a common nuclear configuration at the moment of transfer". According to chemical terminology, *IUPAC, 1977*, "The *Franck–Condon* (FC) principle is the approximation that an electronic transition is most likely to occur without changes in the positions of the nuclei in the molecular entity and its environment. The resulting state is called a Franck–Condon state, and the transition involved, is a vertical transition. The quantum mechanical formulation of this principle is that the intensity of a vibronic transition is proportional to the square of the overlap integral between the vibrational wavefunctions of the two states that are involved in the transition" (*Marcus, R., 1964; UPAC, 1977; Albery, W.J., 1980; Marcus, R., 1982; Marcus and Sutin, 1985; Marcus, R., 1993; Marcus, R., 1997; Bard & Faulkner, 2001; Compton & Banks, 2018*).

The calculation of the rate constant in a classical transition-state theory, of an electron-transfer reaction "involves calculating the probability of reaching the many-dimensional intersection region, due to the fluctuations, multiplied by a suitably weighted frequency for crossing the intersection region and by a transition probability for going from the R to the P surface". Therefore, the net result of the rate constant, ***k,*** of a bimolecular electron-transfer reaction is given by:

Equation 6: $k = KA\sigma^2 \exp(-\Delta G^*/RT)$

K is the transition probability, ***K*** ~ 1 for an adiabatic process.

$A\sigma^2$ has dimensions of collision frequency ($A\sigma^2$ is replaced by a related quantity which has dimensions of a collision frequency of the ion with unit area of the electrode ~ 1 x 10^4 cm. s^{-1}).

σ is the average center-to-center distance in the reacting pair during the electron transfer (the mean separation distance in the transition state of the reaction).

ΔG^* is the Gibbs-free energy of activation (Gibbs-free energy difference between the activated complex and the precursor complex) that is related to **λ**, where:

Equation 7: $AG^* = w^r + \lambda/4\ (1 + \Delta G^{O\prime}/\lambda)^2$ and $\Delta G^{O\prime} = \Delta G^O + w^p - w^r$

ΔG^O is the "standard" Gibbs-free energy change of reaction in the medium and to the work of bringing the reactants ($\mathbf{w^r}$) or products ($\mathbf{w^p}$) to the mean separation distance σ,

$\Delta G^{O\prime}$ is the free energy of the reaction when the reactants are a distance σ apart in the medium,

w^r is the electrostatic work involved in bringing the reactants to the mean reactant separation distance in the activated complex,

w^p is the analogous work term for dissociation of the products,

λ represents the reorganization energy, corresponds to the energy required to distort the atomic configurations of the reactant and its solvation shell to those of the equilibrium product state in the absence of electron transfer, has two contributions:

i. λ_i changes in the intramolecular vibrations (the inner-sphere reorganization energy, and means the free-energy change associated with changes in the bond lengths and angles of the reactants),

ii. λ_o Changes in solvent orientation coordinates (the outer-sphere reorganization energy, and reflects changes in the polarization of solvent molecules); λ represents both energies as $\lambda = \lambda_i + \lambda_o$;

Equation 8: $\Delta G^{O\prime} = \Delta G_i^{O\prime} + \Delta G_o^{O\prime} = \frac{1}{4}(\lambda_i + \lambda_o)$

$\Delta G_i^{O\prime}$ the activation energy arising from distortion of the inner coordination shell in the transition state geometry,

$\Delta G_o^{O\prime}$ activation energy that arises from rearrangement of the solvent dipoles between the reactants and the transition state (*Marcus, R., 1964; Albery, W.J., 1980; Marcus, R., 1982; Marcus and Sutin, 1985*). The rate of electron-exchange reactions was strongly influenced by the Franck-Condon principle: the more similar the inner coordination shells of the donor and acceptor atom, the less difficult would be the electron transfer (*Libby, W.J., 1952*).

The important simplifying feature of all these mechanisms is that the free energy of activation varies as the square of the distance of the displacement along the reaction coordinate. In its preferred equilibrium solvation, the reactants or the products nestle in a parabolic minimum. To reach the transition state, the reactants change their solvation. This change to a less stable form of solvation alters the energy of the electron to be transferred until the electronic energy levels in the "reactants" and "products" are equal. The electron transfer then takes place and is followed by relaxation of the solvent and ligands to the most stable configuration of the products. The variation of free energy on the solvent coordinate is parabolic, whereas the electron transfer is isoenergetic (*Albery, W.J., 1980*):

Equation 9: $O_I + R_{II} \rightarrow R_I + O_{II}$

Equation 10: $d\Delta G^*_{I,II} = 2\alpha(1-\alpha)\, d\,(\Delta G^*_{I,I} + \Delta G^*_{II,II}) + \alpha d\Delta G^0$ α kinetic coefficient,

Kinetic ***Thermodynamic***

According to Marcus, 1964 theory or model for the kinetics of chemical reactions, where electrons, and protons can be transferred the "electron-transfer reactions constitute one type of oxidation-reduction process and includes both chemical and electrochemical systems. A simple electron transfer, in an electron-transfer reaction, between two species differing only in their oxidation states where there is no difference in stability of products compared with reactants, (also called an electron-exchange reaction due that the products are chemically indistinguishable from the reactants)" (*Marcus, R., 1964*). No covalent bonds are formed or broken, and the reaction would be a diffusion-controlled process. *Newton et al, 1984* analyzed and described the steady-state as "The probability of electron transfer increases with increasing electronic interaction between the redox centers. Consequently, electron transfer is favored by small separations of the two reactants. In addition, the equilibrium nuclear configurations of the two reactants will generally be different before and after electron transfer: reorganization of the reactants prior to the electron transfer is necessary so that the transfer can occur with minimal change in nuclear configuration and momentum" (*Marcus, R., 1964; Newton et al, 1984*).

DET of electrons can be applied in biological studies on mechanisms and metabolic processes involving also redox transformations of enzymes, and the use of nanostructures to facilitate effectively the DET shortens the electron tunneling distance at the immobilized enzyme on the surface of the nanotube electrode. Electron transfer of protein is controlled mainly by three factors (*Marcus & Sutin, 1985*): ***i.*** reorganization energies; ***ii.*** potential differences and orientations of involved redox-active sites and ***iii.*** distances between redox-active sites and mediator.

The direct electron transfer of enzymes working onto the surface of electrodes can be applied in the study of reactions catalyzed by enzymes over biological systems, and can develop an electrochemistry basis for the research models that are involved in a selective electron transfer of

the redox transformations in the metabolic process (inter-biomolecular), mechanisms of this redox transformations in the structure of the enzyme molecules (intra-biomolecular). The electrical contacting of redox enzymes with electrodes is the basis for the development of enzymatic electrodes for amperometric biosensors (*Katz et al, 1997*). *Armstrong in 1987,* working with promoters (aminoglycosides as gentamycin or neomycin) to modify the surface of the electrode, achieved a fast-interfacial electron transfer of the enzyme cytochrome c peroxidase (CCP). *Katz et al, in 1997* this showed that modifying the surface the Au-electrode with PQQ-FAD (pyrroloquinoline quinone-flavin-adenine-dinucleotide) cofactor redox unit, this can act as an electron relay, and the surface reconstituted enzyme apo-glucose oxidase (Apo-GOX) exhibits direct electrical communication with the electrode and acts as bio-electrocatalyst for the oxidation of glucose. *Cai et al, 1989* immobilizing the enzyme in redox polymer matrixes, this experiment showed that the oxidized forms of these polymers are electronically conductive, and the conductivity increases when the fiber diameter approaches nanometers values. *Guo in 1997,* worked with adsorbed enzyme horseradish peroxidase (HRP) on a glassy carbon electrode surface can show the direct electron transfer for the catalytically active HRP.

Albery & Knowles, in 1976, proposed the efficiency function for an enzyme-catalyst process, which describes the effectiveness of a catalyst in accelerating an enzyme-catalyzed reaction, "involving one substrate, one product, and a single step for their interconversion". "If an enzyme becomes a more efficient catalyst, then a lower concentration of it can maintain the same flux in the metabolic pathway; the enzyme will be catalytically more efficient if it can increase the net velocity of the reaction, for the same concentrations of enzyme, substrate, and product; enzyme will be catalytically more efficient if the same quantity of enzyme can produce the same net

velocity from a smaller concentration of substrate; the enzyme will be catalytically more efficient if it can maintain the same net velocity with a larger quantity of product present". They proposed a quantitative assessment to evaluate the efficiency of an enzyme as a catalyst basis on, efficiency function (for a perfect catalyst which equals the unity) and for the function dependence of ***y***, which represent all the rate constants and the substrate concentrations (four variables of enzyme concentration, reaction velocity, concentrations of substrate and product). Also, they proposed that it can improve the catalytic efficiency of the enzyme according to alteration to the Gibbs-free energy: ***i.*** "Uniform binding (the free energies of the bound states remain the same relative to each other but are altered with respect to those of unbound states); ***ii.*** differential binding (require the enzyme to discriminate between different bound intermediates); and ***iii.*** catalysis of elementary steps (an enzyme must discriminate between the transition state and the ground state of the kinetically significant step)". One enzyme operating under reversible conditions assumes the follow equation:

Equation 11: $y = e_0 (1-b / K_c . a)/v$

y is the reciprocal of the turnover number of the enzyme,

K_c overall equilibrium constant for the interconversion of A and B,

e_0 is the enzyme concentration,

v is the moles of A converted to B per unit volume and time,

a and ***b*** are the concentrations for the substrates A and the products B (*Albery & Knowles, 1976*).

Reactions characterized by strong electronic interaction or coupling between the acceptor and donor centers are referred to as adiabatic because the probability that the activated complex will proceed to products is, or is near, unity. The rate of electron transfer is affected for two dominant

factors: ***i.*** the distance separating the donor and acceptor centers and ***ii.*** the thermodynamic driving force of the reaction. Many experimental efforts have been done to improve these relationships to quantified the nature of these relationships, modifying the distance separation between the redox center and the acceptor centers and the electrode plates, allowing the redox centers to approach each other sufficiently to transfer electrons ("the Free energy of activation varies as the square of the distance of the displacement along the reaction coordinate") assess and modifying the biological electron-transfer enzyme proteins behavior. The standard free energy of an oxidation–reduction reaction is defined by the difference between the reduction potentials of the two reactants:

Equation 12: $\Delta G^o = -nF(\Delta E) = -23.06(\Delta E)$ ***kcal/mol (T=298 K),***

where ***n*** is the number of electrons transferred,

F is the Faraday constant and

E (the cell potential at standard state) is expressed in volts, an electron volt being the equivalent of 23.06 kcal/mol, the energy acquired by an electron while passing through a potential of 1 V. The equilibrium constant for the reaction can be calculated for the follow equation:

Equation 13: $\Delta G^o = - RTLnK$

$k = Z \exp(-\Delta G^*_{I,II} / RT) \rightarrow \Delta G^*_I / RT = \log(k/Z)^{1/2}$

z is the frequency factor of collision between electrostatically neutral molecules in an aqueous solution and is often estimated to be $\approx 10^{11} dm^3 M^{-1}. s^{-1}$

$\Delta G = \Delta G^o + RTLn[(products)^x / (reactants)^y]$ ***substituting*** $\Delta G = -nFE = \rightarrow$ we have:

Equation 14: $E = Eo - RT/nF \ ln[(products)^x / (reactants)^y]$ ***at 298oK (Nernst Equation)***

$E = E^o + 0.0592/n \log[(reactants)^y / (products)^x]$

Equation 15: $E_{app} = E_m + 2.3\ RT/\ nF.\ log\ [(Ox)\ /\ (Red)]$

"slope of 59 mV (= 2.3RT/F at 298^{o}K) with ***n*** in the Nernst of 1, is indicative of a well-behaved equilibrium; the midpoint potential $\boldsymbol{E_m}$ is the solution potential at which the reduced and oxidized forms of the protein are present in equals amounts ***log [(Ox) / (Red)] = 0"*** (*Marcus, R., 1964; Newton & Sutin, 1984; Mauk, G., 1999*).

We will analyze the enzyme that interests us, its characteristics, and some aspects of vital importance for an ideal functioning. We will review some of the work done to improve its function regarding glucose detection without mediators and promoting a faster direct electron transfer. GOX obtained from Aspergillus Niger is a glycoprotein, a homodimer with a molecular weight of 150 to 180 kDa, and it has two tightly bound FAD molecules. Direct electron transfer for enzymes especially GOX, involves major difficulties due that the communication between the enzyme and the surface of the electron, and becomes more difficult because the FAD portion of the GOX enzyme is deeply embedded within the protein shell. "Direct electron tunneling from the $FADH_2$ of GOX to an electrode is much too slow, because the $FADH_2$ is buried at a depth of about 13–15 Å below the electrode-contacting periphery of its glycoprotein" (*Hecth et al 1993)*. *Kulys et al, 2006* working with GOX from Aspergillus Niger yielded an electron transfer distance of 8.1Å–11.8 Å. "This electron transfer distance reduced by the Van Der Waals contact (1.85 Å) gave the shortest distance from the active site to the surface of the protein. This distance varied from 6.3Å to 10 Å". One of the more important aspects to build a sensor is related to the distance between the redox center of the enzyme GOX and the surface electrode plate. Both the electrode surface plate and the redox center of the enzyme GOX function as a donor-acceptor pair. *Willner et al,*

2007, proposed that the electron transfer rate-constant between these units will be given by the ***Marcus equation***:

Equation 16: $k_{et} \propto exp[-\beta(d-do)]\ exp\ [-(\Delta G^{\circ}+\lambda)^2/4RT\lambda]$

Where ***d*** and ***do*** correspond to the distance separating the donor–acceptor pair and to the Van der Waals distance, respectively,

β is the electronic coupling constant, and

G° and λ correspond to the free energy change and reorganization energy accompanying the electron transfer (*Willner, et al 2007).*

GOX is relatively highly specific for β-D-glucose, with a reductive half reaction, the GOX-FAD is reduced to GOX-$FADH_2$, to produce gluconolactone and an oxidative half reaction, GOX-$FADH_2$ is oxidized to GOX-FAD, to produce hydrogen peroxide (H_2O_2). GOX immobilized on an electrode surface, give an electrochemical response due to a redox reaction of FAD to $FADH_2$, where FAD is undergoing a reaction of two-electrons coupled with two-protons causing a redox reaction as: $\boldsymbol{GOX\text{-}FAD + 2e^- + 2H^+ = GOX\text{-}FADH_2}$. Electrochemically reductive half-reaction glucose is oxidized by FAD-GOX, about 5×10^3 glucose molecules are oxidized per second (*Willner et al 2007, Yang et al, 2008*). The redox potential of GOX is due to its' own prosthetic FAD/$FADH_2$ group resulting in the redox reaction and is -0.048 V at pH 7.2 (*Kulys et al, 2006*). The potential for redox produced in the anode should be as negative (lower operational potential) as feasible to give a maximum potential difference between the anode and the cathode, and the potential range must be closer to the redox potential of the enzyme (FAD/$FADH_2$ redox center) to achieve an optimums DET in a system comprising the GOX immobilized on an electrode surface. This results in greater system efficiency and to avoid interfering substances reactions which are

substantially reduced [interfering substances: acetaminophen (AAP), ascorbic acid (AA), oxygen (O_2), uric acid (UA)] (*Guiseppi-Eli et al, 2002; Ivnitski et al, 2006; Kurusu et al, 2006; Wang et al, 2009*).

Immobilization of GOX either using modified carbon nanotubes, modified carbon electrodes, modified gold electrodes or graphene modified electrodes to build a matrix, have been done and they showed important contributions to detect glucose. *Cai et al, in 2004* working with GOX immobilized onto the surface of carbon nanotubes (CNT) can obtained a direct electron transfer happening between the active center of immobilized GOX and the surface of the CNT electrode. Also, they showed the enzyme retained its bio-electrocatalytic activity in the glucose oxidation. A single walled carbon nanotubes (SWCNT) modified gold electrodes, to immobilize GOX, was made by *Liu et al, 2005* to investigate the electrochemistry of GOX and the direct electron transfer. The rate constant of electron transfer was determined and calculated using the Laviron method, (0.3 s^{-1}). *Liu et al 2007* working with molecular wires (MW) to modified GCE and GOX can achieved direct electron transfer to detect glucose with a redox system of $\boldsymbol{E_{1/2}}$ of -0.443 V and the rate of electron transfer for immobilized GOX on GC surfaces was calculated to be 78 s^{-1} using the Laviron method. *Hui et al, 2013* developed a nafion-graphene-GOX modified gold disk electrode, to immobilize GOX, reached a direct electrochemistry system with a stability, bioactivity and electron transfer rate of $\boldsymbol{Ks}$ 1.96s^{-1} for GOX to detect glucose. The use of a matrix appropriate to immobilize GOX is a more convenient way to achieve the purpose of DET and even with greater sensitivity and better stability to act as biosensors for glucose, other studies can be found in the next references (*Chen et al, 2003; Wang et al, 2003; Liu et al, 2005; Liu et al, 2010; Unnikrishnan et al, 2013; Dervisevic et al, 2014; Kong et al, 2014; Haghighi et al, 2017; Baghayeri et al, 2017)*. CNT can promote DET due to the presence of oxygen groups (carboxylic

acid groups) on the surface (*Wang et al, 2002; Chou et al, 2005; Yang et al, 2008; Liu et al, 2018),* and can be ideal conducting nanowires due to the range of electrical conductivity (*Wang et al, 2009*). Modified electrodes with MWCNTs and have been shown as a faster electron transfer rate, but *Compton group, 2006* and other authors as well, have shown that SWCNTs and modified graphite electrodes had an increased electron transfer, due to the electrochemical properties are dominated by the oxygenated species, shown at CNT edge-plane defects at the side walls and defect sites located at the ends (*Chou et al, 2005; Ji et al, 2006: Kurusu et al, 2006; Liu et al, 2010; Liu et al, 2018*).

And now I want to explain the other part of my research. HbA_{1c} measures electrochemically (Amperometric methods) are based in the recognition of amino-phenyl-boronic acid (APBA) which interact with the sugars and can bind glucose and glycated proteins through boronic acid-diol bound. Boronic acid could covalently bind to 1, 2 or 1, 3-diol group and the cis-diol group of the surface sugar from glycated proteins under weak alkaline conditions, to form reversible cyclic boronic esters. Under bound sugar, the behavior of boronic acid-modified electrode surface, is more negatively charged (*Takahashi & Anzai, 2005; Song et al, 2009*). The catalytic reduction of H_2O_2 by HbA_{1c} can be monitored as an analytical signal in a sensor HbA_{1c} electrode, due to Hb having four iron heme groups, that catalyze the reduction reaction of H_2O_2 *(Zhang & Oyama, 2004; Kim & Shim, 2013*)

Reduction of hydrogen peroxide at a platinum electrode generates the number of electron transfers, and this electron flow is proportional to the number of HbA_{1c} molecules present in blood *(Kim & Shim, 2013*). This reduction of H_2O_2 is specifically catalyzed by HbA_{1c} (*Bunn et al, 1978*). This

amperometric assay of HbA_{1c} is a direct electron transfer detection, without enzymes for the intact glycated protein recognition. APBA serves 2 functions: ***i.*** selective binding to HbA_{1c} over the other immobilized hemoglobin's (using boronic acid part) and ***ii.*** Participation in the electrochemical reaction for HbA_{1c} measurement through its ferrocene part. DET of HbA_{1c}, immobilized on the surface of the electrode, can undergo DET, the bio-electrocatalysis is required to build a mediation APBA and immobilized glycated protein (HbA_{1c}) for continuous and efficient electron transfer from the glycated protein to the electrode surface (*Park et al, 2008; Chuang et al, 2012*). The anodic and cathodic peak potentials should be pH dependent, around pH 7.4, like a physiology condition, the redox potential for the APBA-Hb is sufficiently negative for anode operation (*Kim & Shim, 2013*).

One of the most important reasons for the DET to happen is the presence of carboxylic group, which can be found in a range of the Fourier transform infrared (FTIR) at 1715 cm^{-1} and carboxylate groups with FTIR at 1574 cm^{-1}, (–C=O, -COOH, -OH) (*Liu et al, 2010; Prasad et al, 2012*). The use or application of redox mediators versus the stimulation by the pre-anodization method to increase surface carboxylic and carbonyls groups functionalities on the edge planes (*Prasad et al 2012)*, shifts the redox potential of the APBA-HbA_{1c} anode to a more positive potential range, than the redox potential of APBA systems (*Song & Yoon, 2009; Wang et al, 2015*). The new generation of HbA_{1c} biosensor are reagent less, basically an amperometric HbA_{1c} biosensor with different modified methodologies and modified surface electrode technologies for the support for HbA_{1c} immobilization. The HbA_{1c} enzymatic assay based on the glycated peptide fructosyl valine (FV) oxidation with a further oxidation by fructosyl amino acid oxidase (FAO) on a modified zinc oxide nanoparticles/polypyrrole (ZnONPs/PPy) hybrid film gold (Au) electrode was developed by *Chawla & Pundir, 2012* to detect H_2O_2 produced enzymatically. *Stollner et al,*

2002 developed an affinity matrix composed by a membrane-immobilized haptoglobin and immobilized anti-hemoglobin antibodies to a specific detection of the bound HbA_{1c} by GOX labeled anti-HbA_{1c} antibody, this HbA_{1c} bound reflects the ratio of HbA_{1c} to the total Hb.

Biosensors that incorporates derivates of boronic acid as: ***i.*** An anti-HbA1c anti-body binding to the glycated site of HbA_{1c} and subsequent tagging of the of the carbohydrate molecule of the antibody molecule with ferrecene-boronic acid (FcBA), the hemoglobin (Hgb) was incubated with (FcBA) on deoxycholate (DOCA)-modified piezoelectric quartz crystal gold electrodes by *Halamek et al, 2007,* showing an increase in the peak current due to the accumulative amount of HbA_{1c} respect of the Hb***; ii.*** a self-assembled monolayer (SAM)-covered gold electrode to immobilized thiophene-3- boronic acid (T3BA) reported by *Park et al, 2008 and Chuang et al, 2012* showing that the impedance change reflects the amount of surface-bound HgA_{1c}. ***iii.*** a dendrimer-FPBA (4-formyl-phenyl-boronic-acid) modified gold electrode was used as a boronic acid-functionalized electrode to a backfilling assay between HgA_{1c} and GOX to detect HbA_{1c} by *Song & Yoon, 2009*. ***iv.*** Boronic acid as amino-phenyl-boronic acid (APBA) modified graphene oxide (GO)-polished glassy carbon electrode by *Krishna et al, 2011* and a modified APBA gold nanoparticles (AuNPs) coated-screen printing paper (APBA-pTTBA) made by *Kim & Shim, 2013*. ***v.*** Poly (3-amino-phenyl-boronic acid) (PAPBA) modified Nafion ® screen-printed carbon electrode showed that binding to HbA_{1c} decreased the redox current of PAPBA by *Wang et al, 2015*. ***vi.*** Phenylboronic acid-modified pyrroloquinoline quinine (PBA-PQQ) reduced graphene oxide (ERGO) on the glassy carbon (GC) electrode by *Zhou et al, 2015* showed that the oxidation peak current decreased upon increasing the concentration of HbA_{1c}. ***vii.*** Toluidine blue O (TBO)-p-benzoic acid (TBA)-MWCNT on a screen-printed carbon electrode (SPCE) to detect both HbA1c and Hb by *Moon et al, 2017*. Basically all are on DET either by measuring oxygen (O_2)

consumption and/or the amount of H_2O_2 produced in the reaction (*Kim & shim, 2013; Fang et al 2009*), by increased electrochemical signal compared (*Halamek et al, 2007*), between the cofactor APBA and HbA_{1c} and the electrode surface without mediators (*Song & Yoon, 2009).* Other references can be found in an excellent review by for *Sheikholeslam et al, 2011; Pundir & Chawla in 2014; Wang et al. 2015.*

2. 4. Electrochemical Techniques.

Chronoamperometry (CA) is a controlled-potential step voltammetry technique, which measure current (***i***) at a fixed potential (***E***). Cyclic voltammetry (CV) is a reversal linear potential sweep technique ("the potential scan equivalent to a double potential-step chronoamperometry"), which measure current (***i***) as a function of a potential (***E***) applied over a time. Square-wave voltammetry (SWV) is a linear potential sweep voltammetry applied to a stationary electrode, that combines a staircase potential and square wave, which measure current (***i***) as a function of applied potential (***E***). CA, CV and SWV use a three-electrode method: the counter electrode (CE), the reference electrode (RE), and the working electrode (WE). The experiments consist of measuring the current flowing through the WE during a triangular potential disturbance. The system handles a potential that is changing when the current is flowing and affects the current/potential (energy of electrons) at the WE, where the redox reaction occurs. The three-electrode system allows the current flow through the WE and the CE, but can measure the current between the WE and RE. The CE becomes more stable to the system, when the current is flowing. The CE can supply the current required by the WE, without limiting the measured response of the cell and the closed circuit. The role of the RE is to provide a stable and reproducible voltage to the WE, without changes in the electrical potential, but allow explore modifications in the electrode potential, during the experiment and

measurements. The electrical potential value should not vary over time and should be reproducible from electrode to electrode. The working electrode's potential is varied linearly with time (*Evans et al 1983; Kissinger et al, 1983; Eklund et al, 1999; Mirceski et al, 2013; Compton et al, 2018).*

The experimental electrochemistry process make through the electrochemistry methods, means a heterogeneous redox reaction that occurs only in the interface between the electrode and the electrolyte. According *Bard & Faulkner, 2001* factors that affect the electrochemistry process basically, are the mass transfer, electron transfer and the chemical reactions, that happen at the electrode surface. As well as these factors can modify the current generate at the electrode surface. The electrochemistry process is governed by a mass-transfer controlled electrode reaction and the concentration of gradient determines the rate of the mass transfer. If the concentration gradient is the only mechanism that control the mas transfer the electrochemistry process is a diffusion-controlled electrode reaction. If a redox process is in equilibrium, [the potential of the electrode and the concentrations of Oxidation ***(Ox.)*** and Reduction ***(Red.)*** are in equilibrium on the surface of the electrode], and there is a rapid kinetic of electron transfer the process complies with the requirements for a Nernstian reaction, and the ***Nernst equation*** for a half-reaction can be written as:

Equation 17: $E = E^{0'} + RT / nF \ln [(Ox.) / (Red)]_{x=o}$

where ***E*** is the potential applied,

$E^{0'}$ is the formal potential,

R is the gas constant ($8.314 JK^{-1}mol^{-1}$),

T is the absolute temperature (^oK),

n = number of electrons transferred/molecule,

F= Faraday's constant (96,4853 C. mol^{-1}),

[Ox.] and ***[Red.]*** represent the surface concentrations at the electrode/solution interphase (*Mabbott, 1983; Bard et al, 2001; Wang, 2006; Vedharathinam, 2011*).

In CV "the potential is scanned back and forth linearly with time between two extreme values, the switching potentials use a triangular potential waveform. When the potential of the working electrode is more positive than that of a redox couple that is present in the solution, then the corresponding species may be oxidized (flow of electrons going from the solution to the electrode) and produces an *anodic (oxidation)* current. On the return scan, as the working electrode potential becomes more negative than the reduction potential of a redox couple, reduction (flow of electrons flowing away from the electrode) may occur to cause a *cathodic (reduction)* current" *(Kissinger et al, 1983; Bard et al, 2001; Wang, J., 2006; Vedharathinam, V., 2011*).

Anodic currents are positive and cathodic currents are negative by IUPAC convention.

The potentiostat, is the electronic hardware, which controls the three-electrode cell and can run most of the electroanalytical experiments and allows us to record the curve for the current-potential polarization. The potentiostat does not control the potential of the working electrode, but it controls the voltage that occur between the RE and WE, while measuring the current that flow through the CE. The potentiostat guaranteed that the potential of the WE will not be affected by the reaction that takes place. It can control the potential of the counter electrode only (relative to the WE). In the order of significance, the most important electrode is the CE follow by the RE (*Harnisch et al, 2012; Mott et al, 2014*).

2. 4. 1. Chronoamperometry (CA).

CA is defined as an electroanalytical technique, characterized by an excitation waveform in variation of an applied potential. CA is a potential-step method which uses a voltage applied to the electrodes to measure the current before, and after, the voltage has been applied. CA is an electrochemistry technique based using a stationary electrode and a process without agitation (unstirred process). CA has a mass transport by controlled-diffusion; with a constant controlled-potential (voltage) applied, and that can measure the current generated against the time, this current is proportional to the concentration of the substance to be analyzed *(Delahay, 1963; Bard et al, 2001*).

CA assumes that the redox process happens when the oxidation (Ox.) step, plus electrons, gets to the reduction (Red.) step, ***(Ox + n*** e^- ***⇐⇒ Red***) and both Ox. and Red. steps are soluble. This is a reversible reaction (electrochemically) and the potential set for the reduction to be completed on the surface of the electrode (*Wang, J., 2006*). The current originated in a potential-step method (CA), is a current-spike due to an initial electrolysis of the species on the surface of the electrode (the current is directly proportional to the rate of electrolysis), which is followed by a time-dependent decay due to the diffusion of the molecules to the level of the electrode surface. In CA, the current is monitored as a function of time and it is recorded during the experiment as a function of time. After the experiment, the data can also be displayed as charge as a function of the time (the charge could by calculated by integrating the current, as is the case in the ***Cottrell integrated equation:***

Equation 18: $Q_d = 2nFAD^{1/2} C t^{1/2} \pi^{-1/2}$ (*Anson, F., 1966; Compton et al, 2018*).

The CA uses a time scale in milliseconds and seconds.

Faradaic currents (***I*** $_{Far}$) are related to an oxidation or reduction reaction and the result of the electrochemical reactions at the electrode surface. I_{Far} decreases because oxidation used up at electrode surface and, oxidation is only replenished by diffusion (*Wang, J., 2006*).

Faraday's law defines "The amount of chemical reaction caused by the flow of current is proportional to the amount of electricity passed". "A Faradaic (electrochemistry) process occurs when electrochemistry is characterized by the flow of current to/from electron donor/acceptor species present at the electrode surface". For a diffusion-controlled current, in a reversible redox reaction, the current-time (***i-t***) curve is described by the Cottrell equation, which reflects the net flux, (the change in the concentration gradient), and the change of the current as well, (the measured Faradaic current is proportional to the concentration target analyte at the electrode surface). "The ***Cottrell equation*** describe the behavior that happen during a potential-step experiment as long as the thickness of the diffusion layer is small relative to the electrode dimension":

Equation 19: $i = nFACD^{1/2}\pi^{-1/2} t^{-1/2}$

where: ***n*** = number of electrons transferred/molecule,

F= Faraday's constant (9.64853×10^4 C. mol^{-1}),

A= electrode area (cm^2); ***C***=concentration (mol. cm^{-3}),

D= Diffusion coefficient (cm^2. s^{-1}).

The current response is inversely proportional to the square root of the time, so the relationship between current and time ($it^{1/2}$) can be called a "Cottrell behavior" and is direct proportional to the concentrations of the species (*Delahay, P., 1963; Macdonald, D, 1977; Heineman et al, 1984; Bard et al, 2001; Wang, 2006*).

CA can measure the concentration by measuring ***(i***) current vs. concentration at any fixed time. CA studies the occurrence of coupled chemical reactions analyzing the shape of the current-time curve and measuring the coefficient of diffusion for the electroactive species (blood glucose test stripes). The graphic between the anodic current vs. time generates a straight line and according the equation of Cottrell means a process controlled by diffusion (*De Guibert et al, 1979*). Biosensors with screen-printing technology for glucose detection through the glucose oxidase, the meter control operation is built up over potential-step method as chronoamperometry. CA is important because it is a fundamental method on which other techniques are based (*Leroux et al, 2008; Laxmibai, 2019*).

CA has proven to be an excellent technique for understanding the effects of electrode potential and time, in mechanistic studies related to the redox process of enzymes (*Fourmond, 2009*). CA is useful for monitor changes in the current that results from the enzyme switching between the catalytical active and inactive states, under certain redox conditions (*Leger et al, 2008*).

2. 4. 2. Cyclic Voltammetry (CV).

CV is defined as an electroanalytical technique, characterized by the current response, based in a stationary electrode, excited by a triangular voltage waveform in variation on applied potential. CV is an electrochemical method to characterize the behavior of analytes that can be oxidized or reduced electrochemically. CV can locate redox potentials and acquire the qualitative ("the half-wave potential $E_{1/2}$ is related to the standard potential for the half-reaction and is often used for qualitative identification of species") and quantitative ("the limiting current ***i***, is proportional to the analyte concentration and is used for quantitative analysis") information from these electrochemical reactions *(Skoog et al, 2007*). CV is an unstirred process (without agitation), with

a mass transport by diffusion-controls. “CV specifies the relationship between the potential of an electrode and the concentrations of the two species (designated Ox and Red) involved in the redox reaction at that electrode”. This assumes that the redox process happens when the Oxidation (Ox.) step, plus electrons, gets to the Reduction (Red.) step, (***Ox + n e^- ⇆ Red***) and both Ox and Red steps are soluble. These are a reversible reaction (electrochemically) and the potential set for the reduction to be completed on the surface of the electrode. CV distinguishes a reversible redox process (controlled diffusion) through the kinetics of the potential scan-rate electrode process, where the reagent transport is proportional to the square root of the scanning speed *(Kissinger et al, 1983)*.

CV is an electrochemistry technique with control of a constant potential (voltage) applied at the electrode. The potential of the working electrode is swept at a specific scan rate (Volts/second), and the resulting current can be measured against the time curve. The sweep potential is reversed at a specific switching potential. The sweep potential rate is constant and the initial and switching potentials are known, the time value can be converted to a potential and then it can be recorded as the current against applied potential. The relationship between the potential applied to an electrode and the concentration of redox species (oxidized and reduced form) at equilibrium, is described by the equation of Nernst on the surface of the electrode as:

Equation 14: $E = E^0 + (0.0591/n) \log [Ox/Red]$ at T of 298 ^oK

where ***E*** is the potential applied,

E^0 is the formal potential,

[Ox.] and ***[Red.]*** represent the surface concentrations at the electrode/solution interphase (*Nicholson et al, 1964; Mott et al, 2014; Compton et al, 2018*).

Applied potential (***E***) is a function of sweep rate and the potential varies linearly with the time, rate of potential change with time $\boldsymbol{E(t) = E_1 - \nu t.}$

One full cycle occurs in CV scan for reversible systems, when a linearly dependent potential (in relation to the RE) is applied, with a certain scan rate (***v***), to the WE. The swept from $\boldsymbol{E_1}$ (initial potential), where no reaction undergoes to $\boldsymbol{E_2}$, (final or reverse potential) where electron transfer is rapid, the potential is reversed when it reaches $\boldsymbol{E_2}$ and is swept back to $\boldsymbol{E_1}$. The scan rate (***v***) is the change of potential as function of time $\boldsymbol{v = dE/dt"}$, and the current flow is also a time function, there could be interrelates and plot the current as a function of applied electrode potential (*Mabbott, 1983; Heineman et al, 1984; Harnisch et al, 2012*).

Figures 2.4.1. left side and right side shows the conventional cyclic voltammogram obtained by measure the current at the WE during the potential scans which describe: the cathodic peak potential ($\boldsymbol{E_{pc}}$), anodic peak potential ($\boldsymbol{E_{pa}}$), cathodic peak current ($\boldsymbol{i_{pc}}$) and anodic peak current ($\boldsymbol{i_{pa}}$) as the more important magnitudes (*Nicholson et al, 1964*); and also, the different steps than happen in the redox reaction.

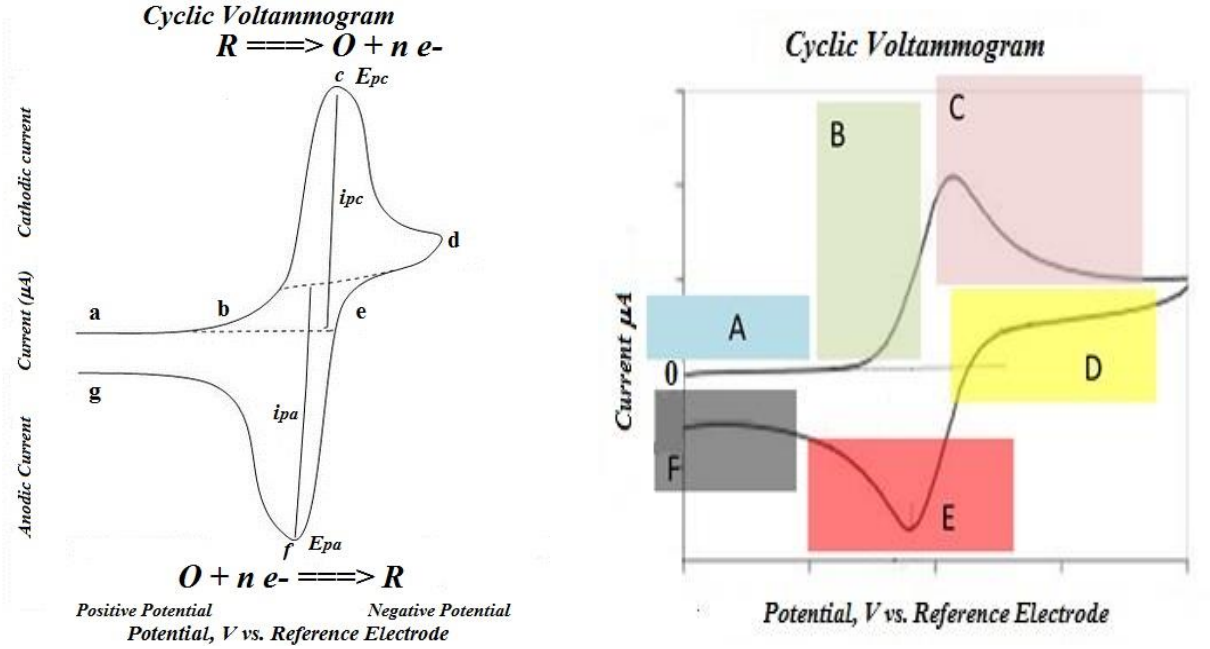

*Figure 2.4.2.1. left side shows: "the reduction process occurs from (a) the initial potential to (d) the switching potential. In this region the potential is scanned negatively to cause a reduction. The resulting current is called cathodic current (**i_{pc}**). The corresponding peak potential occurs at (c) and is called the cathodic peak potential (**E_{pc}**). The **E_{pc}** is reached when all of the substrate at the surface of the electrode has been reduced. After the switching potential has been reached (d), the potential scans positively from (d) to (g). This results in anodic current (**I_{pa}**) is because the oxidation occurs. The peak potential at (f) is called the anodic peak potential (**E_{pa}**) and is reached when all of the substrate at the surface of the electrode has been oxidized" (Nicholson et al, 1964; Kissinger et al, 1983). Figure Right side shows: "Region A where the current remains unchanged. Region B which shows increasing current as the potential difference is increased. This is due to the oxidation of the species in solution. Region C shows that the current then peaks before dropping off as the rate of reaction is limited by the diffusion rate of the species in solution. Region D shows the potential difference being decreased. As the potential difference decreases, the current decreases because the reaction rate decreases. Region E shows the species produced in the forward scan is being reduced. Region F shows the reaction being limited by the diffusion of the oxidised species to the electrode" (Nicholson et al, 1964; Kissinger et al, 1983; Wang, J., 2006).*

The Electrode potential (***E***) is calculated: $E=E_i + v\,t$. where E_i is the initial potential in volts, ***v*** is the sweep rate in volts/s, and ***t*** is the time in seconds. When the direction of the potential sweep is switched, the equation becomes, $E=E_s - v\,t$. where E_s is the potential at the switching point.

Formal potentials as mid-point potential (half-wave potential of the current plateau) $E_{1/2}$ from a reversible cyclic voltammogram or in a sigmoid curve in steady-state voltammetry (qualitative information) could be calculated by the anodic (E_{pa}) and cathodic (E_{pc}) peak potentials:

Equation 20: $E_{1/2} = E_{pc} + E_{pa}/2 = E^{o'} + RT / nF\ [\ Ln\ (D_{red}^{1/2}) / (D_{ox}^{1/2})]$

Where $E^{o'}$ is the redox potential,

R is the gas constant (8.1314 $JK^{-1}mol^{-1}$),

T is the absolute temperature (^{o}K),

F= Faraday's constant (96,4853 C. mol^{-1}),

D_{ox} and D_{red} are the diffusion coefficients for the oxidized and reduced halves of the couple (*Nicholson et al, 1964; Bard et al, 2001; Skoog et al, 2007; Compton et al, 2018*).

The formal electrode potential for a redox process $E^{o'}$, can be determine through the CV, averaging the two peak potentials due to the presence of a return potential peak: $E^{o'} = E_{pc} + E_{pa} / 2$. The corresponding peak potentials E_{pa} ***and*** E_{pc} are independent of scan rate and concentration (*Bard et al, 2001; Aristov et al, 2015).*

ΔE_p means the separation between the two peak potentials, $(\Delta E_p = E_{pa} - E_{pc})$ is characteristic for a redox species and can be used to determine the electrochemical reversibility for a redox process, (number of electrons transferred) close as $\Delta E_p = E_{pa} - E_{pc} = 59 / n\ mV$ at 25oC ($2.3RT/nF$), where ***n*** is the number the electrons participating in the redox reaction. ΔE_p allows the identification of the mass-transfer regime for reversible redox process which is controlled by diffusive mass transfer [according to Nernst equation, in the interface between the electrode and the electrolyte, the ***(Ox.)*** and ***(Red.)*** reactions occur at high enough rates that the equilibrium point is broken]. The cathodic and anodic peak potentials do not change with the scan rate, their difference, ΔE_p is always ***59/n mV*** at 25.8^{o}C in a steady state (*Kissinger et al, 1983; Bard et al, 2001; Wang, J., 2006*).

The heterogeneous electron transfer rate constant ***(Ks)*** for the redox reaction can be calculated through the value of the ΔE_p, ***59/n*** mV for ΔE_p. The Electron stoichiometry (***n***) is calculated: $E_{pa} - E_{pc}/2 > 0.0565/n$.

where E_{pa} is the anodic peak potential,

E_{pc} is the cathodic peak potential, and

n is the number of electrons participating in the redox reactions.

CV allows it to be observed that the product generated electrochemically is stable, on the time scale of the experiment. An electronic transfer reaction usually involves the reaction of the electrode that is influenced by the potential of the electrode. If the product is stable the peak current observed by return potential peak scan (i_{pa}), should be equal to the potential peak forward (i_{pc}), $i_p(red.)/ip(Ox.) = 1$. The forward potential scan (i_{pc}) gives a reversible electron transfer reaction in both directions, means the ratio for the reverse and the forward current is: $I_{pa}/I_{pc} = 1$ *(Kissinger et al, 1983; Aristov et al, 2015).*

The peak current i_p in a reversible system with a forward sweep at ***T*** of 298°K is given by the ***Randles-Sevcik equation*** (quantitative information):

Equation 21: $i_p = (2.69 \times 10^5)\, n^{3/2} AD^{1/2} v^{1/2} C$

where i_p is the peak current (in amperes),

n is the number of electrons passed per molecule of analyte oxidized or reduced,

A is the electrode area (cm^2),

D is the diffusion coefficient of analyte (cm^2 /sec),

v is the potential sweep rate (volts/sec), and

C is the concentration of analyte in bulk solution (moles/cm^3) (*Bard et al, 2001; Wang, J., 2006; Skoog et al, 2007*). So, the peak currents are proportional to the square root of the scan rate $(v^{1/2})$, and anodic peak potential (i_{pa}) and cathodic peak potential (i_{pc}) increases as $v^{1/2}$ increase; and it is

directly proportional to the concentration. A graph of the *Randles-Sevcik* equation generates a straight line. The slope can be used to determine the system's diffusion coefficient (***D*** $\boldsymbol{cm^2/s}$) (*Mabbott, G., 1983; Heineman et al, 1984*).

2. 4. 3. Square-Wave Voltammetry (SWV).

SWV due to its high analytical sensitivity, can determine concentrations at the picomolar level (***pM*** $\boldsymbol{= 10^{-9}\ mol/m^3}$). It has the capability to reduce capacitance currents significantly, and with a very short time of analysis. SWV allows simultaneous inspection of the redox system of both reduction processes and oxidation processes and, therefore, gives an idea of the mechanism of the electrode reaction. SWV is an electrochemical election method for many analytic studies (sensitivity of pulse techniques), electrochemical measurements and mechanistic studies in electrode operation (kinetic information for impedance techniques) and has valuable capabilities to determine compounds simultaneously present in physiological and/or pharmaceutical samples with similar chemical structures. According to *Bard & Faulkner, 2001,* combine "the best aspects of several pulse voltammetric methods, including the back-ground suppression and the sensitivity of differential pulse voltammetry, the diagnostic value of normal pulse voltammetry, and the ability to interrogate products directly in much the same manner as a reverse pulse voltammetry. It also offers access to a wider range of time scales than can be achieved by any pulse polarographic techniques". The voltammogram peaks obtained show their high sensitivity and exclusion of currents from the background. SWV integrates the advantages of a CV technique and the increased sensitivity of pulse voltammetric techniques, and invariably performed through a potentiostat-system controlled by a computer *(Barker & Jenkins, 1952; Krause & Ramaley, 1969; Lovric et al, 1991; Bard & Faulkner, 2001; Mirceski et al, 2013; Mirceski et al, 2018*).

SWV is a linear potential sweep voltammetry applied to a stationary electrode, that combines a staircase potential and square wave in an unsteering process. The waveform of the SWV combines a large-amplitude square wave modulation with a stair-case waveform. SWV has a stair-case potential ramp which it is modified with a square-shaped potential pulse, and at each step of the stair-case ramp, there are two potential pulses with equal height but with opposite direction, this shows a single potential cycle in the SWV, and this single cycle potential is repeated at each step in the full experiment.

The height of the single potential pulse is termed square wave amplitude ($\boldsymbol{E_{sw}}$), also correspond to the magnitude of each pulse, which is one-half of the peak-to-peak amplitude on the square-wave signal *(Lovric et al, 1991; Mirceski et al, 2007*).

In a surface electrode reaction, the voltammetric response consists of forward (anodic direction) and backward (or reverse, cathodic direction) potential pulses, with their corresponding current measurements anodic ($\boldsymbol{I_{for}}$) and cathodic ($\boldsymbol{I_{rev}}$) currents, taken at the end of each cycle. The first pulse per cycle, at the end of the positive direction, corresponds to the forward current or oxidation current ($\boldsymbol{I_{for}}$), which is in the direction of the stair-case scan, and at the end of the second pulse at the end of the negative direction which correspond to the reverse or backward current or reduction current ($\boldsymbol{I_{rev}}$), which is in the opposite direction of the scan. The two different currents generate a peak for each of these processes. The difference between $\boldsymbol{I_{for}}$ and $\boldsymbol{I_{rev}}$ is termed the difference current ($\boldsymbol{\Delta I}$) or net current $\boldsymbol{I_{net}}$ ($\boldsymbol{I_{net} = I_{for} - I_{rev}}$), which is "recorded as a function of the mean potential of each SW period". Also, the $\boldsymbol{\Delta I}$ assess the displacement of the redox equilibrium that occurred at the electrode surface (electrode reaction) and gives the respective information of the oxidation or reduction of the redox species through anodic and cathodic direction (also different surface concentrations), with subsequent diffusion of mass transfer close to the electrode. In the

voltammogram plot (difference current plotted versus the sweep potential), the plot displays a peak-shaped which is proportional to the concentrations of the redox species at the electrode surface *(Lovric et al, 1991; Bard & Faulkner, 2001; Mirceski et al, 2018; Dias et al, 2017).*

A critical time for the experiment, is represented by the duration of a single potential cycle (***τ***) or by the duration of a single potential pulse $t_p = \tau/2$. The square-wave frequency (frequency of the potential modulation and number of potential cycles in a unit of time) is the reciprocal of the stair-case period $f = 1\tau$ or $f = 1/2\ t_p$, (correspond to the critical time parameter of the SW voltammetric experiment). The potential increment (***ΔE),*** is the height of the stair-case waveform (*Mirceski et al, 2018).*

Bard & Faulkner, 2001 and Mirceski et al, 2018 define the principal parameters for the SWV as:

a. the scan increment, ***ΔE*** of the staircase ramp; the square wave is characterized by a pulse height, ΔE_p, measured with respect to the corresponding tread of the staircase, and a pulse width t_p, which can be related to the square wave frequency and expresses the scan rate as $v = \Delta E/2t_p$ **if** $f = ½\ t_p$ **therefore** $v = f\Delta E$ (***ΔE*** correspond to the step of the staircase ramp).

b. Square wave amplitude (E_{sw}) and

c. The duration of the potential pulse t_p.

Osteryoung in 1993, described "the theoretical response by means of a dimensionless current function, ***ψ*** for the surface reaction, which is related to the current, ***i*** by a factor containing parameters of the experiments and the system:

Equation 22: $i = (nFAD^{1/2}C^b/\sqrt{\pi t_p})\ \psi\ (\Delta E_s, E_{sw})$

n is the number of electrons transferred,

F Faraday constant,

$\boldsymbol{A}$ is the area of the electrode,

$\boldsymbol{D}$ is the reactant diffusion constant (typical value is $\boldsymbol{10^{-6}\ cm^2.s^{-1}}$),

$\boldsymbol{C^b}$ is the bulk concentration of the reactant,

$\boldsymbol{t_p}$ is the pulse width (half of the staircase period),

$\boldsymbol{\psi}$ is the dimensionless current function, which depends on the amplitude ($\boldsymbol{E_{sw}}$) and the scan increment ($\boldsymbol{\Delta E}$),

$\boldsymbol{\Delta Es}$ is the step height (the potential increment from one cycle to the next),

$\boldsymbol{E_{sw}}$ is the square wave amplitude (*Osteryoung, J., 1993).*

In a reversible reaction, the current response, described in terms of a normalized current function, which occurs in a voltammetry pulse technique, depends only on the sequence of potential applied to the electrode regardless of time. According to *Miscerki et al, 2018* the "real current $\boldsymbol{I}$, that includes the net peak current $\boldsymbol{\Delta I_p}$, is a linear function of the square-root of the frequency and corresponds at the first diagnostic criteria of a reversible electrode reaction of a dissolved redox couple". The voltammogram graphic obtained by plotting the normalized current function versus the normalized potential $\boldsymbol{n(E-E_{½})}$ "is independent of pulse width, concentration or identity of reactant" (*Osteryoung & Osteryoung, 1985; Osteryoun, J. 1993; Mirceski et al, 2018).*

"The peak potential separation ($\boldsymbol{\Delta E_p}$) is a function of normalized amplitude ($\boldsymbol{nE_{sw}}$, $\boldsymbol{n}$ is the number of electrons exchanged in the electrode reaction)" (*Mirceski et al, 2013*).

CHAPTER 3. EXPERIMENTAL AND DISCUSSION FOR GLUCOSE & GOX

3. 1. Materials and Method

3. 1.1. Materials and apparatus

Glucose Oxidase (GOX), EC 1.1.3.4 from Aspergillus Niger, β-D-glucose: oxygen 1-oxidoreductase, (CAS 9001-37-0) lyophilized power containing 100,000 – 250,000 units/g solid; Glucose (D-(+)-glucose >99.5% power (CAS 50-99-7) bioreagent; 1-ethyl-3(3-dimethylaminopropyl) carbodiimide hydrochloride (EDC) (CAS 25952-53-8) reagent; N-hydroxysuccinimide (NHS) (CAS 106627-54-7) reagent; Ru (NH_3) Cl_2 (hexamine-ruthenium III chloride) 98% (CAS 14282-91-8) reagent; phosphate buffered saline (PBS) 10X concentrate (CAS 7558-79-4) with a pH 7.2-7.6 at 25^{o}C; ascorbic acid (AA) 99% power (CAS 50-81-7) reagent; salicylic acid (SA) power (CAS 69-72-7) and lactic acid (LA) 85% viscous liquid (CAS 50-21-5) were all purchased from Sigma Aldrich Co and used as received.

Highly concentrated graphene oxide (HC-GO) composition ≥79% carbon and ≤20% oxygen, viscosity at 25^{o}C 1,000-2,000 mPa.s, sheet resistance 50 Ω/sq. at 25 μm thickness; Ag/AgCl ink, surface resistivity <75mΩ/square/mil and viscosity 5,570-14,600 CPS; Carbon ink 79% C-220 carbon resistive ink make by Conductive Compounds, with a surface resistivity 10.68 Ω/Sq. and viscosity at 25^o C. 43,050 CPS and oxygen 20% was purchased from Graphene Laboratories (Calverton, NY.).

Deionized water (>18MΩcm) was obtained from a Millipore purification system (Biomedical solutions Inc. Bedford, MA.), to prepare all aqueous solution.

Potassium ferricyanide [K_3Fe $(CN)_6$] (CAS 13746-66-2) power reagent was purchased from Fisher.

SU-8 50 negative tone photoresist formulation 50, with a thickness of 50 mms as purchased from Micro-Chem, Newton. MA.

Chromatographic paper Whatman 1 chr. 1030-025, grade 3MM, from Tish scientific, cellulose, with a thickness of 0.34mm and diameter 25 mm.

3. 1. 2. Preparation of solutions.

The phosphate buffer solution (PBS) 0.01 M phosphate buffer, 0.0027 M potassium chloride and 0.137 M sodium chloride with a pH 7.4 was used in all studies, it is made for dissolved 1 tablet of PBS compound from Sigma Aldrich Co., in 200 ml of deionized water at 25^{o}C.

The EDC/NHS (0.35M/0.1M) solution was prepared as follow: 0.0033 g of EDC plus 0.0012 g of NHS dissolved in 50 μL of deionized water and kept at 4^{o}C.

The 5 mM potassium ferricyanide solution was prepared by passing 0.074 g of KCl dissolved in 10 ml of deionized water through a 0.0164 g of $K_3Fe\ (CN)_6$ in 10 mL of deionized water. The solutions were stored at room temperature (25^{o}C).

The 5 mM hexamine-ruthenium chloride solution $Ru\ (NH_3)_6\ Cl_2$, which was prepared by dissolving 0.0154g of $Ru\ (NH_3)_6\ Cl_2$ in a 0.1 M of KCl (0.074 g KCl in 10 mL of deionized water). The solution was sored under N_2 and keep at 4^{o}C.

20 mM GOX solution was prepared by dissolving 0.0020 g of GOX (lyophilized power) in 1 mL of PBS. The solution was stored at 4^{o}C.

Solutions of varying glucose concentrations solution were prepared by dissolving different known amounts of glucose (D-(+)-glucose) power, in 1 mL of PBS at room temperature (25^{o}C).

Ascorbic acid, salicylic acid and lactic acid solutions were prepared to achieve a glucose equivalent concentration of 0.1 M.

3. 1. 3. Specific surface area

The specific surface area the sample was calculated using the Brunauer, Emmett and Teller (BET) surface adsorption method and theory, through the accelerated surface area and porosimetry system (ASAP) 2020 Sorptometer made by Micromeritics, by measuring N_2 adsorption on the surface of the sample. The sample was degassed at 150ºC for 70 min at 10 mm Hg, in order to remove any remaining solvent and ensure complete dryness and emptiness of the pores. After this result of the amount of adsorbed N_2 at a bath temperature of 76 K were obtained.

3. 1. 4 Electrochemical measurements.

Voltammetry measurements CV, CA, and SWV were carried out with a CH Instrument (CHI 730E, Electrochemical Analyzer, Austin TX.) electrochemical workstation in a three-electrode cell assembly, at room temperature (25ºC), with electrodes which consists of the printed paper-carbon electrode (PPE) microfluidic device. The modified electrodes such as graphene oxide-PPE (PA-PPE-GO) and pre-anodized-PPE (PA-PPE) were analyzed with the different electrochemical techniques, and, the modified PA-PPE-GO-GOX and PA-PPE-GOX electrodes were analyzed and compared with the identical electrochemical techniques. All the PA-PPEs have a working electrode area of 0.03141 cm^2.

CV measurements were carried out at a different scan rates range 30 mV/s to 500 mV/s. We used different probes as 5 mM potassium ferricyanide, 5 mM hexamine ruthenium III chloride and 0.01 M PBS in PA-PPE-GOX- biosensor, through direct electron transfer, to evaluate the electrochemical oxidation in order to demonstrate the presence of immobilized GOX and therefore the analysis of glucose. All the experiments were carried out at room temperature 25ºC, with different scan rates to find the best scan rate for the experiment.

CA experiments were carried out with glucose concentrations range 30 μM to 50 mM.

The SWV experiments were carried out with different concentrations of glucose range from 0.2 mM to 0.84 mM and analyzed with tht PA-PPE-GO-GOX and PA-PPE-GOX biosensors.

3. 1. 5. Spectrometers studies.

The FT-IR spectrum was recorded by using Spectrum 100 FT-IR Spectrometer, Perkin Elmer. Spectrum is Perkin Elmer's premier software package for collecting, viewing and processing FT-IR spectra., all the studies were testing at room temperature (25^{o}C). The optical module contains a Class II/2 Helium Neon (HeNe) laser, with an achievable precision of ca 0.008 cm^{-1}, which emits visible, continuous wave radiation at a wavelength of 633 nm and has a maximum output power of 1 mW, reduces signal artifacts and improves response linearity, high-quality, low-angle, off-axis optics minimize aberrations and provide the highest optical efficiency. The PPE, PA-PPE and PA-PPE-GOX biosensors 5 of each, were prepared according to details showed in next two sections, to carry out the experiments and compare and analyze the results obtained.

3. 1. 6. X-ray photoelectron spectroscopy studies.

XPS is a powerful technique that provides us with information about a sample surface, which is located on the surface of a platform or electrode, about its molecular composition and its chemical bonding. The XPS analysis were carried out with a PHI 5600 spectrometer with a hemispherical energy analyzer, using an aluminum (Kα) source of 1487 eV at 100 Watts. The sample was maintained at high vacuum. The pressure in the analysis chamber during XPS analysis was in the low range of 10^{-9} Torr. All spectra were recorded at 54^{o} take-off angle, the analyzed area being currently about 1 mm^2. All spectra were recorded with 1.0 eV step, 10 cycles, 20 sweeps and

corrected using carbon signal (C1s) at 284.5 eV. XPS spectra were analyzed using Casa-XPS software version 2.3.18. The Shirley method was used for extracting the background necessary for curve fitting.

3. 1. 7. Fabrication of paper electrodes.

The PPEs were designed through the adobe illustrator graphic design software and were subsequently manufactured using the template printing technique. A template print mask with the electrode pattern was created by means of low-adhesion laser-cut films with an internal Zing 16 laser cutter (Epilog, Golden, CO). The prepared electrode patterns were placed on the SU-8 2010 photographic resistance treated chromatographic paper, which was previously prepared using the photolithography technique. SU-8 epoxy-based is a negative photoresist, and negative refers to a photoresist whereby the parts exposed to UV rays crosslink and needs to bake again after UV exposure to complete the polymerization. The photolithography technique consists in: applied SU-8 photoresist over the chromatography paper; baked in a hot plate for 20 min at 135ºC; a selectively polymerization with UV (350-400 nm) exposure at 100% for 20 sec. using a mask 0.7 cm diameter that show the design area, in black ink printed, to generate a hydrophobic and hydrophilic areas; transfer the chromatography paper to the hot plate por 5 min at 135ºC and later developed with acetone and isopropyl alcohol at 70%. Them left to dry at room temperature x 20 min. See figure 3.1.

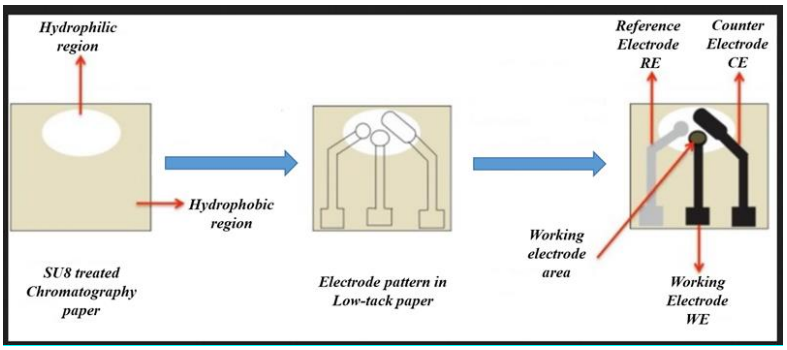

Figure 3.1. Design showing the process of making the disposable paper electrode (pictures not drawn to scale).

The conductive carbon ink paste was careful impregnated into the electrode patterns to make 2 of the 3-electrode system consisting of a: carbon-based counter electrode (CE), a carbon-based working electrode (WE) with a surface area of 0.03141 cm^2 and a conductive Ag/AgCl ink-based pseudo-reference electrode (RE) as a 3^{er} electrode system, see fig. 3.1. and fig. 3.2. After each step, following the application of carbon ink to the two electrodes WE and CE, and next the Ag/AgCl ink over RE, the PPE were backed at 95^oC for 25 min in an oven *(Dungchai et al, 2009; Martinez et al, 2010; Nie et al, 2010; Lan et al, 2013; Liu et al,2014*).

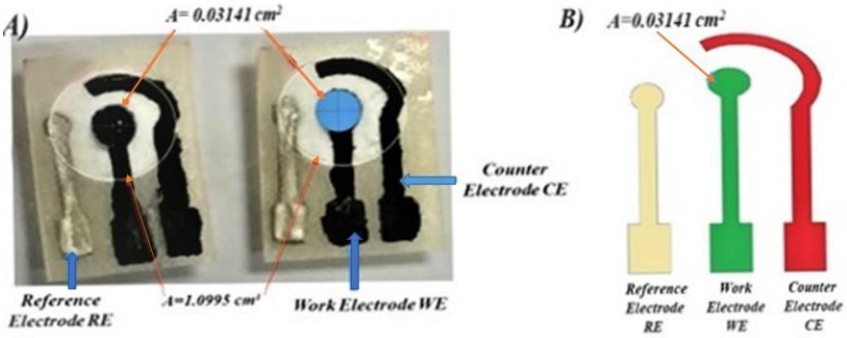

Figure 3.2. (A) Digital photo image of the PPE. (B) the electric circuitry for the electrode. The circuitry consisted of working electrode (WE), counter electrode (CE), and reference electrode (RE).

3. 1. 8. Fabrication of Modified Electrode.

After the PPE has been prepared, then the pre-anodization process is done by applying a potential at 2.0 V, through the ***i-t*** electrochemical technique method, over working electrode vs Ag/AgCl counter electrode, for 300 s., placing the PPP in a beaker which contained a pH 7.4 PBS. With a pre-anodized time of 300 s. the ratio between O_{1s} and C_{1s} (O_{1s}/C_{1s} ratio) has more changes and as well as create more carbonyl-groups functionalities (*Evans et al, 1979; Notsu et al, 1999*). The pre-anodization method create more edge plane sites and can make the modified carbon electrode (CE) more electroactive, but also provides low susceptibility to electrode fouling (*Prasad et al, 2007; Yang et al, 2008; Prasad et al, 2008; Thiyagarajan et al, 2014*). The next step was add the EDC/NHS (0.35M/0.1M) solution, which was prepared with 0.0033g of EDC and 0.0012g of NHS and dissolved in 50 mL of deionized water, and drop coated 5 mL over the WE at the PA-PPE and left for 30 min at room temperature (25^{o}C), after that, the excess was removed and washed with 0.01 M PBS 1 μL. Then GOX was coupled through EDC and NHS cross-linkers. The GOX solution was prepared by dissolving 20 mg GOX in 1 mL 0.01M PBS and drop coated 5 μL on to EDC/NHS activated PA-PPE. The electrodes (PA-PPE-GOX) were then dried at room temperature for 2h, and subsequently washed with 0.01M PBS 1 μL to remove unbounded GOX. The prepared electrodes including, also modifies electrodes prepared with GO (PA-PPE-GO-GOX) was further used for the voltammetry measurements and evaluated the electrochemical oxidation of glucose through direct electron transfer without utilizing any mediators. The figures 3.3 & 3.4 show the schematic diagram and the representation for the full process done to prepare and tested the modified electrode.

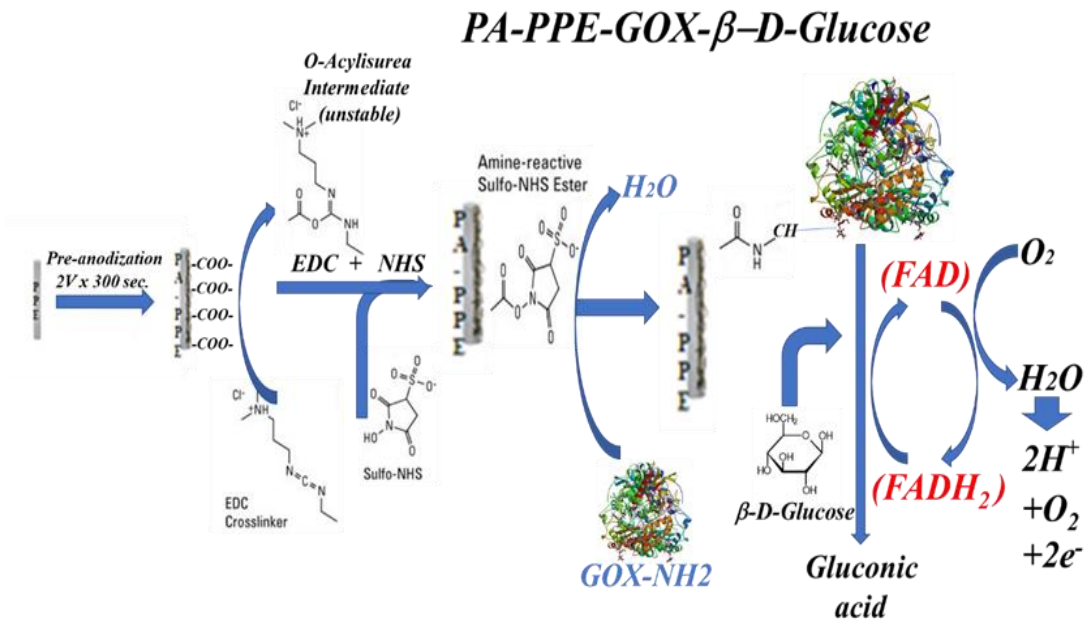

Figure 3.3. Schematic diagram and representation of modified electrode: PA-PPE-EDC/NHS-GOX-Glucose.

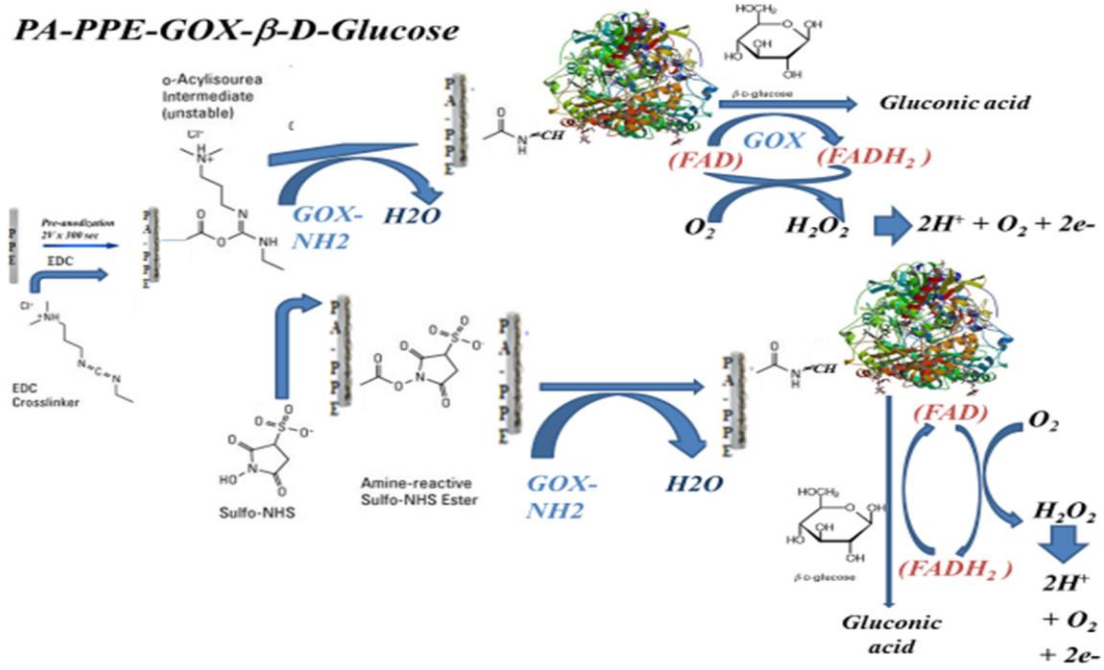

Figure 3.4. Schematic diagram and representation of modified electrode: PA-PPE-EDC/NHS-GOX-Glucose, showing the two enable ways to immobilize the GOX and final products of the process.

3. 2 Results and discussion

3. 2. 1. Specific surface area

The BET surface area report shows a 5.07 m^2 of area per gram of the material. The geometric surface area for the working electrode is 0.03141 cm^2. The Braunauer-Emmett-Teller *(BET*) surface area is 12.675 cm^2 with a pore size of 92.607 Å and pore volume of 0.016736 cm^3/g. (*Brunauer et al. 1938*).

3. 2. 2. Pre-anodization technique

The pre-anodization as a cleaning technique and performed as a pretreatment, the carbon electrode is cleaned and exposed to the application of a potential, and the functional groups are formed on the surface as a multiple edge plane formation. The fig. 3.5 shows the electrochemical oxidation process that happens when a positive potential (2V) is applied versus time (300 s). The current or the flow of electrons going from the solution to the electrode and produces an anodic (oxidation) current.

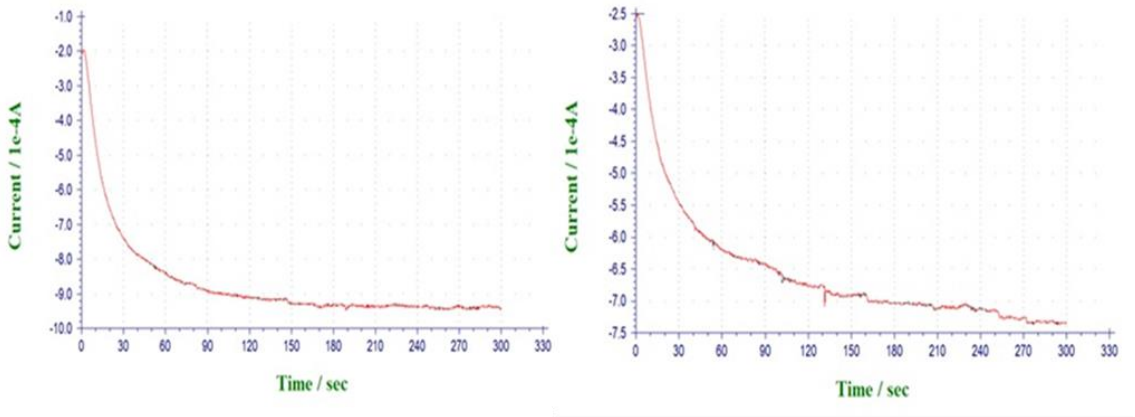

Figure 3.5. Pre-anodization (PA) graphic.

3. 2. 3. Surface Characterization of PA-PPE-GOX.

a. Fourier transform infra-red (FT-IR).

The FT-IR spectrum of GOX exhibits basically two peaks with additional bands:

i. The Amide I band (is an overlapping spectrum of α-helices, β-sheets, turns and random coils, which form the basic structure of the protein) peak at 1650 cm^{-1} and 1715 cm^{-1} caused by C=O stretching vibrations of peptide linkages in the backbone of the protein GOX, (*Zhao et al, 2010*). Identified C=O stretching vibrations of peptide linkages in the GOX backbone, at 1600cm^{-1} to 1700 cm^{-1} (*Liang et al, 2003)* and 1650 cm^{-1} to 1750 cm^{-1} (*Hui et al, 2013*).

ii. Amide band II peak at 1462 cm^{-1} caused for combinations of N-H in a plane bending and C-N stretching linkages for the peptide groups, (1490 cm^{-1} identified as the combination of N-H in-plane bending and C-N stretching of the peptide groups) (*Liang et al, 2003; Hui et al, 2013; Malasevic et al, 2008*).

iii. Amide band III on 1239 cm^{-1}, predominantly β-sheet (Mainly C=O) correlated with Delfino datas (*Delfino et al, 2013; Boyaci, et al, 2015*).

Additionally, we founded two wide bands in the region 3400 to 2900 cm^{-1} representing the amide A and the bond linkages to -CH_3 stretching at 3400 cm^{-1} and 2958 cm^{-1}, respectively, correlated with Prasad study (*Prasad et al, 2015*). According to a consensus of research's, the presence of the amide I region between 1600 cm^{-1} to 1700 cm^{-1}, with their different C=O stretching vibrations, and amide II region at 1550 cm^{-1} to 1462 cm^{-1} with the C-N stretch coupled to N-H bending, that correspond to the peptide groups, they provide information on the type of secondary structure, these types of vibrations are the α-helix, β-strands, and different kinds of turn structures as β-turns and β-antiparallel. The α-helix structure can be assigned in the range of 1655 cm^{-1} and 1545 cm^{-1}, and the β-strands has been assigned in 1630 cm^{-1} and 1530 cm^{-1} bands. (*Goormaghtigh et al, 2006;*

Alhazmi, H. 2019). Amide I and amide II bands in the FT-IR spectrum of the free enzyme is generally accepted as indicative of the enzymatic activity and could be used to monitor the GOX characteristics after immobilization.

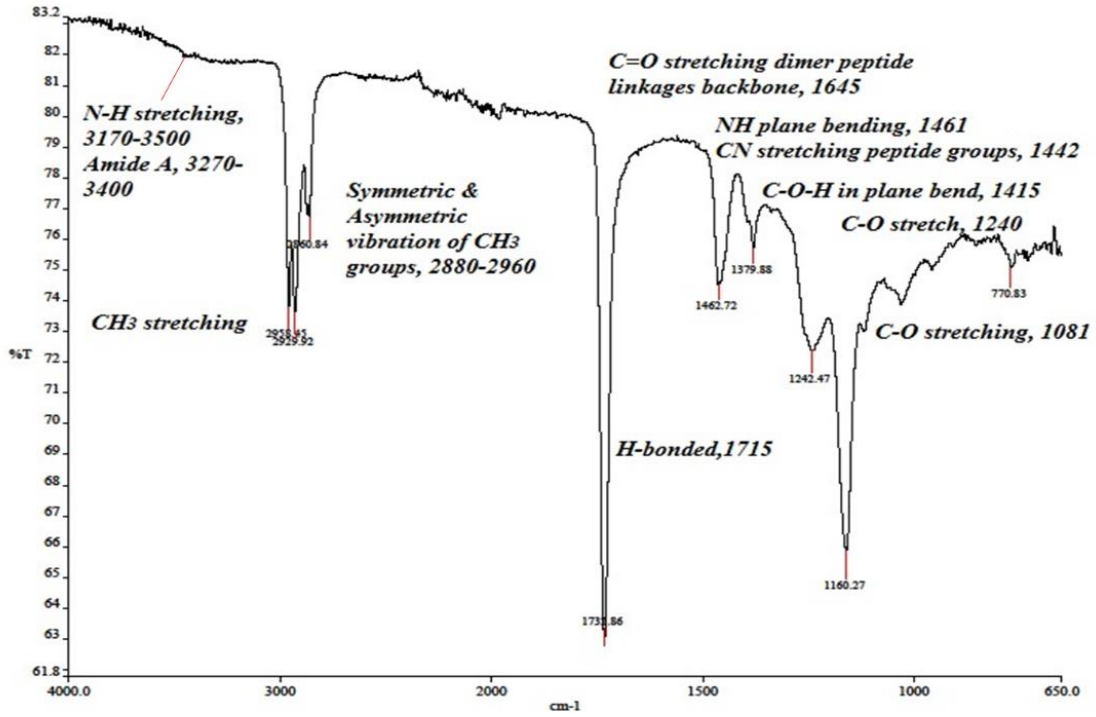

Figure 3.6. FT-IR Spectrum for PA-PPE-GOX.

b. **X-ray photoelectron spectroscopy (XPS).**

XPS studies conducted on the PA-PPE-GOX sensor to demonstrate the immobilization of GOX show us that the data with C is fitted by a mix of pure C(1s), with C-C and C-O-C bonds in the proportions shown in the figure 3.7. B & C. Pure C would peak at 284 eV. The peak of C(1s) moves from 284 eV and focuses around 285.8 eV corresponding the (overlap C-C, C-H, C=C bonds) (*Libertino et al, 2007; Ni et al, 2008).* C(1s) centered peak around 288 eV with two binding energy, 288.3 (N-C-O bond) and 286.3 (C-O bond), which be assigned to overlap groups such as

[R-CH2-NH-(C*O)-] and [(R-CH2*-NH-(CO)-] respectively *(Libertino et al, 2008)* and overlap 286.3 eV (C≡N), 287.7 eV (C-N) and 288.2 eV (C-O) bonds) (*Ni et al, 2008).*

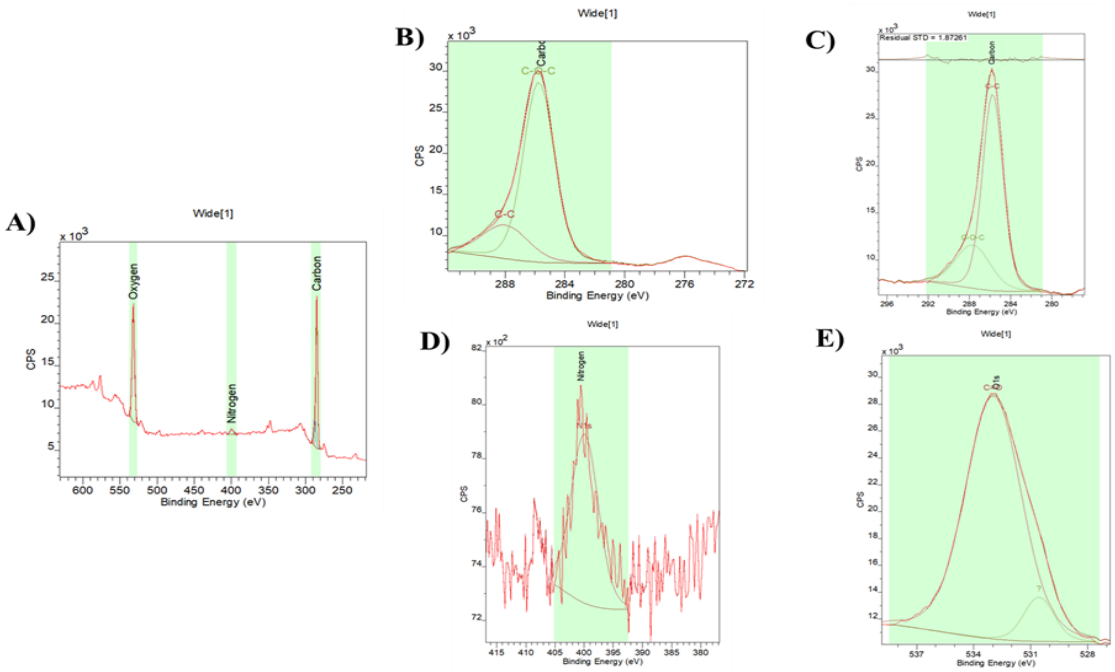

Figure 3.7. XPS for GOX (A) found C(1s) (B & C), N(1s) (D) and O(1s) (E) graphics.

The following works in XPS on the C(1s) core-level spectra set out the principles for compound configurations associated with proteins. *Boyd et al, 1995* use the peak of C(1s) identified in 284.6 eV, as an adventitious carbon to evaluate the reference of the spectra, the peaks obtained at 285.9 eV and 287.7 eV were assigned to the carbon and (nitrogen sp2 and sp3) bonds and the peak obtained at 288.2 eV is assigned to the (C-O) bond. Five peaks at C(1s) core-level spectra were identified by *Bhattacharyya et al, 1998,* which were assigned the binding energy to the respective bond, 284.7 eV (pure carbon C1), 285.3 eV [C=N (C2) bond], 286.7 eV [C≡N (N3)], 287.7 eV [C-N bond (C4) bond] and 289.6 eV [C-O bond (C5)]. *Dementjev et al, 2000* found a peak with a union energy at 287.9 eV, which identifies it as C(1s) and a good indicator of the interaction

between C and N (C-4N), characteristic of carbon atoms (four bonds) that has a single or double bond with nitrogen atoms.

To validate our findings, we will review some work that focuses on demonstrate the presence of GOX, based on the different configurations of C(1s) spectra. *Li et al, 1998* found that the successful immobilization of GOX on the surface of a film, shows two significant changes in relation to the peaks obtained by the binding energy (BE), the first corresponds to the reduction in intensity of the carboxyl group by 288.7 eV and the second to increase in intensity at the peak of the peptide union at 287.8 eV. *Libertino et al, 2007 and 2008* assigned 288.3 eV (N-C-O) to [R-CH2-NH-(C*O)-], and 286.3 eV (C-O) to (R-CH2*-NH-(CO)-), as chemical groups of the proteins, characteristic of the GOX immobilization. We can see the C(1s) binding energy shift for the functional groups and the main compounds in the figure 3.8.

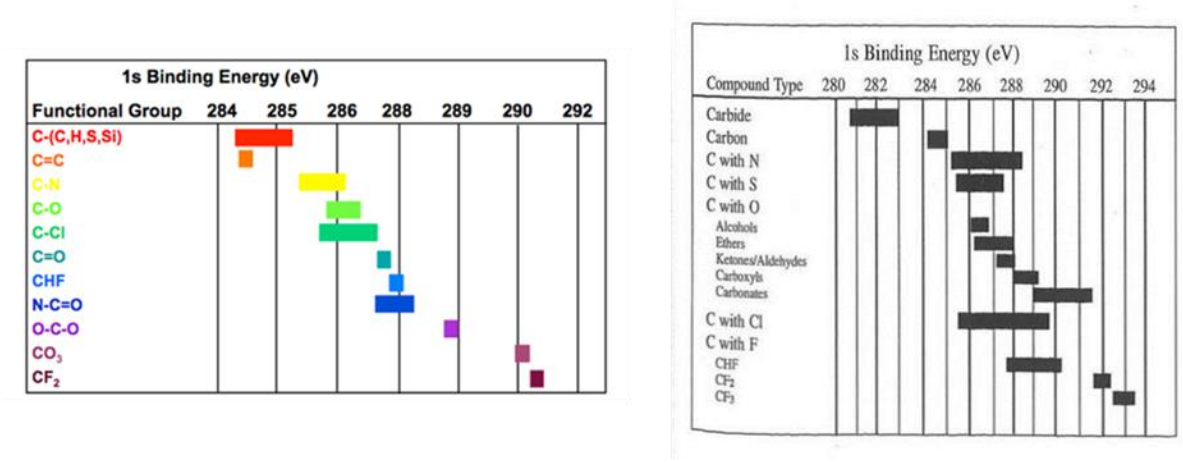

Figure 3.8. Binding energy (BE) for the functional groups, and compound type of the carbon chemical state C(1s). Moulder et al, 1992, and Web-EAG laboratories. Assessed in March 2020

For the binding energy of N(1s) spectrum, figure 3.7. D, we found a centered peak at 400 eV, which is the correct one corresponding to pure N(1s) peak at 399 eV (*Libertino et al, 2007* shows that the intensity of the N(1s) peak was centered at 400 eV). Also, the N(1s) spectra core-level

found the following binding energies at different peaks and was attributed to their respective union. 398.3 eV (overlap N^1 sp^3 as N-C and C-NH_2 bonds) (*Boyd et al, 1995; Dementjev et al, 2000; Ni et al, 2008*). 399.1 eV (overlap N≡C and C=N-C bonds) (*Dementjev et al, 2000).* 399.9 eV (N=C bond) (*Ni et al, 2008).* 400.6 eV (N-C sp^2 bonding) *(Boyd et al, 1995*) and 400.8 eV [NO (N4)] (*Bhattacharyya et al, 1998).*

The next works confirms the presence of organic molecules, due to the configurations of N(1s) and C(1s) spectrum, in the surface of the biosensor and support the immobilization of GOX. The centered peaks overlapping binding energy for the 398.5 eV (C-NH_2 bond) assigned by *Dementjev et al, 2000*. 398.8 eV (N-C sp3 bonding) assigned by *Boyd et al, 1995*, and 399.1 eV (C=N-C bond) assigned by Dementjev et al, 2000. 400.7 eV (overlapping N-C sp2 bonding and NH2 groups) according to *Ni et al, 2008.* All of them, contributed to identify different bounds between the N(1s) and C(1s) as part of the configurations of carbon nitride compounds. Also, *Libertino et al, 2007* detect a centered signal at 400 eV, in the spectra of N(1s) for the GOX immobilized.

Our oxygen data, figure 3.7.E, is fitted by a mix of pure O(1s) at 532 eV and some carbonates such as C-O (almost at the same energy as C, see figure below) in the proportions shown in the figure 3.7. E. Pure O would peak at the vertical line (almost at the same energy as C-O). See figure 3.9 for more details of the binding energy of O(1s) and compounds type.

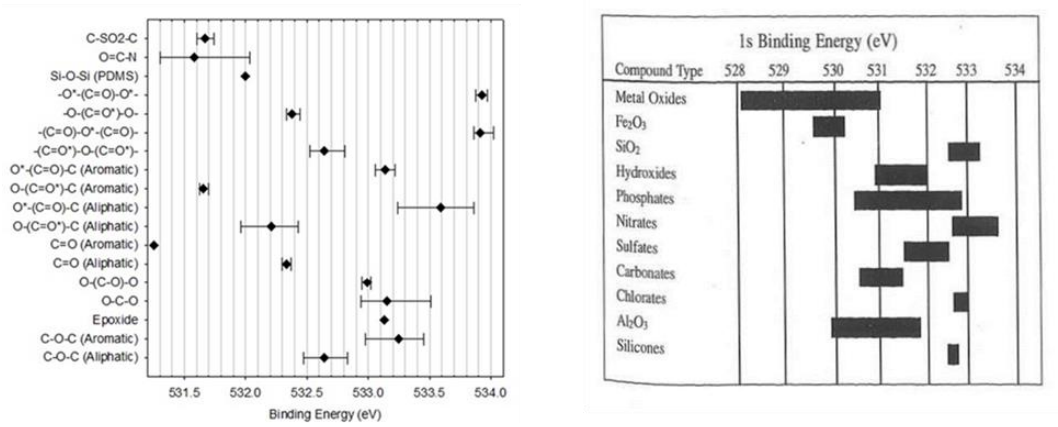

Figure 3.9. Binding energy for oxygen. Moulder et al, 1992. Internet archive, open library. Assessed March 2020.

According to our data obtained especially the changes in the spectrum of C(1s) peak, related to the chemical group's characteristic of the proteins, and the spectrum of N(1s), we can suggest that the GOX is successfully immobilized in our PA-PPE-GOX biosensor. These changes are in accordance with the revised literature by *Boyd et al, 1995; Bhattacharyya et al, 1998; Li et al, 1998; Libertino et al, 2007; Libertino et al, 2008; Ni et al, 2008.*

3. 2. 4. Electrochemical characterization of PA-PPE-GOX.

After immobilizing GOX onto PA-PPE, the electrochemical studies were carried out in 0.01M PBS under N_2.

***a*. The cyclic voltammetry (CV)** profile for PA-PPE-GOX exhibited a pair of well-defined and nearly symmetric redox peaks with a formal potential of -0.44 V (Fig. 3.10. A), which is like the previous reports (*Yang et al, 2008*), and close to the standard electrode potential of GOX (*Kang et al, 2009*).

We compare the CV for PPE-PA-GOX tested with 5mM K-Ferricyanide which get an anionic probe-left side with increased current, and we tested with 5mM Ruthenium-Hexamine Chloride 5mM which get a cationic probe-right side graphics (Fig. 3.10. B), at 0.050 V/s scan rate. Two

different probes towards the same electrode, explain the electron transfer involved and interaction between electrodes (negative charge) and electrostatic interaction between electrode and probe molecules (specific potential for oxidation and reduction).

The difference in potential between the peaks of the reduction (E_{pc}) and oxidation (E_{pa}) curves is $\Delta E_p = (E_{pa} - E_{pc}) = 0.0599$ V (a value that is close to the theoretical value of 0.059 V for the ferrocene redox pair) for all scan rates between 50 and 500 mV s^{-1}, the peak current ratio (i_{pa}/i_{pc}) is equal to 1.01, and the and the formal electrode potential for a redox process Eo' = 0.43145.

In addition, the CV clearly indicate that the redox peaks are derived from the immobilized GOX, when compared to the unmodified electrodes without GOX. The electrochemical response of GOX immobilized onto the PA-PPE is attributed to the direct electron transfer of GOX for the conversion of FAD/$FADH_2$ (*Wang et al, 2002: Cai & Chen 2004; Yang et al, 2008*), (Nernstian-electrochemical reaction in which the rate of reactions is governed by the diffusion of the electroactive species to the surface of a planar electrode, as a reversible and surface-confined process). The direct electron transfer reaction of GOX/FAD redox reaction involved two-electron coupled with two-proton transfer: $GOX/FAD + 2e^- + 2H^+ = GOX/FADH_2$.

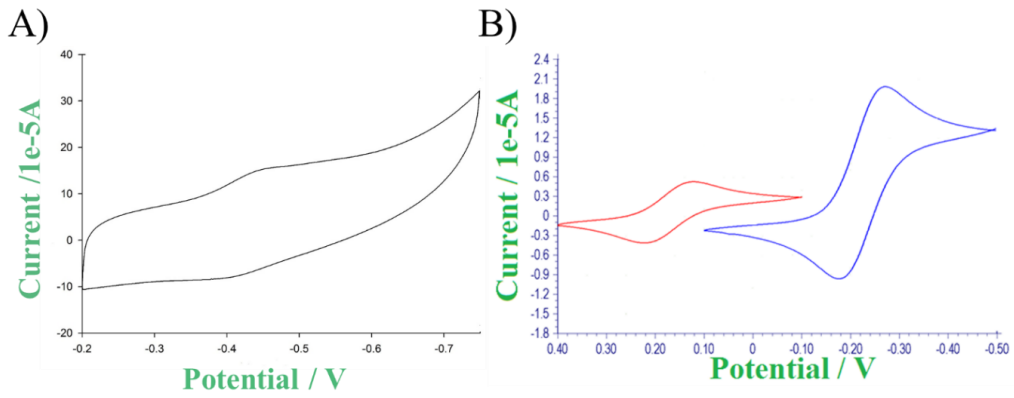

Figure 3.10. (A) CV response of PPE-PA-GOX immobilized with 0.01 M PBS at a scan rate of 50 mV/s. (B) CV for PPE-PA-GOX with 5mM K-ferricyanide (anionic probe-left side, red color) and 5mM ruthenium-hexamine chloride 5mM (cationic probe-right side, blue color) comparative.

CV studies allow us to show the behavior of the electrode with respect to the scan rate, if there is any change in the current and allows us to determine what type of reaction take place in the electrode. The scan rate effect on PA-PPE-GOX electrodes is shown in Fig. 3.11, the CV's at different scan rates (*v*) ranged from 50 to 200 mV/s (Fig. 3.11.A). The anodic and cathodic peak currents changed appreciable and increased with respect to the change in scan rate and exhibited a good linear relationship for both the anodic and cathodic current and scan rates (Fig. 3.11.B). The relationship between the log peak current versus log scan rate, in the plot was linear with a slope of 0.561714 (***α = transfer coefficient***) which indicates a surface-diffusion controlled redox electrode process.

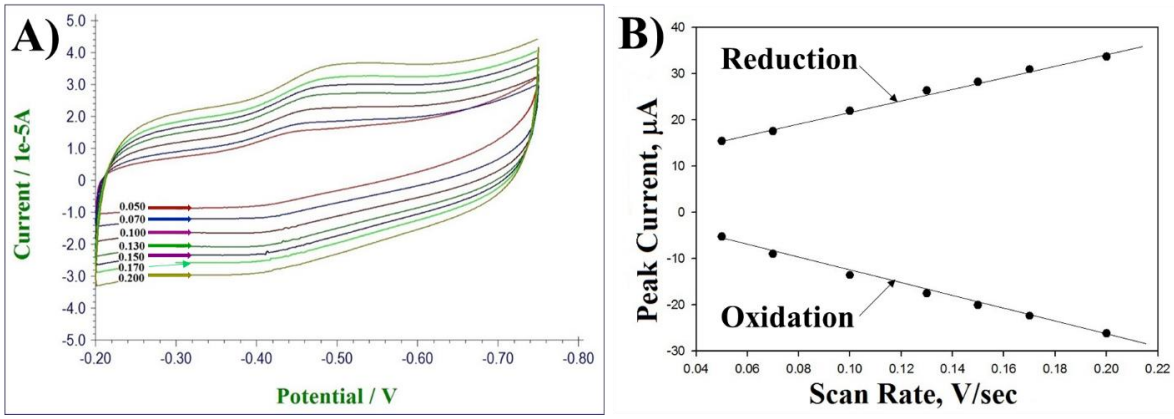

Figure 3.11. (A). CV response of PA-PPE immobilized with GOX in 0.01 M PBS at a scan rate of 50-200 mV/s, and (B), plots of anodic (i_{pa}) and cathodic (i_{pc}) peak current versus scan rate.

The heterogeneous electron transfer rate constant, k_s on the PA-PPE-GOX electrode was calculated with Laviron equation (Laviron, 1979).

Equation 23: Log k_s = α log (1-α) + (1-α) logα-log (RT/nF v)-α (1-α) nFΔEp /2.3RT

R is the universal gas constant (8.314 J $mol^{-1}K^{-1}$),

T room temperature at Kelvin degree (298^{o}K),

F is the Faraday constant (9.64853 x 10^{4}C),

n number of electron transfers and

v is the scan rate.

The calculated charge transfer coefficient ***(α)*** was 0.5617 and with two electron transfers ***(n***=2). The heterogeneous electron transfer rate constant k_s was calculated to be 3.363 s^{-1}, which is higher than the k_s reported for the carbon nanostructured materials: (K_s of 1.69 s^{-1} for *Janegitz et al 2011*); (K_s of 2.83 s^{-1} for *Kang et al, 2009*); (K_s of 3.273 s^{-1} for *Hua et al, 2012*); (K_s of 1.713 s^{-1} and 1.12 s^{-1} for *Razmi et al, 2013*); and gold nanoparticle incorporated matrices: (K_s of 1.713 s-1 for *Wu et al, 2007*); and (K_s of 2.2 s-1 for *Zhang et al, 2011*). From this it is evident that the carbonyl functionalities and edge plane-like sites formed during the pre-anodization process at PPE, play an important role in improving the electron transfer communication between the redox centers of GOX and electrode.

The surface average concentration of electroactive GOX ***(Γ)*** value was calculated from the ***equation 24: Γ= Q/nFA.*** ***(Q)*** charge involved in the reaction, ***(n)*** number of electrons transfer, ***(F)*** Faraday constant, (***A)*** area of WE.

Γ= 8.30013 e-9 mol/cm^2, which is bigger than *Liand & Zhuobin, 2003* (***Γ***= 5.1 x 10e-11 mol/cm^2); *Kang et al, 2009* (***Γ***= 1.12e-9 mol/cm^2); *Zhang, et al. 2011* (***Γ***= 2.56 e-10 mol/cm^2); *Razmi et al, 2013* (***Γ***= 1.8e-9 mol/cm^2) *and Baghayeri, M. 2015 (****Γ***= 4.65± 0.76 e-10 mol/cm^2), means that the higher heterogeneous direct electron transfer rate constant is directly influenced by the multilayer coverage of GOX.

Different experiments of calibration conducted through CV on the PA-PPE-GOX-Glucose biosensor show good performance to identify glucose at different concentrations with a sensitivity of 60.8723 $\mu AmM^{-1}cm^{-2}$ (SE 1.544, CV% 1.336) which, was calculated as the current density (current/area) and plotted against the concentration of glucose. The calculated sensitivity is higher than *Zhang et al, 2011* (16.6 $\mu AmM^{-1}cm^{-2}$); *Unnikrishnan et al, 2013* (1.85 $\mu AmM^{-1}cm^{-2}$*); Razmi & Mohammad-Rezaei, 2013* (0.085 $\mu A\mu M^{-1}cm^{-2}$).

b. **Square wave voltammetry (SWV) analysis**. The electrocatalytically activity of the PA-PPE-GOX towards glucose is studied by conducting square wave voltammetry experiments with different concentrations of glucose ranging from 0.2 mM to 0.84 mM and 0.01 M PBS under N_2. Successive additions of glucose resulted in a gradual decrease in reduction current (Fig. 3.12. A), and it is linearly proportional to the increased concentration for glucose (fig.3.12. B). This trend could be explained by the fact that with the addition of glucose triggers, the enzyme-catalyzed reaction of GOX and glucose by formation of $FADH_2$ from FAD, at the level of the biosensor surface with subsequent decreases of the cathodic peak current (*Janegitz et al, 2011; Liu et al, 2014*). This reaction causes a decrease in the amount of oxidized GOX on the PA-PPE electrode and reduces the electrode reduction current.

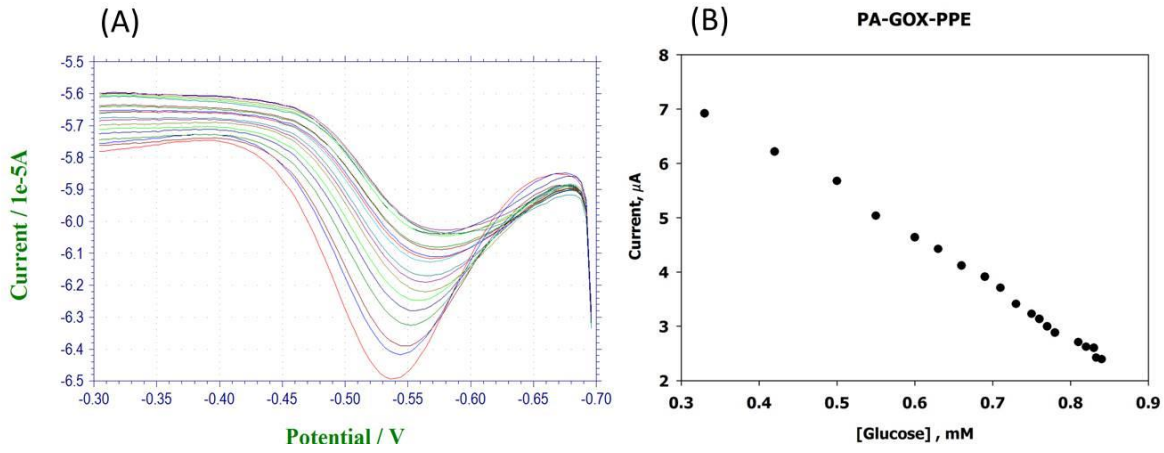

Figure 3.12. (A) Square wave voltammogram for different concentration of glucose at GOX immobilized in PA-PPE, (B) the plot peak current μA versus glucose concentration in mM showing the linear progression decrease at the surface of the electrode.

In order to establish the increased sensitivity of the newly developed electrode, PA-PPE-GOX towards glucose detection, we compared the current response developed for GOX immobilized on graphene oxide through EDC/NHS cross coupling method, GO-PA-PPE-GOX with PA-PPE-GOX. As can be seen from the calibration plots of PA-PPE-GOX and GO-PA-PPE-GOX (Fig. 3.13. B), the pre-anodized electrode exhibited, quantitatively, 2.612 times higher current response than GO modified electrodes. The improved electro-catalytical activity at PA-PPE-GOX again points towards the better electron transfer communication between GOX at the surface of the electrodes electrochemically activated or pre-anodized electrodes than with GO modified electrodes.

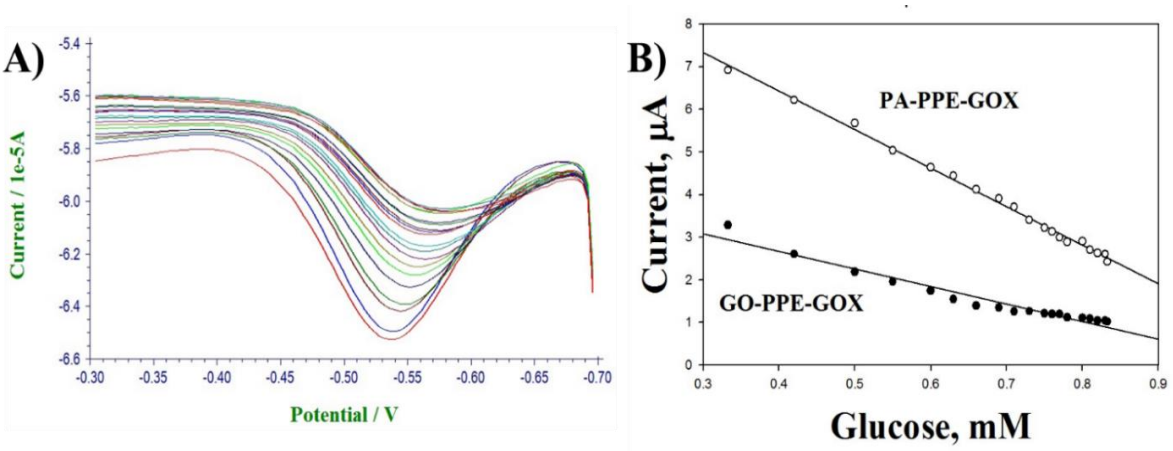

Figure 3.13. Square wave voltammogram (SWV) for different concentration of glucose at PA-PPE-GOX (A) and corresponding calibration curve for PA-PPE-GOX and GO-PPE-GOX (B).

***c*. Chronoamperometry analysis (CA).** CA is one of the more sensitivity methods and can reach lower detection limits. The electro-catalytical activity of PA-PPE-GOX was further characterized by conducting CA experiments for the reduction of glucose, with a constant controlled potential of -0.55 V, comparing the response with 0.01 M PBS (pH 7.4) and different concentrations of glucose that ranging from 30 µM to 50 mM. Different experiments were carried out, measuring current against time, at high and low glucose concentrations, until a minimum and maximum glucose level was optimized. Since the current is proportional to the glucose concentration, the current graph against time shows changes in glucose concentration on the electrode surface, also obtaining a linearity in the graphic response.

Figure 3.14.A and Figure 3.14.B depicts the chronoamperometric responses of glucose reduction at 0.01 M PBS and a different concentration of glucose with a fixed potential of −0.55 V. Because of the negative operating potential, for the detection of glucose, that eliminates the interference from other electroactive species such as, ascorbic acid, uric acid, and dopamine present in the real blood samples.

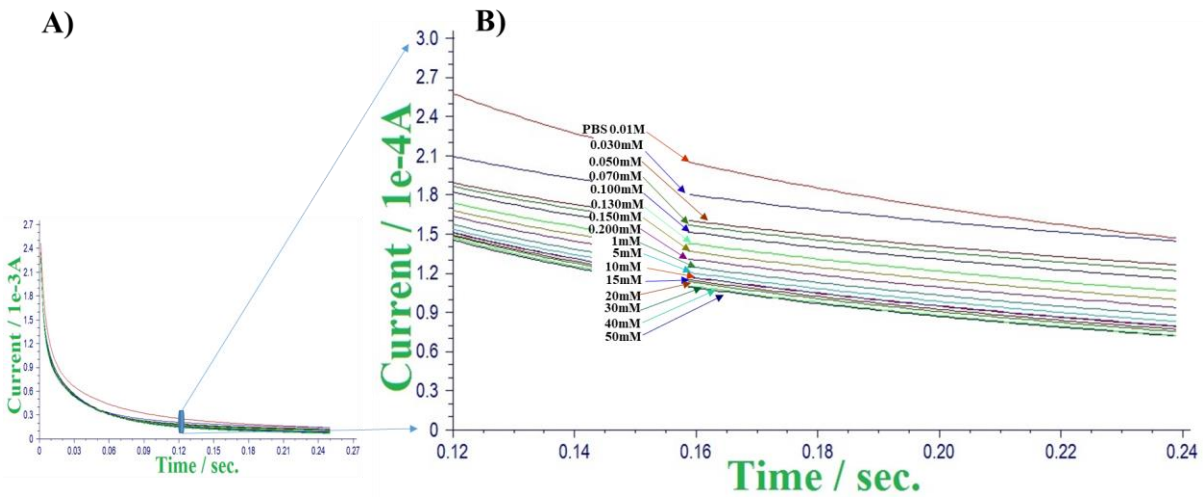

Figure 3.14. Chronoamperometric response for PA-PPE-GOX towards different concentrations of glucose (30 μM to 50 mM).

As the concentration of glucose increases, there is a shift from the linearity between concentration and current (Fig. 3.14. A and fig. 3.14. B), exhibiting a typical Michaelis-Menten kinetics, see figure 3. 15. A, (*Marcos et al, 1993; Shirale et al, 2006*). The line-weaver-Burk plot (*Liu et al, 2014*) a double reciprocal plot, show a linear curve graphic, based in the following equation:

$$\textbf{\textit{Equation 25: } } 1/v = (1 / v_{max}) + (K_m / v_{max}).\ (1 / [S]),$$

Where v is the initial reaction rate at a given substrate concentration,

v_{max} is a constant reaction rate,

K_m is the Michaelis-Menten constant,

$[S]$ is the substrate concentration.

($V_{max} = 0.021714$, $m = 1.38343$, $b = -46.05323$), which corresponds with the linear equation $y = b + mx$, with a direct correlation between current ***1/v (1/mA)*** and glucose concentration ***1/[S]*** (***1/mM***) (*Shirale et al, 2006*).

The K_m calculated was found to be 0.03 mM (3.0×10^{-2}mM), values of Km of GOX which is lower than GOX immobilized on graphene quantum dot (K_m of 0.76 mM for *Razmi et al, 2013*), GOX

immobilized reduced graphene oxide (K_m of 0.215 mM for *Sehat et al, 2014*), poly (p-phenylenediamine)-based nanocomposite (K_m of 0.42 mM for *Baghayeri, M., 2015*), and with the GOX adsorbed pre-anodized screen printed-carbon electrodes (K_m of 1.07 mM for *Yang et al, 2008*).

A lower K_m means a higher enzymatic activity of immobilized GOX at PA-PPE; thus, the results suggests that the present PA-PPE-GOX have a high affinity towards glucose, with a limit of detection as low as 1.8 x 10^3 ug/5µL. The Figure 3.15. B shows a linearity relationship range for glucose 1mM through 50mM (target range of 18 mg/dL – 900 mg/dL), (SD: 0.879, SE: 0.0265, R^2: 0.9890), which include the normal range of blood glucose in humans as well the abnormal range values of hypoglycemia or hyperglycemia.

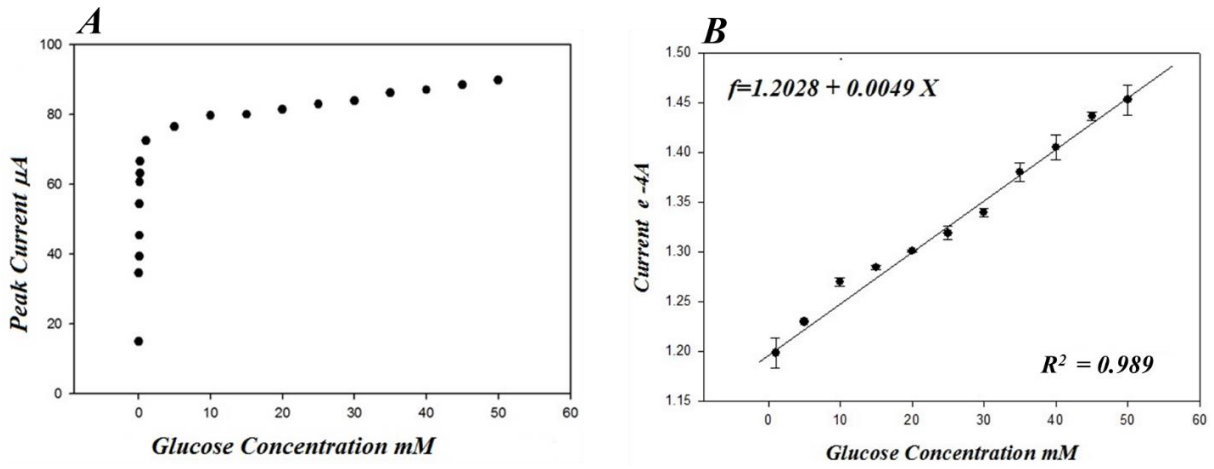

Figure 3.15. characteristic response of Michaelis-Menten kinetics (A), corresponding linearity range of 1mM through 50 mM (B).

Glucose serum is linear from 5 mg/dL to 900 mg/dL (0.28 mmol/L to 44.40 mmol/L).

3. 2. 5. Interfering species.

The total blood level of glucose is around 100 mg/dL and may reach values above 400 mg/dL in uncontrolled diabetic patients. There are substances in the blood considered interference species, and their blood levels are minimal, comparable to glucose. These types of substances can interfere

with glucose readings in biosensors. We conducted multiple studies in amperometric ***i-t*** technique, to validate the specificity of the biosensor, PA-PPE-GOX, on glucose (Glc), ascorbic acid (AA), salicylic acid (SA) and lactic acid (LA), as interfering species. Concentrations of interfering species were adjusted to a glucose equivalent of 0.1 M. Different experiments were carried out to achieve an adequate amount of volume samples, which was 5 μL. All the studies were conducted in ***i-t*** mode with a potential of 0.5 V, time of 1000 sec, and non-stirring process, as well as, the 0.1 M glucose samples and AA (0.1M), SA (0.1M) and LA(0.1 M) samples, were applied at different times, allowing the system to stabilize between samples.

The graph shows two large initial peaks, 200 sec and 300 sec, corresponding to glucose 0.1 M, the following peaks around 360 sec, 420 sec and 485 sec correspond to SA, LA and AA respectively. Amperometric readings are shown in the graph and the currents of the interfering species are very small, and there was a need to adjust the graph to assess their values. We calculate the current ratio between glucose and interfering species, which was for SA (1.65%), LA (5,354%) and AA (4.99%) respectively. See figure 3.16.

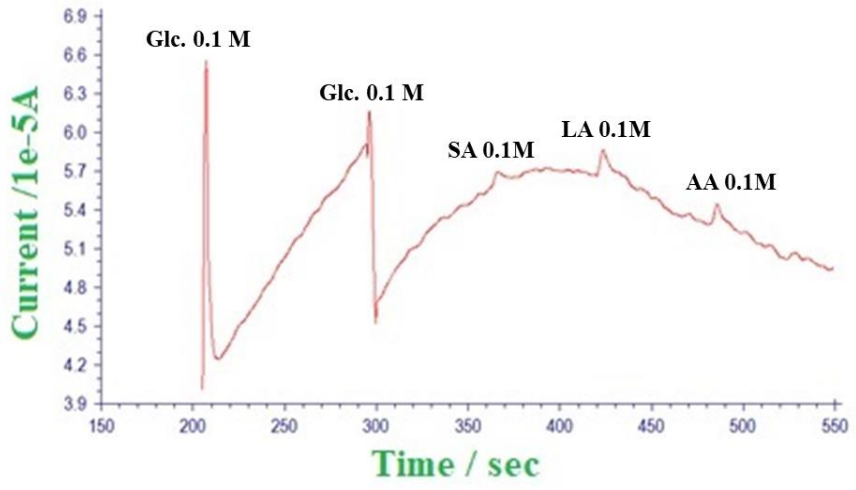

3. 16. Amperometric studies (i-t) for interfering species in glucose sensing experiments.

The current ratio between the glucose and the interfering species allow us to infer that our sensor shows great affinity for glucose. The current value of the interfering species represents a higher concentration (0.1M) than the concentrations that these species can obtain in total blood. Therefore, we observe a minimum current response of the interfering species with respect to glucose, suggesting that there is a selectivity and specificity of the biosensor towards glucose.

3. 2. 6. Discussion and inferences.

The modified prepared electrodes PPE-PA-GOX and PA-PA-GOX-glucose have:

i. A well-defined redox peak, due to improved electrochemical conductivity through the pre-anodization and covalent immobilization techniques with cross-linking agents. The redox peak has a formal potential of -0.44 V, close to the standard electrode potential of GOX (*Yang et al, 2008; Kang et al, 2009*), and this electrochemical response is due to the direct electron transfer for the reaction of the FAD/$FADH_2$ happening in the immobilized GOX (*Yang et al, 2008; Cai & Chen, 2004; Wang et al, 2002*).

ii. Through FT-IR we were able to demonstrate GOX immobilization, due to the presence of the Amide I and amide II bands which is accepted as indicative of enzymatic activity and has been used to monitor the GOX characteristics after immobilization.

iii. The spectrum of C(1s) and N(1s) found in studies conducted through XPS, allows us to demonstrate the presence of glucose oxidase enzyme, immobilized in our electrode PA-PPE-GOX, which goes according to what is described in the literature *(Boyd et al, 1995; Li et al, 1998; Bhattacharyya et al, 1998; Libertino et al, 2007; Libertino et al, 2008; Ni et al, 2008).*

iv. The direct electron transfer, K_s 3.363 s^{-1} is much higher than previous studies from carbon nanostructured materials (*Janegitz et al, 2011; Kang et al, 2009; Hua & Wang, 2012; Razmi & Mohammad-Rezaei, 2013*), gold nanoparticle incorporate matrices (*Wu & Hu, 2007; Zhang et al, 2011*), and comparable with SPCE-Nafion® film (*Yang et al, 2008*), with a rapid detection time less than 10 sec.

v. The surface average concentration of electroactive GOX ***(Γ)*** value was calculated Γ = 8.30013 e-9 mol/cm^2, means that the higher heterogeneous direct electron transfer rate constant is directly influenced by the multilayer coverage of GOX.

vi. The PA-PPE-GOX exhibits higher current response, 2.612 times, comparable with Graphene Oxide (GO) modified electrodes.

vii. PA-PPE-GOX has a higher affinity for glucose, K_m 0.03 mM, with a wide range to detect glucose from 5 mg/dL to 900 mg/dL as well as low detection limit of 1.8 ug/5μL, which involved the glucose human range of measurements of diabetes variability in both hypoglycemic and hyperglycemic states. A lower value of the K_m suggests that immobilized GOX maintains enzymatic activity and displays an outstanding attraction to glucose. The linearity of the Glucose concentrations range for precision evaluations in the human glucose range is between 30 mg/dL through 400 mg/dL. Our PA-PPE-GOX-glucose biosensor meet both recommendations addressed by the FDA and to be used for SMBG, to minimize hypoglycemia state and maximize the euglycemia. “Blood glucose monitoring systems (BGMSs) intended for prescription-use in the hospital setting should be able to measure blood glucose accurately down to 10 mg/dL and up to 500 mg/dL, or a clinical justification should be provided for alternate measuring ranges and BGMSs intended for use outside of a hospital setting, and which will not reasonably be used to test neonatal samples, should be able to measure blood glucose accurately down to 20 mg/dL”

(*FDA, 2016*), and "To meet the clinical needs of the user population, Self-Monitoring Blood Glucose, should minimally be able to measure blood glucose accurately between 50 mg/dL and 400 mg/dL, or a clinical justification should be provided for alternate measuring ranges" (*FDA, 2018*).

viii. Calibration experiments of the PA-PPE-GOX-Glu. biosensor showed good performance to identified glucose at different concentrations with a sensitivity of 60.8723 $\mu AmM^{-1}cm^{-2}$ (SE 1.544, CV% 1.336) calculated as the current density (current/area) and plotted against the concentration, higher than *Zhang et al, 2011* (16.6 $\mu AmM^{-1}cm^{-2}$); *Unnikrishnan et al, 2013* (1.85 $\mu AmM^{-1}cm^{-2}$*); Razmi & Mohammad-Rezaei, 2013* (0.085 $\mu A\mu M^{-1}cm^{-2}$).

ix. In order to review the reproducibility, 4 electrodes were tested for a period of 3 months, two times for the first and second month, and once on the third month. The PA-PPE-GOX-Glucose showed an error percent of 3.76%, which means they have good reproducibility after 90 days, and showing that the electrodes have good shelf life, reproducibility and stability.

x. The validation for the electrode, PA-PPE-GOX towards glucose, was carried out through the analytical recovery experiments, which were performed with different samples of whole blood and the percentage of recovery was calculated from the data (calculated value of glucose, original concentration or spiked concentration) x 100. The values are (94%, 90% and 101%) e-Average of 95%. GOX have specificity for glucose, but due to complex systems of substances found in the blood, GOX is not completely specific for glucose, that means we need to work with this kind of variable to improve the sensitivity and chemical stability of the biosensor.

xi. By analyzing the interfering species, which represent a higher concentration (0.1M) than the concentrations in total blood and the calculated current ratio found between the glucose and the interfering species, allows us to infer that the biosensor shows a great affinity for glucose.

Therefore, the minimum current response obtained for the interfering species, suggests that the biosensor has a higher selectivity and specificity towards glucose.

3. 3. Conclusions.

Our electrode (PPE-PA-GOX-Glucose), showed good stability and selectivity in a physiology range of pH and temperature, and by the negative operating potential eliminates the interference from ascorbic acid, salicylic acid, lactic acid, uric acid, and dopamine.

We characterize the biosensor (PA-PPE-GOX-Glucose) through the FT-IR and XPS studies to demonstrate the immobilization of the enzyme GOX.

Excellent electrochemical reversibility, high stability, reproducibility, technically simple and possibility of preparation at short period of time are of great advantages of this glucose biosensor. The amperometric biosensor has feasibility, portability and low costs and offers new possibilities for the development of portable and customized equipment for better glucose control.

The biosensor meets addressed recommendations for the FDA to use in both, blood glucose monitoring systems (BGMSs) and self-monitoring blood glucose (SMBG), due to its wide range of values (5 mg/dL to 900 mg/dL).

The biosensor has the ability to distinguish between glucose and interfering species, high selectivity and specificity.

Our next step as future work, is conducting a clinical field research, and analyze each of these previous aspects, to obtain a stronger biosensor electrode to handle diabetic patients, and to have a better SMBG and BMGSs. The glucose variability, (hypoglycemic and hyperglycemic states), has a poor glycemic control and has an increased risk for complications, such as diabetic retinopathy prolonged hospital admission and mortality (*Mendez et al, 2013; Nathan D., 2014*).

CHAPTER 4. EXPERIMENTAL AND DISCUSSION FOR GLYCATED HEMOGLOBIN (HbA_{1c}.) ELECTRODE

4. 1 Materials and methods.

4. 1.1. Materials.

A Human blood hemolysate as lyophilized glycated hemoglobin (HbA1c) reference, RM 405 (lyophilized form to about 0.5 ml of a solution of hemolysate of human erythrocytes with a substance concentration of total hemoglobin of 0.23 mmol/L(15g/L.); 1-ethyl-3(3-dimethylaminopropyl) carbodiimide hydrochloride (EDC) (CAS 25952-53-8) reagent; N-hydroxysuccinimide (NHS) (CAS 106627-54-7) reagent; Ru (NH_3) Cl_2 (hexaaminеruthenium III chloride) 98% (CAS 14282-91-8) reagent and phosphate buffered saline (PBS) 10X concentrate (CAS 7558-79-4) with a pH 7.2-7.6 at 25^{o}C, were all purchased from Sigma Aldrich Co and used as received.

Amino-phenyl-boronic acid (APBA) 98% (CAS 30418-59-8) power reagent was purchased from VWR International Alfa Aesar.

Fresh human whole blood purchased from Interstate blood Zen Bio. Inc.

Ag/AgCl ink, surface resistivity <75mΩ/square/mil and viscosity 5,570-14,600 CPS; Carbon ink 79% C-220 carbon resistive ink make by Conductive Compounds, with a surface resistivity 10.68 W/Sq. and viscosity at 25^o C. 43,050 CPS and oxygen 20% was purchased from Graphene Laboratories (Calverton, NY.).

Deionized water (>18MΩcm) was obtained from a Millipore purification system (Biomedical Solutions Inc. Bedford, MA.), to prepare all aqueous solution.

Hydrogen peroxidase (H_2O_2) 30 wt.% solution (CAS 772-84-1) oxidizing agent and potassium ferricyanide [$K_3Fe\ (CN)_6$] power reagent (CAS 13746-66-2) was purchased from Lab Chem Fisher.

SU-8 50 negative tone photoresist formulation 50, with a thickness of 50 mms as purchased from Micro-Chem, Newton. MA.

Chromatographic paper Whatman 1 chr. 1030-025, grade 3MM, from Tish scientific, cellulose, with a thickness of 0.34mm and diameter 25 mm.

4. 1. 2. Solutions preparation.

The phosphate buffer solution (PBS) 0.01 M with a pH 7.4 was used in all studies, it is made for dissolved 1 tablet of PBS compound from Sigma Aldrich Co., in 200 ml of deionized water at 25^{o}C.

The EDC/NHS (0.35M/0.1M) solution was prepared as follow: 0.0033 g of EDC plus 0.0012 g of NHS dissolved in 50 mL of deionized water and keep the solution at 4^{o}C.

The 5mM potassium ferricyanide solution was prepared passing chloride through a solution of potassium ferrocyanide as dissolving $K_3Fe\ (CN)_6$ 0.0164 g in 10 mL of deionized water and 0.074g of KCl in 10 mL of deionized water, keep at room temperature (25^{o}C).

The 5 mM hexaaminеruthenium chloride solution $Ru\ (NH_3)_6\ Cl_2$, which was prepared as: 0.0154g of $Ru\ (NH_3)_6\ Cl_2$ dissolved in a 0.1 M of KCl (0.074 g KCl in 10 mL of deionized water, and later the solution was put in N_2 x 30 min. and keep at 4^{o}C.

The 10 mM APBA solution was prepared as follow: 0.0136 g of APBA 98% power dissolved in 10 mL of 0.01 M PBS keep at 4^{o}C.

The glycated hemoglobin was reconstituted lyophilized HbA_{1c} and with hemolyzing reagents. A volume of 1 mL of deionized water was added to the lyophilized HbA_{1c} to reconstitute, allow standing for 15 minutes at room temperature, mixed gently and then stored at 4ºC. The reconstituted RM 405 was diluted with (26mM NaH_2PO_4/ 10 mL, + 7.4 mM Na_2HPO_4/ 10 mL) 0.5 mL + 0.5 ml of 13.5 mM KCN) hemolyzing reagent, the final concentration of HbA_{1c} was obtained to be a 6.25% in a 0.23 mM hemoglobin solution.

The 5mM H_2O_2 solution was prepared as follow: 0.0025 ml of H_2O_2 30% dissolved in 5 ml of 0.01M PBS and keep at 4ºC.

4. 1. 3. Specific surface area

The specific surface area the sample was calculated using the Brunauer, Emmett and Teller (BET) surface adsorption method and theory, through the accelerated surface area and porosimetry system (ASAP) 2020 Sorptometer made by Micromeritics, by measuring N_2 adsorption on the surface of the sample. The sample was degassed at 150ºC for 70 min at 10 mm Hg, in order to remove any remaining solvent and ensure complete dryness and emptiness of the pores. After this result of the amount of adsorbed N_2 at a bath temperature of 76 K were obtained.

4. 1. 4 Electrochemical measurements.

Voltammetry measurements CV, CA were carried out with a CH Instrument (CHI 730E, Electrochemical Analyzer, Austin TX.) electrochemical workstation in a three-electrode cell assembly, at room temperature (25ºC), with electrodes which consists of the printed paper-carbon electrode (PPE) microfluidic device. All the PA-PPEs have a working electrode area of 0.03141

cm^2. We analyze and compare the results obtained with the different modified electrodes made, through CV and CA electrochemical techniques.

CV measurements were carried out at a different scan rates range 30 mV/s to 500 mV/s. We used different probes as 5 mM potassium ferricyanide, 5 mM hexamine ruthenium III chloride and 0.01 M PBS in PA-PPE-APBA and PA-PPE-APBA-HbA_{1c} biosensors, through direct electron transfer, to evaluated the electrochemical oxidation in order to demonstrate the presence of immobilized APBA and therefore the immobilization of APBA-HbA_{1c}. We also carried out experiments with modified electros such as PA-PPE-APBA-HbT y PA-PPE-APBA-HbA_{1c} with 0.01 M PBS and different concentrations of H_2O_2 to determine the best response obtained through H_2O_2. All the experiments were carried out at room temperature 25ºC, with different scan rate to find the best scan rate to the experiment.

CA experiments were carried out the PA-PPE-APBA-HbA1c electrodes with different % of concentrations of HbA_{1c}, range 0.0015% to 6.25%, different scan rate, we select 0.100 V/s as the best option scan rate and 0.55 V of potential, and at room temperature 25ºC.

4. 1. 5. Spectrometers measurements.

The FT-IR spectrum was recorded by using Spectrum 100 FT-IR Spectrometer, Perkin Elmer. Spectrum is Perkin Elmer's premier software package for collecting, viewing and processing FT-IR spectra., all the studies were testing at room temperature (25ºC). The optical module contains a Class II/2 Helium Neon (HeNe) laser, with an achievable precision of ca 0.008 cm^{-1}, which emits visible, continuous wave radiation at a wavelength of 633 nm and has a maximum output power of 1 mW, reduces signal artifacts and improves response linearity, high-quality, low-angle, off-axis optics minimize aberrations and provide the highest optical efficiency. Different electrodes 5

each, were prepared to carry out the experiments to compare and analyze the results through the PA-PPE-APBA, PA-PPE-APBA-HbT and PA-PPE-APBA-HbA_{1c} biosensors. The electrodes used was prepared according to details showed in the next two sections.

4. 1. 6. X-ray photoelectron spectroscopy studies.

The XPS analysis were carried out with a PHI 5600 spectrometer with a hemispherical energy analyzer, using an aluminum (Kα) source of 1487 eV at 100 Watts. The sample was maintained at high vacuum. The pressure in the analysis chamber during XPS analysis was in the low range of 10^{-9} Torr. All spectra were recorded at 54º take-off angle, the analyzed area being currently about 1 mm^2. All spectra were recorded with 1.0 eV step, 10 cycles, 20 sweeps and corrected using carbon signal (C1s) at 284.5 eV. XPS spectra were analyzed using casa-XPS software version 2.3.18. The Shirley method was used for extracting the background necessary for curve fitting.

4. 1. 7. Fabrication of paper electrodes.

The PPEs were designed through the adobe illustrator graphic design software and were subsequently manufactured using the template printing technique. A template print mask with the electrode pattern was created by means of low-adhesion laser-cut films with an internal Zing 16 laser cutter (Epilog, Golden, CO). The prepared electrode patterns were placed on the SU-8 2010 photographic resistance treated chromatographic paper, which was previously prepared using the photolithography technique. SU-8 epoxy-based is a negative photoresist, and negative refers to a photoresist whereby the parts exposed to UV rays crosslink and needs to bake again after UV exposure to complete the polymerization. The photolithography technique consists in: applied SU-8 photoresist over the chromatography paper; baked in a hot plate for 20 min at 135ºC; a selectively

polymerization with UV (350-400 nm) exposure at 100% for 20 sec. using a mask 0.7 cm diameter that show the design area, in black ink printed, to generate a hydrophobic and hydrophilic areas; transfer the chromatography paper to the hot plate por 5 min at 135ºC and later developed with acetone and isopropyl alcohol at 70%. Them left to dry at room temperature x 20 min. See figure 4.1.

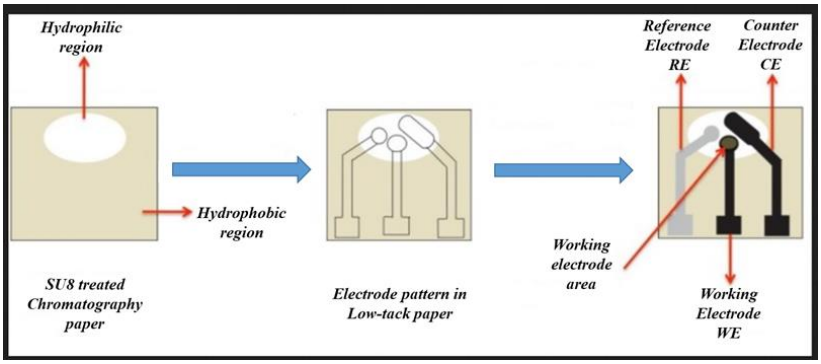

Figure 4.1. Design showing the process of making the disposable paper electrode (pictures not drawn to scale).

The conductive carbon ink paste was careful impregnated into the electrode patterns to make 2 of the 3-electrode system consisting of a: carbon-based counter electrode (CE), a carbon-based working electrode (WE) with a surface area of 0.03141 cm^2 and a conductive Ag/AgCl ink-based pseudo-reference electrode (RE) as a 3er electrode system, see fig. 4.1. and fig. 4.2. After each step, following the application of carbon ink to the two electrodes WE and CE, and next the Ag/AgCl ink over RE, the PPE were backed at 95ºC for 25 min in an oven *(Dungchai et al, 2009; Martinez et al, 2010; Nie et al, 2010; Lan et al, 2013; Liu et al,2014*).

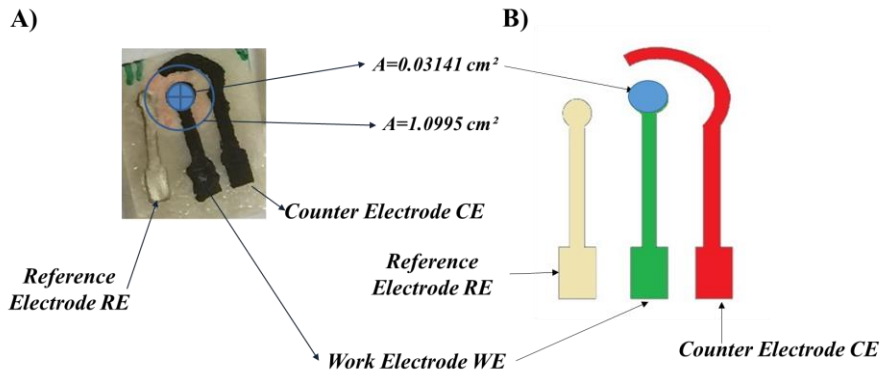

Figure 4.2. (A) Digital photo image of the PPE. (B) the electric circuitry for the electrode, (picture not drawn to scale). The circuitry consisted of working electrode (WE), counter electrode (CE), and reference electrode (RE).

4. 1. 8. Fabrication of modified electrode.

After the PPE has been prepared, then the pre-anodization process is done by applying a potential at 2.0 V, through the ***i-t*** electrochemical technique method, over working electrode vs Ag/AgCl counter electrode, for 300 s., placing the PPP in a beaker which contained a pH 7.4 PBS. With a pre-anodized time of 300 s. the ratio between O_{1s} and C_{1s} (O_{1s}/C_{1s} ratio) has more changes and as well as create more carbonyl-groups functionalities (*Evans et al, 1979; Notsu et al, 1999*). The pre-anodization method create more edge plane sites and can make the modified carbon electrode (CE) more electroactive, but also provides low susceptibility to electrode fouling (*Prasad et al, 2007; Yang et al, 2008; Prasad et al, 2008; Thiyagarajan et al, 2014*). The next step was add the EDC/NHS (0.35M/0.1M) solution, which was prepared with 0.0033g of EDC and 0.0012g of NHS and dissolved in 50 mL of deionized water, and drop coated 5 mL over the WE at the PA-PPE and left for 30 min at room temperature (25^{o}C), after that, the excess was removed and washed with 0.01 M PBS 1 μL. Then APBA was coupled through EDC and NHS cross-linkers and immobilized in the PPE. The 10 mM APBA solution was prepared by dissolving 0.0136 g of APBA 95% power in 10 mL 0.01M PBS and drop coated 5 μL on to EDC/NHS activated PA-PPE. The electrodes

(PA-PPE-APBA) were then dried at room temperature (25°C) for 2h, and subsequently washed with 0.01M PBS 1 µL to remove unbounded APBA. The $HgbA_{1c}$ solution was reconstituted lyophilized HbA1c and with hemolyzing reagents. 5 µL of HbA1c was added to the working electrode and left dry four 1 hour at 4°C. Then washed with 1 ml of 0.01 M PBS to removed unbounded HbA_{1c} and evaluated with electrochemical experiments. The PA-PPE-APBA-HbT biosensors was prepared adding an aliquoted the sample of Hb with 100 µL of deionized water and drop 5 µL over the modified electrode, left at 4°C x 1 hour. Then washed with 1 µL of 0.01M PBS. The figures 4. 3 show the schematic diagram and the representation for the full process done to prepare and tested the modified electrode.

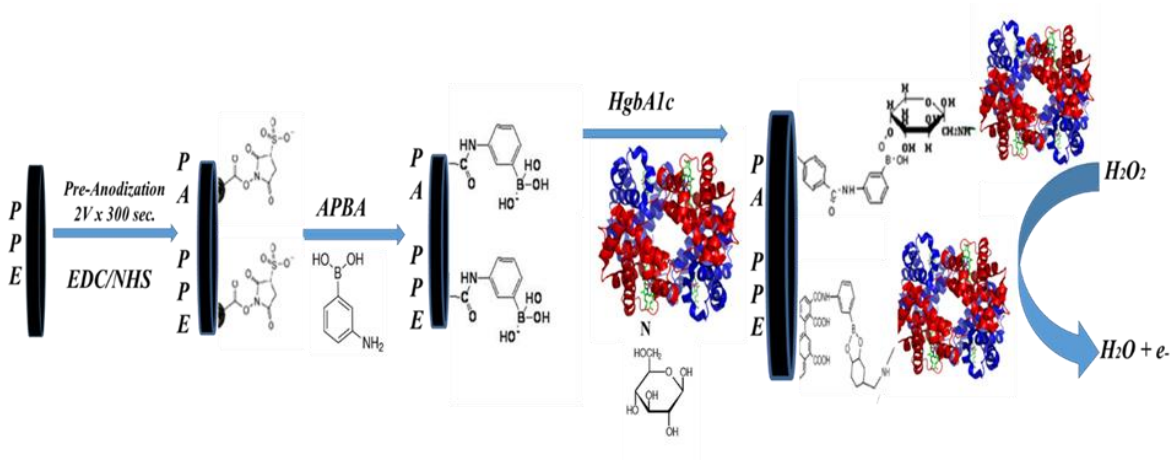

Figure 4.3. Design of the PA-PPE-APBA-$HgbA_{1c}$ electrode showing the different steps to immobilization of HgbA1c and the catalytic reaction with H_2O_2.

4. 2 Results and discussion

4. 2. 1. Specific surface area

The BET surface area report shows a 5.07 m^2 of are per gram of the material. The geometric surface area for the working electrode is 0.03141 cm^2. The Braunauer-Emmett-Teller *(BET*)

surface area is 12.675 cm^2/g with a pore size of 92.607 Å and pore volume of 0.016736 cm^3/g. (*Brunauer et al. 1938*).

4. 2. 2. Pre-anodization technique

The pre-anodization as a cleaning technique and performed as a pretreatment, the carbon electrode is cleaned and exposed to the application of a potential, and the functional groups are formed on the surface as a multiple edge plane formation. The fig. 4.4 shows the electrochemical oxidation process that happens when a positive potential (2V) is applied versus time (300 s). The current or the flow of electrons going from the solution to the electrode and produces an anodic (oxidation) current.

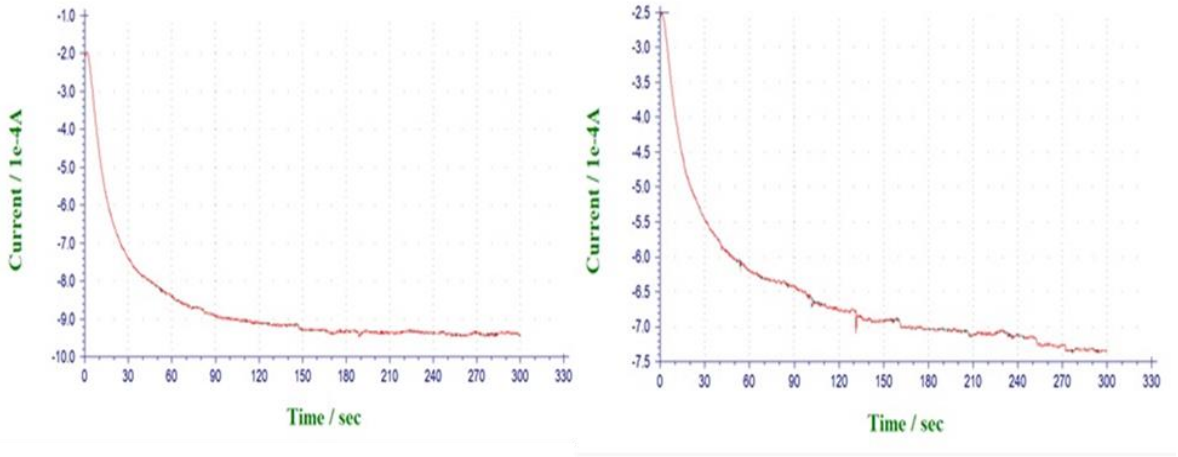

Figure 4.4. Pre-anodization (PA) graphic.

4. 2. 3. Surface characterization of PA-PPE-APBA and PA-PPE-APBA-HbA$_{1c}$.

***a.* Fourier transform infra-red (FT-IR).**

To characterize the electrodes, we compared the Fourier transform infra-red (FT-IR) spectrum between APBA and the APBA-HbA1c, through the PA-PPE-APBA and PA-PPE-APBA-HbA$_{1c}$ electrodes, to show the differences that occur when the HbA$_{1c}$ bound APBA and is immobilized. Also, we compared the FTIR for PA-PPE-APBA-HbT and PA-PPE-APBA-HbA$_{1c}$.

I. The FT-IR spectrum of APBA (Fig. 4.5. A) found exhibits basically two peaks with additionally peaks as characterization associated:

i. amide I band 1732 cm^{-1} peak (1659 - 1841 cm^{-1}) caused by ester bonds, C=O stretching vibrations in carboxylic acid and carbonyl moieties, 1740 cm^{-1} for C=O from carboxylic acids & carbony moieties (*Wang et al, 2013)*; 1452 cm^{-1} for C-N stretching (*Prasad et al, 2015)*; ester bonds at 1,730 cm^{-1} *(Xu et al, 2014*) and the wide band 1600 cm^{-1} to 1700 cm^{-1} identified C=O stretching vibrations of peptide linkages in the backbone.

ii. Amide band II 1456 cm^{-1} peak caused for combinations of N-H in a plane bending and C-N band stretching linkages, at 1457 cm^{-1} for the peptide groups (1490 cm^{-1} identified as the combination of N-H in-plane bending and C-N stretching of the peptide groups at 1442 cm^{-1}) *(Malesevic et al, 2008; Liang & Zhuobin, 2003).*

iii. Third peak, Amide band III on 1239 cm^{-1}, correlated with Delfino data's *(Delfino et al, 2013).*

iv. Fourth peak, B-O stretching vibrations at 1379 cm^{-1} (near 1,370 cm^{-1} broad asymmetric B-O stretching band (*Faniran & Shurvell,1968; Diao et al, 2012; Zhou et al,2014*).

Additionally, we founded:

v. Two wide bands in the region 3400 to 3300 cm^{-1} representing the amide A and B bond linkages to B-OH and NH stretching overlapped with O-H stretching vibration, and -CH$_3$ stretching at 3430

cm^{-1}, correlated with Wang, Xu and Prasad studies (*Wang et al, 2013; Xu et al, 2014; Prasad et al, 2015*).

vi. Sixth peak, characteristic (B–O) stretches at 1380 cm^{-1} and 1350 cm^{-1} and aromatic (B-OH) bending can be also observed at 1029 and 860 cm-^{1} after reaction, suggesting the successful amidation reaction of the anchored carboxyl groups with the amine groups of APBA, (a strong band at 1350 cm^{-1}, and weak absorption band at 850 cm^{-1} (*Faniran & Shurvell, 1968; Diao et al, 2012; Zhou et al, 2014; Wang et al, 2015*).

vii. Seventh peak, (C-O) stretching vibrations at 1239 cm^{-1} and 1158 cm^{-1} (assigned as vCO asymmetric at 1238 cm^{-1} and vCO symmetric at 1,149 cm^{-1} (*Faniran & Shurvell, 1968*).

vii. Eighth peak (C-H) stretching vibrations of phenyl ring at 2,958 cm^{-1} incorporated in the band corresponding to C-H stretching 2,950 cm^{-1} (*Xu et al, 2014; Gu et al, 2012*), for carboxylic acid groups at 2,800 to 3,050 cm^{-1} (*Diao et al, 2012)*.

II. The FT-IR spectrum for glycated hemoglobin (HbA_{1c}) Fig. 4.5. B, we found:

i. Amide I broad band 1588 to 1687 cm^{-1} which correspond to (C=O) stretching of protein amide groups, N-O stretch band for heme group bound NO 1700 to 1620 cm^{-1}, N-O stretch band for heme-bound near 1,617 cm^{-1} with two discrete N-O stretch bands near 1617 cm^{-1} for CI band and 1632 cm-1 for CII band; also will be found absorbance of the amide I band of a protein with α helix near 1656 +/- 2 cm^{-1} (~1654 cm^{-1}) and a protein with β sheet structure near between 1645 and 1632 cm^{-1} (~1633 cm^{-1}) (*Dong & Caughey, 1994; Barth, A. 2007*).

ii. A second broad band Amide II band 1,588 cm^{-1} to 1415 cm^{-1} for N-H bending vibration strongly coupled to CN stretching vibration of peptide groups of proteins (correlated due to an out-phase combination of N-H in plane bending and C-N stretching vibrations of peptide groups (*Dong & Caughey, 1994; Krimm & Bandekar, 1986*).

iii. A third peak 1156 cm-^{1} involved in a wide band O_2 bound to Fe^{+2} for C-O-H and C-O-C bonds ring vibrational mode of C-O-H and C-O-C bonds at 1170 cm^{-1} *(Dong & Caughey, 1994; Gunasekaran et al, 2010)*.

iv. Four wide band with particular variations and absorbance between 1978 cm^{-1} to 1825 cm^{-1} for C-O stretch band in the carbonyl spectrum at the heme bound C-O and cysteine band, also C-O stretch band for heme-bound CO at 1951 cm^{-1} and bisignate cysteine band at 1857 cm^{-1} (*Chen & Spiro, 2002*).

v. A fifth wide band between 3400 to 3050 cm^{-1} for Amide B band and Amide A band due to N-H stretching vibrations, -OH stretching documented by *Gunasekaran et al, 2010 and Prasad et al, 2015*. (3303cm^{-1} Amide-A band due to N-H stretching vibration and 3068 cm^{-1} Amide-B band due to overtone of Amide I band) (*Chen and Spiro, 2002*).

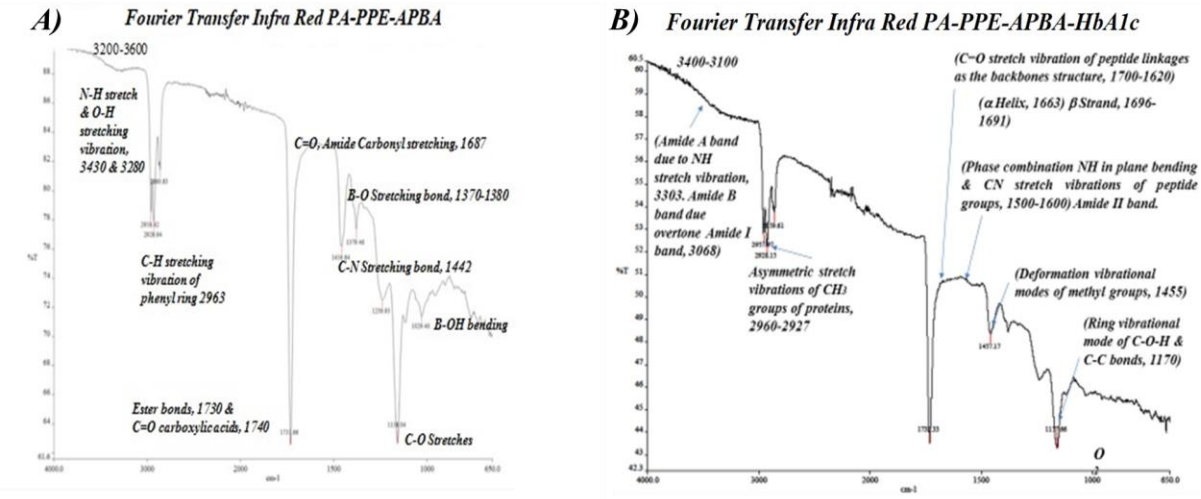

Figure 4.5. Fourier transfer infra-red (FT-IR) for PA-PPE-APBA (A) and FT-IR for PA-PPE-APBA-HbA1c (B).

The fig. 4.6. show the difference observed between the FTIR for PA-PPE-APBA-HbT and PA-PPE-APBA-HbA$_{1c}$. The amide I band between 1600 cm^{-1} to 1700 cm^{-1}, with their different C=O

stretching vibrations, and amide II band at 1565 cm^{-1} to 1462 cm^{-1} with the C-N stretch coupled to N-H bending, that correspond to the peptide groups, they provide information on the type of secondary structure, these types of vibrations are the α-helix, β-strands, and different kinds of turn structures as β-turns and β-antiparallel. The α-helix structure can be assigned in the rage of 1655 cm^{-1} and 1545 cm^{-1} with a strong feature close at 1550 cm-1 in amide II band, and the β–strands has been assigned in 1630 cm^{-1} and 1530 cm^{-1} bands. (*Goormaghtigh et al, 2006; Murphy et al, 2014; Alhazmi, H. 2019*). Human hemoglobin exhibits several exogenous ligands that include O_2, CO and NO bound to Fe^{2+} and CN^-, N_3, OCN^-, SCN^- and NO bound to Fe^{3+}. Positives and keys for identification Hb are N-O stretch band for heme-bound NO close to 1617 cm^{-1}, C=O stretching of protein amide groups close at 1700 cm^{-1} to 1620 cm^{-1}, C-N stretch ligand to HbA Fe^{3+}, four C-O stretch bands near 1969 cm-1 reflecting the interaction between the heme pocket with CO and the nature expression of the Fe-C bond (*Dong & Caughey, 1994*).

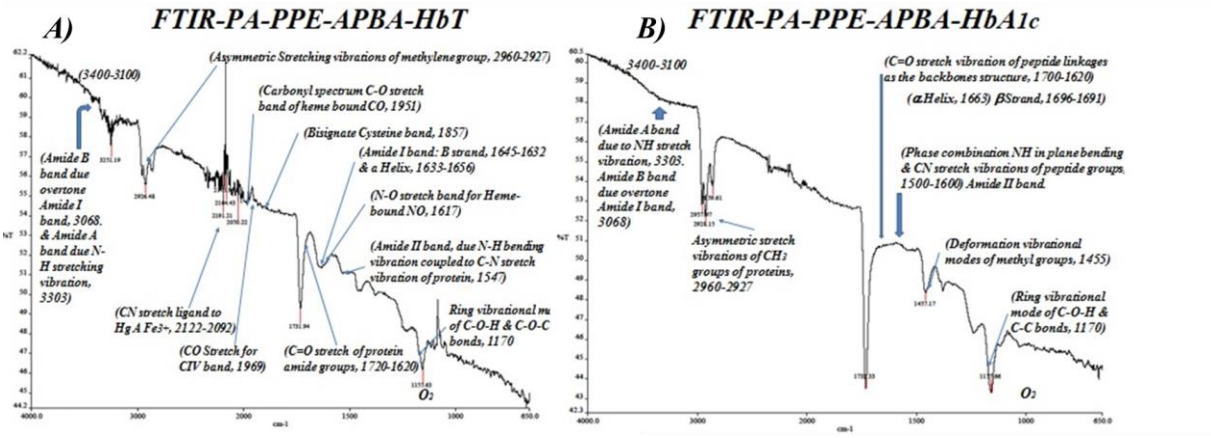

Figure 4.6. FT-IR for PA-PPE-APBA-HbT (A) and FT-IR for PA-PPE-APBA-HbA1c (B).

***b.* X-ray photoelectron spectroscopy (XPS).**

XPS studies were conducted to demonstrate the immobilization of APBA and of course APBA-HbA_{1c} in the biosensor. All our findings are in accordance with the revision of the literature, with greater emphasis on those works that support the objective of the study, the presence of APBA and APBA-HbA_{1c} in the biosensor. We will do a more in depth-analysis of the observations that match ours XPS findings of the different elements.

Boron

We compare sample No. 1 corresponding to the PA-PPE electrode, modified with EDC/NHS and sample 3 corresponding to modified PA-PPE-APBA biosensor. In both cases B(1s) shows several peaks centered between 186.7 eV to 192.5 eV (*Wang et al, 2015*). Sample 3 shows B(1s) core levels peaks at 188.1 eV (pure). 189.9 eV (B-C bond) (*Paul et al, 2012*). 190.5 eV (overlapping C-N and B-C bonds), these peaks correspond to phenylboronic acid binding (*Kim et al, 2007 and Mohapatra et al 2009).* B-$(OH)_2$ (*Wang et al in 2015).* 191.2 eV (overlapping C-B and B-O bonds), (*Ong & Huang, 2004; Kim & Shim, 2013; Fabre et al, 2017)*. 192.5 eV (B-O bond), (*Kim et al, 2007)*, see figure 4.7. F.

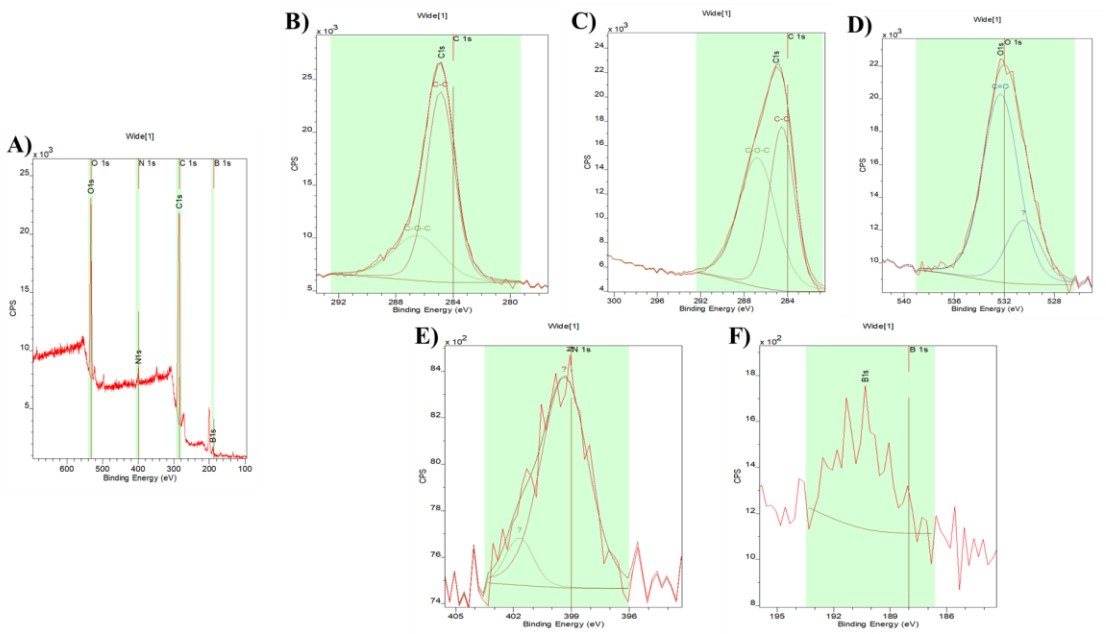

Figure 4.7. PA-PPE-APBA XPS studies showing the complete graphic for the elements funded (A), carbon, C(1s) core-level spectra (B) and (C), oxygen (D), nitrogen N(1s) core-level spectra (E) and boron (E).

Hendrickson et al,1970, found shifts of B(1s) the binding energy in 25 different compounds, with a range between 186.7 eV to 195.1 eV (Δ eV~8.4 eV). The binding energy for ρ-chlorobenzeneboronic acid was at 191.9 eV and that of ρ-mercaptophenylboronic acid was at 191.5 eV with a calculated CNDO of +0.498. *Carey et al, 1994*, working with acid ω-mercaptoalkylboronic found that the binding energy for B(1s) electrons was 192 eV. According to *Ong & Huang in 2004,* boron is usually oxidized as B_2O_3, with the B(1s) energy shifted to 190.5 eV as $E_{b,\ VBM}$ and 193.6 eV as $E_{b,\ FL}$, the peak located at 187.3 eV is assigned to the elemental boron and the peak at 191.2 eV corresponds to the (C-B) bond. These references allow us to assig the binding energy at 192.5 eV (C-B) relate to the presence of boronic acid.

Also, XPS studies conducted by *Kim et al in 2007* show three bands correlated with their binding energies for the B(1s) atom and their respective bonds, located in 189.6 eV as (B-C), 190.7 eV as B-N and 192.5 eV as (B-O) bond. They also analyze different B bonds with other atoms (C&N)

and identify, 283.5 eV (C-B bond) and 397.6 eV (N-B bond). *Barriet et al, 2007* in its analysis of the spectrum of B(1s) obtained a peak at 190.7 eV which can be assigned to different species of boronic phenyl acid in its trigonal sp^2 hybridization and *Mohapatra et al in 2009,* based on its analyses considers it possible that the union (OH^--boronic acid) to form a tetra-coordinated boron corresponds to the peak 190.04 eV as phenyboronic acid. Our changes obtained in the spectrum of B(1s) at 189.9 eV and 190.5 eV validate the presence of boronic acid configurations.

Other studies recently confirmed the existence of boronic acid in different binding energy bonds, which, confirm our findings in the biosensor. *Paul et al, 2012*, assigns the B(1s) spectra with three centered components and their respective bond, 193.0 eV as boron oxide (B-O), 191.6 eV as boron nitride (B-N), and 189.9 eV as boron carbide (B-C). *Kim & Shim, 2013,* found a peak in 191.2 eV in the B(1s) spectrum and identified it as a (C-B) bond. *Wang et al, 2015,* obtained a spectrum of B(1s) between 188.0 to 192 eV. *Fabre et al, 2017*, considers that the peak in the spectrum of union energy in 191.9 eV can be assigned to a (B-O) bond, attributable to boronic acid moieties.

Carbon

XPS studies for PA-PPE-APBA show basically a grand band for binding energy of C(1s) through 280 eV to 291.5 eV which different peaks. Carbon run 1, the data is fitted by a mix of pure C(1s), (C-C bond) and (C-O-C bond) in the proportions shown (figure 4.7.B & C). Pure C(1s) would peak at the vertical line at 284 eV overlapping the (C-B) bonds. Carbon, run 2, the data is fitted by a mix of pure C(1s), (C-C) and (C-O-C) bonds in the proportions shown see figure 4.7. B & C. The centered peak at 284.9 eV could be assigned to overlap (C-C) bond (*Kim et al, 2007*), pure carbon C1 bond *(Boyd et al, 1992)* and (C-N/C=N) bonds (*Wang et al, 2015).* The centered peak at 286.5 eV could be assigned to (C-O-C) bonds and [C≡N (N3)] bond (*Bhattacharyya et al, 1998*), and centered peak at 284.6 eV could be assigned to (C-O), overlapping (C-C/C-H) bonds (*Golczak*

et al, 2008, Mohapatra et al, 2009) and pure carbon C1 bonds (*Bhattacharyya et al, 1998*). See figure 4.7. B & C.

XPS studies for PA-PPE-APBA-HbA_{1c} show a grand band with different binding energy of C(1s), 279.5 eV to 291.5 eV. Carbon run 1, the data is fitted by a mix of pure C(1s), (C-C) and (C-O-C) in the proportions shown, see figure 4.8.B. Pure C(1s) would peak at 284 eV, show for the vertical line, and overlapping a (C-B bonds). Carbon run 2, the data is fitted by a mix of pure C(1s), (C-O) and (C-O-C) in the proportions shown, see figure 4.8.C. The centered peak at 284.6 eV could be assigned to (C-C) bond *(Kim et al, 2007; Mohapatra et al, 2009*). The centered peak at 284.4 eV could be assigned to (C-O) bonds and overlapping (C-C/C-H) bonds *(Golczak et al, 2008; Wang et al, 2015*). A centered peak at 286.9 eV could be assigned to overlapping (C-O-C), (C=O) and (C≡N) bonds *(Kim et al, 2007*), (C≡N) (N3) bond (*Bhattacharyya et al, 1998*) and (C=O/C-O) *(Golczak et al, 2008;Wang et al, 2015).* A peak at 287.7 eV overlapping C1 as sp3 (*Boyd et al, 1995),* (C-N) bond *(Bhattacharyya et al, 1998)* and the (C=O) bond, due to protein chains of the hemoglobin *(Wang et al, 2018*). Overlapped peak at 288.5 eV could be assigned to (C-O) bond *(Boyd et al, 1995*), (O-C=O bonds) as presence of (-COOH) groups (*Wu et al, 2001*), (-NH-CO-bond) (*Liu et al, 2009*) and (C-N and C-O bonds) (*Mohapatra et al, 2009*). See figure 4. 8. B & C and figure 4.9.

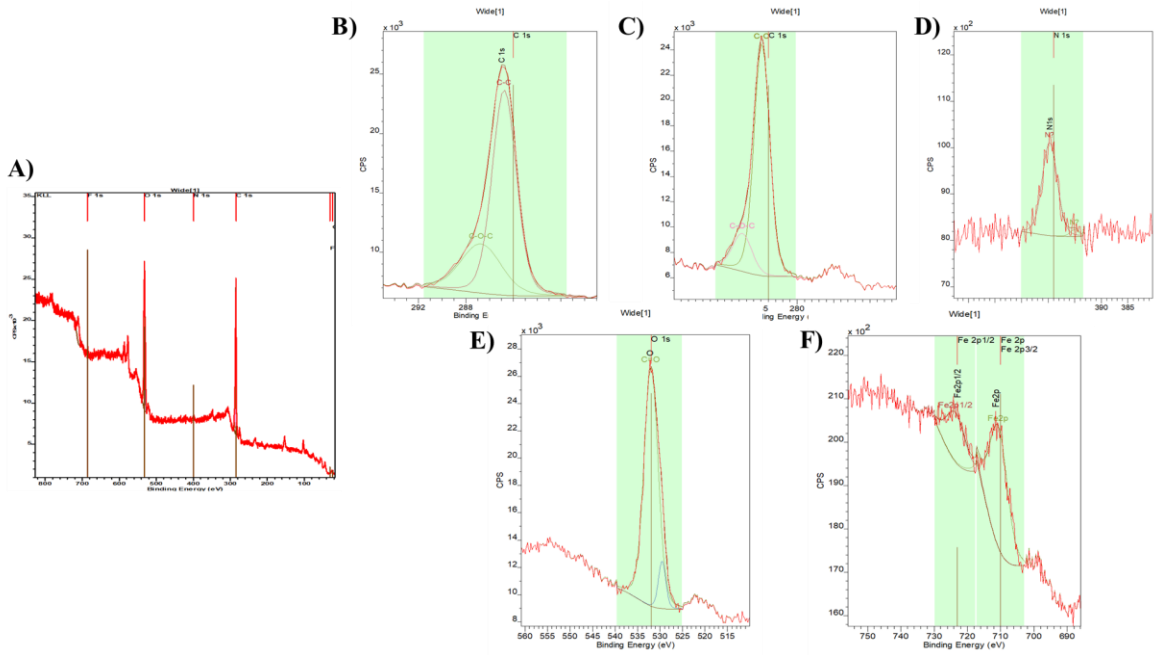

Figure 4.8. PA-PPE-APBA-HbA_{1c} XPS studies showing the complete graphic for the elements funded (A), carbon, C(1s) core-level spectra (B) and (C), nitrogen N(1s) core-level spectra (D), oxygen (E) and boron (F).

The spectrum of C(1s) and N(1s) represent a complex group of atoms that have multiple configurations due to their different bounds and overlap the binding energies. We analyze in more detail the works focused on validating our findings.

The following studies in XPS establish the carbon and nitrogen ratios at their spectral base and electronic properties in surface matrices, simple bonds of each atom and conjugated forms. *Boyd et al, 1995*, basically allocates the existence of four peaks by deconvolution of the spectrum of C(1s) and situate them according to their bonds, 288.3 eV (C-O bond), 287.7 eV (C^1) sp3 bonding, 285.9 eV (C^2) sp2 bonding and 284.6 eV (AC bond). The two middle binding energy they assigned as (C-N) bonding. We mentioned early five peaks at C(1s) core-level spectra were identified by *Bhattacharyya et al, 1998*, which were assigned to a respective binding energies (BE) located, 284.7 eV (pure carbon C1), 285.3 eV [C=N (C2) bond], 286.7 eV [C≡N (N3) bond], 287.7 eV [C-N (C4) bond] and 289.6 eV [C-O (C5) bond].

The following section analyzes the integration of C(1s), N(1s) and B(1s) into matrix structures with nanoparticles and confirm the presence of (C-B), (C-N), (C-C), (B-N), as part of the boronic acid and functional groups. XPS studies conducted by *Wu et al, 2001,* deconvolution the spectrum of C(1s) in four components and relate each binding energy to their respective bonds, 283.92 eV (C-C or C-H), 285.02 eV (C-N or C=N), 285.80 eV ($C-N^+$ or $C=N^+$) and 286.59 (C=O). Also, they found an extra higher binding energy level which was related with (O-C=O) bonds at 288.14 eV to 288.81 eV and they assigned to the presence of (-COOH) groups. *Kim et al in 2007,* found a broad band deconvoluted in three bands centered, 283.5 eV (C-B bond), 284.6 eV (C-C bond) and 286.3 eV (C-N bond) which, will incorporate other binding energies for (C=O and C≡N bonds). *Golczak et al, 2008,* found the same four components with some differences, 284.4 eV (C-C/C-H), 285.0 eV (C-N/C=N), 285.8 eV ($C-N^+/C=N^+$/C-Cl), and 286.72 eV (C=O/C-O) which it to be assigned to functional groups. *Liu, et al, 2009,* found a peak overlapping other peaks at 288.41 eV and identifies it as amide bond (-NH-CO-).

Studies conducted in XPS, in the next section, analyze and confirm the findings in the biosensor about the presence of boronic acid, C-O functional groups, and hemoglobin protein components. According a *Mohapatra et al, 2009,* the peak found at 284.6 eV represents the carbon and aromatic carbons that characterize the benzene ring of the imine. Also, they assigned the peak at 283.2 eV with the (C-B) bond, another two peaks, 285.86 eV (C=N bond) and 288.5 eV (C-O bond). They suggest that all these changes found are important evidence for the presence of boronic acid imine on the electrode surface. *Wang et al, 2015,* has found the same four components of the C(1s) spectrum and relates them to their respective bonds, 283.8 eV (C-B), 284.4 eV (C-C/C-H), 285.0 eV (C-N/C=N), 286.1 eV (C=O/C-O) and suggest that the C-O/C=O bonds correspond to the

functional groups. *Wang et al, 2018* suggest that one peak located at 287.6 eV assigned to the (C=O) bond could be attributed due to of the protein chains of Hb.

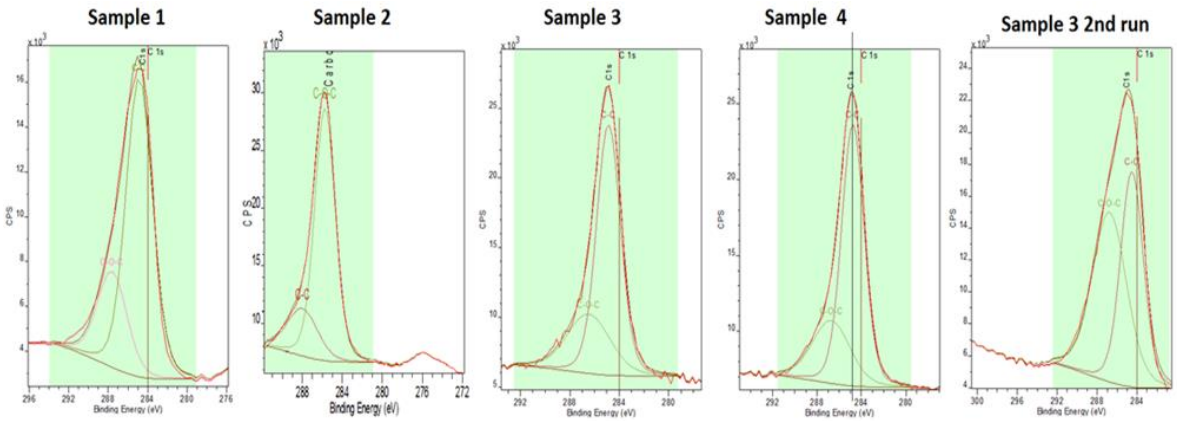

Figure 4.9. XPS studies for carbon. Sample 1 (PA-PPE), sample 2 (PA-PPE-GOX), sample 3 (PA-PPE-APBA), sample 4 (PA-PPE-APBA-HbA$_{1c}$).

Nitrogen

XPS studies for PA-PPE-APBA for the N(1s) core-level showed a grand band centered at 399.3 eV and another small band overlapping the first centered at 401.7 eV. Nitrogen it peaks at the right energy showing it is pure at 399.5 eV *(Baranton & Belanger, 2005)*, the rest correspond to mixtures of N (pure) and NO at 399.8 eV, see figure 4.7. D and figure 4. 10, sample 3. Other binding energies found, 399.3 eV could be assigned to (C-N) bonds and overlapped (C=N) bond (*Chan et al, 1992)* and 401.8 eV will be attributed to overlapping (C=N) bonds or (C-N) bonds and a pyrolic N bond *(Chakraborty et al, 2018).*

XPS studies for PA-PPE-APBA-HbA$_{1c}$, N(1s) peaks about 0.8 eV to the left, with a grand band starting at 393.4 eV and finish over 405.0 eV. Sample may contain different peaks located at different binding energy which can maybe overlap bounds. 398.3 eV which will be assign to the

overlapped N^1 bounds as (C-N) bond *(Boyd et al, 1995; Bhattacharyya et al, 1998)* or (C-NH_2) bond *(Dementjev et al, 2000*). 399.0 eV (overlapping C-NH_2 and C=N-C bonds) (*Dementjev et al, 2000; Kim et al, 2007)*. 399.5 eV [pure N(1s)] *(Kim & Shim et al, 2013),* (C=N bond) *(Chan et al, 1992),* amine nitrogens (-NH-) *(Wang et al, 2015)*. 400.1 eV overlapping (C-N bond) (*Chan et al, 1992*), (C=N bond) and N_2 in the N-C sp^2 binding energy *(Boyd et al, 1995*). 400.4 eV which it would assign to conversion of the amine group (NH_2) into an amine group (NH-CH) *(Song et al, 2009*). 402.4 eV (C-N^+ or N-O bond) and could be assigned to higher energies for the N-radicals *(Boyd et al 1995*). The peak at 400.1 eV as considered as (C-N) which could be assigned to the bonds from hemoglobin *(Chakraborty et al, 2018),* overlapping (C-N=N-C) bonds (*Baranton & Belanger, 2005)*. See figure 4.8. D. and figure 4. 10. sample 4.

We will review the complexity of interactions between C(1s) and N(1s) and analyze the basic structure of the nitrogen and its potential electronic interrelationship properties, through the following works done in XPS. *Chan et al in 1992,* determined four peaks for the N(1s) nucleus, for polymers, based on the increase in the positive charge for the nitrogen atom which causes an increase in the binding energy, and interpreted according to their bond, 399.4 eV (C=N bond), 400.2 eV (C-N bond), 401.2 eV (C=N^+ bond) and 402.5 eV (C-N^+ bond). XPS studies conducted by *Boyd et al in 1995,* they found that the binding energies are deconvoluted in three basic peaks which interpret as: N^2 assigned to the N-C(sp^2) bonding with an binding energy of 400.0 eV, N^1 attributed to the sp^3 bonding with an energy of 398.3 eV, and the N-O bond with an energy of 402.5 eV, which can be attributed to high-energy components for N-radicals.

The following section allows us to analyze the presence of organic molecules and combined structures of C(1s), N(1s) and B(1s) as an addendum to the previous carbon revisions. N(1s) spectrum studies conducted by *Bhattacharyya et al in 1998,* show that this compound of different binding energies, which were assigned to their respective bonds, 398.3 eV [C-N (N1)], 398.8 eV [C≡N (N2)] and 400.8 eV [NO (N4)], closing these binding energies for C(1s) and N(1s) for organic molecules. *Dementjev et al 2000,* assigned the binding energies for the peaks with the bonds, 398.5 eV (C-NH_2), 399.1 eV (C=N-C) and 400.7 eV (-NH_2 bond). *Baranton & Belanger, 2005,* found a peak at 399.5 eV and they considered these was por presence of the N-$(C_2H_5)_2$ substituent, another peak at 400.0 eV which assigned to a (C-N=N-C) linkage, in a DEA modified electrode. *Kim et al, 2007,* finds a band centered at 399 eV and performed a deconvolution, finding three centered peak at 397.6 eV (PN0) assigned to (N-B) bond, 398.6 eV (PN1) assigned to (N-C) structures (graphite-like N-C) and 400.7 eV (PN2) assigned to N atoms bonding to C atoms (pyridine-like N-C) structures.

The presence of boronic acid and the immobilization of APBA in our biosensor is validated by the following studies in XPS. *Song et al, 2009,* working on Dend-FPBA, found a peak at 400.2 eV which was assigned to the binding energy of the (NH_2) group, and they attributed this response due to the modification at electrode by the boronic acid, and the spectra changes in C(1s) and N(1s) due to the conversion of the amino group (NH_2) into a imine group (NHCH). *Kim & Shim in 2013,* showed through the N(1s) spectrum a different peak located at 399.4 eV after the APBA immobilization. *Wang et al in 2015,* through to the modified electrode to detect HbA_{1c}, found basically three peaks located, 398.8 eV assigned to the protonation of the imine nitrogens (=N-) as emeraldine state, 399.6 eV assigned to amine nitrogens (-NH-) as leucoemeraldine state and 401.1 eV assigned to the N^+ as to positively charged nitrogens:oxidized amine.

The following study allows us to validate the presence of hemoglobin in our biosensor. *Ummam et al, 2017*, working with a gold-nanoparticles modified boron-doped diamond (AuNPs-BDD) to detect hemoglobin found a peak at 400 eV which was attributed to (C-N bonds) from the hemoglobin. *Chakraborty et al, 2018* found a spectrum of the N(1s) which showed different peaks and related them to their respective bonds, 397.8 eV (pyridinic N), 398.8 eV (pyrolic N), 399.6 eV (N-Fe), 400.8 eV (quaternary N) and 401.8 eV (pyrolic N), signaling another peak at 400. eV as part of the hemoglobin spectrum.

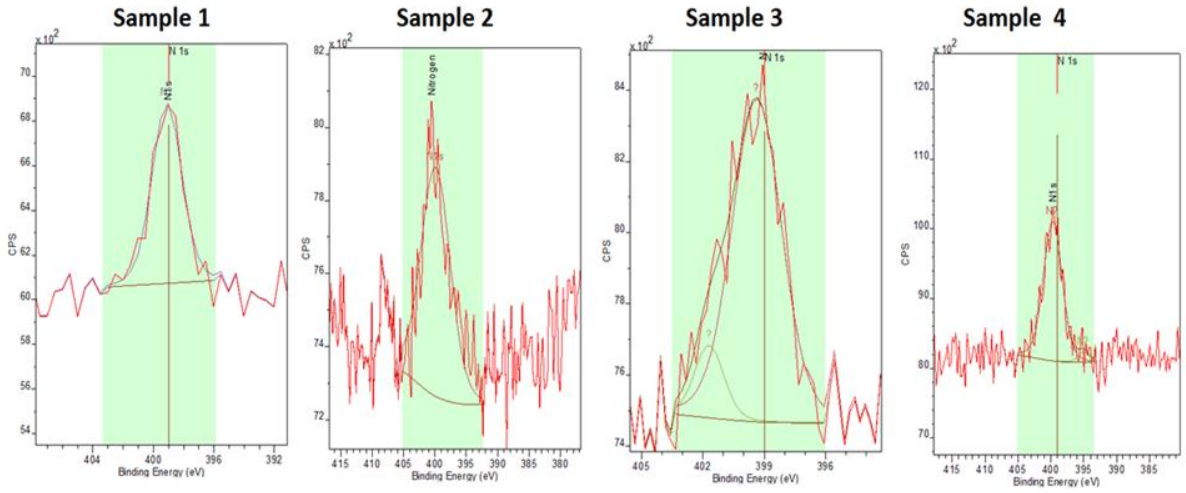

Figure 4. 10. XPS studies for nitrogen. Sample 1 (PA-PPE), sample 2 (PA-PPE-GOX), sample 3 (PA-PPE-APBA), sample 4 (PA-PPE-APBA-HbA_{1c}).

Oxygen

XPS studies for PA-PPE-APBA, sample 3, for the spectrum of O(1s) showed a grand band range 527.0 eV to 536.0 eV, with a centered peak 532.1 eV and 532.4 eV which could correspond to overlap (C=O and C-O bonds) which could be considered representative of the groups of boronic acid (*Barriet et al, 2007*). Another band centered at 530.4 eV which will assigned to overlap (Fe-O bond) (*Mohapatra et al, 2009*) and FeO_2 bonds. The sample at the correct energy for pure O(1s)

at 532.0 eV at the vertical line. The peak at 533.0 eV may have some (C-O-H) bonds and (B-O) bond (*Chan et al, 1992; Wu et al, 2001)*), see figure 4.7. D and figure 4.11.

XPS studies for PA-PPE-APBA-HbA1c, sample 4, had a band range starting in 526.0 eV and finishing at 538.5 eV for the O(1s) spectrum with a centered peak at 532.0 eV for a correct energy for pure O(1s) overlap (C=O and C-O bonds) (*Chan et al, 1992: Barriet et al, 2007*). Another centered peak at 529.0 eV overlapping (Fe-O) bonds (*Woo et al, 2001; Mohapatra et al, 2009*), a centered peak at 533.0 eV may it for some (C-O-H), (B-O) and (Fe-O-C) bonds (*Wu et al, 2001; Mohapatra et al, 2009; Song et al, 2009; Liu et al, 2011*). Notice that it may also contain (C-O bond) as they both peak at almost the same energy (532.3 eV) (*Chan et al, 1992*) and bonds for modification surface as Fe_2O_3 particles. Also, a centered peak at 531.0 eV (C=O bond) and the centered peak at 532.0 eV (C-O bond), due to C(1s) spectrum on the protein chains of Hb (*Wang et al, 2018*), see figure 4.7. E and 4.11

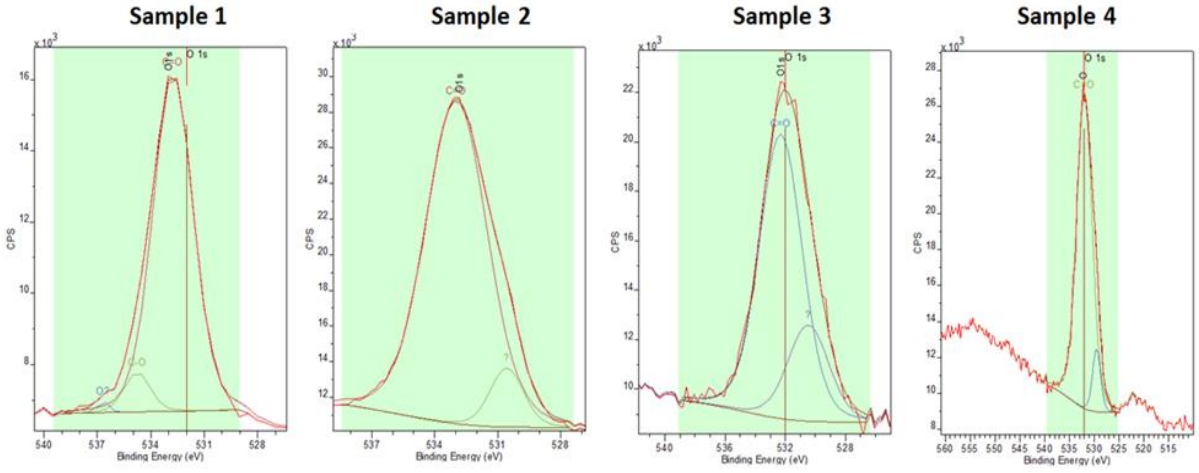

Figure 11. XPS studies for oxygen. Sample 1 (PA-PPE), sample 2 (PA-PPE-GOX), sample 3 (PA-PPE-APBA), sample 4 (PA-PPE-APBA-HbA_{1c}).

The O(1s) spectrum is a multifunctional complex which can have water and waste as part of its configurations, it is interesting to find the specific points and document the relationships with our biosensor. The spectra of O(1s) range in binding energy at 530.9 eV to 533.8 eV, in organic compounds according to *Beansom & Griggs, 1992.* In the range between 532.0 eV to 533.7 eV they found the more common organic species with oxygen as alcohols, esters, ketones, ethers and organic acids.

To understand the usefulness of the O(1s) in our reading we will review some works that analyze the structure and configurations of the oxygen as functionals groups. XPS studies conducted by *Chan et al in 1992,* in copolymers and PANA-HCl found that the O(1s) spectrum has three components, to different binding energy, which it was able to assign to their respective bond, 531.0 eV (C=O bond), 532.5 eV (C-O bond), 533.4 eV (H_2O) and they suggest that this results indicate a concurrent self-doping by the (-COOH) groups. *Woo et al 2001*, working with silane (Si) as a coupling agent between an interfacial interaction between a magnetic particle and a binder, found that the binding energy at 530.2 eV can be assigned to the (Fe-O) bond, as well as, found another peak for the O(1s) at 531.9 eV which it considers can be attributed to the (Si-O-Fe) bond. *Wu et al in 2001,* found similarity between O(1s) spectrum with small differences in the binding energies, which they compared with the studies of *Chan et al, 1992*. The O(1s) spectrum for copolymer and poly-diphenylamine (PDPA) films, was assigned to 531.68 eV (C=O bond), 532.63 eV (S-O bond) and 533.2 eV (O-H bond). They also, assigned another peak in the range at 532-49 eV to 533.75 eV, in copolymers, as (C-O) bond.

The following detailed studies support the presence of boronic acid, in our samples, through the O(1s) links with other atoms such as C(1s), B(1s), Fe(sp^2) and therefore the presence of glycated hemoglobin. *Barriet et al in 2007,* working with 4-mercaptophenylboronic acid (MPBA) and other

compounds containing boronic acid in its structure, found that the localized peak approximately at 532. eV shows that the samples have water, in addition they observe other peaks with binding energy at 531.2 eV and at 532.7 eV and could correspond to the (C=O) and (C-O bonds). They also argue that the peak at 532.2 eV is considered representative of the groups of the boronic acid. *Mohapatra et al, 2009,* found two peaks in the binding energy of the O(1s) spectra and was able to deconvolution in three peaks assigning to each peak with its respective bond: 530.5 eV (Fe-O bond), 531.5 eV (B-O bond) and 532.08 eV (Fe-O-C bond) which it to be attributed boronic acid functionalized iron oxide nanoparticles. *Song et al 2009,* found a peak on the spectrum of O(1s) at 533.31 eV, in a modified dendrimer layer 4-formyl-phenylboronic acid (Dend-FPBA) electrode to detect HbA_{1c}, which was assigned to the (B-O) bond by a modified-boronic acid. *Liu et al 2011,* working with 4-formyl-phenylboronic acid (FPBA) modified-electrode for determination of glycated hemoglobin found in the O(1s) spectrum a new peak at 533.31 eV which was assigned to the (B-O bond). *Wang et al in 2018*, working with Hb and Hb-polydopamine (Hb-PDA) nanoparticles, found two peaks in the O(1s) spectrum located at 531.0 eV and 532.0 eV, which was assigned to the (C=O) and (C-O) bonds, which indicated the presence of Hb-PDA at the surface.

Iron

XPS studies for iron (Fe) spectrum in PA-PPE-APBA-$HbA_{1c,}$ modified electrode, see figure 4. 8. F, showed a most likely pure and mixed with Fe bound to something else (peak is shifted by about 1.2 eV to lower energies). A band range 705.0 eV to 729.5 eV was found at the spectrum of Fe(1s). A centered peak at 710.0 eV which will be assigned to the Fe(2p) orbitals (Fe3O4) (*Mohapatra et al, 2009; Chakraborty et al 2018*). A peak at 710.4 eV which could correspond to (Fe-OOH)

bounds (*Grosvenor et al, 2004*). Overlapping between 710.0 eV and 710.3 eV one peak at 710.2 eV assigned to ($Fe_3O_4^{3+}$) which will be attribute to satellite structure for Fe (III) present and it will be like Fe (II) ($Fe2p_{1/2}$) (*McIntyre et al, 1977; Lin et al, 1997*). Peak at 709.8 eV [Fe(p2)] as (Fe-O) bond (*McIntyre et al, 1977; Grosvenor et al, 2004*). The centered peak at 721.5 eV could be assigned to satellite peaks to the Fe(2p) as the Fe (II) ($2p_{3/2}$) and Fe (III) ($2p_{3/2}$) states binding energies. An overlap centered peak at 726.5 eV for satellite Fe (III) ($2p_{1/2}$) y Fe (II) ($2p_{1/2}$) (*Lin et al, 1997).*

The following two sections review the multiple configurations of the Fe(sp2) spectrum, with their different ferric, Fe (II) and ferrous, Fe (III) states. *McIntyre & Zetaruk in 1977*, analyzed the spectrum of Fe(2p) and they found similarities between, 711.0 eV ± 0.15 [α-Fe_2O_3 ($Fe2p_{3/2}$)] with a satellite band at 719.0 eV [α-F_2O_3 (Fe2p)], predicted component of the Fe($2p_{1/2}$) line. 711.0 eV ± 0.2 [γ-Fe_2O_3 ($Fe2p_{3/2}$)] with the same intensity distribution but, it is reduced by 0.2 eV compared to (α-Fe_2O_3). Another peak at 709.5 ± 0.2 (Fe-O, Fe2p bond). *Lin et al in 1997*, found that the spectrum of Fe(2p) can have a range as wide as from 700 eV to 730 eV containing different peaks which will be correspond to the pure iron (Fe^0) state, doublets for both 709.3 eV [Fe (II)] and 711.6 eV [Fe (III)] states, a double line for the Fe (II) shake-up satellite, and a simple line for the Fe (III) state shake-up satellite. They found two shake-up satellite peaks, 714.5 eV [$Fe^{2+}(2p_{3/2})$], 719.0 eV [$Fe^{3+}(2p_{3/2})$] and two satellite peaks for, 723.3 eV [$Fe^{2+}(2p_{1/2})$], 724.7 eV [$Fe^{3+}(2p_{1/2})$].
Grosvenor et al in 2004, analyzed the spectra of $Fe^{3+}(2p_{3/2})$ and they found different oxide species and relating each with different peaks that vary in its binding energy around 3.2 eV as maximum to 2.5 as a minimum, 709.8 eV (ΔV=2.5 eV) (α-Fe_2O_3), 709.8 eV (ΔV=3.2 eV) (γ-Fe_2O_3), 710.2 eV (ΔV=3 eV) [α-FeO(OH)] and 710.3 eV (ΔV=3 eV) [γ-FeO(OH)]. *Biesinger et al in 2011*,

analyzes the Fe (II) and Fe (III) spectra finding similarities between the two spectrums compared to the different components for Fe (III) analyzed by *Grosvenor et al in 2004*. All Fe (II) exhibit a high spin with multiple peaks and low spin ones do not exhibit these peaks. Also, they found different components like Fe (III), which vary in their binding energy, with 6 peaks for each component, 709.8 eV-719.3 eV (α-Fe_2O_3), 709.8 eV–719.3 eV (γ-Fe_2O_3), 710.2 eV-719.8eV [α-FeO(OH)], 710.3 eV–719.5 eV (γ-Fe_2O_3) and another two, a single 706.6 eV [Fe(0)] and a multiple (5 peaks) binding energy, 708.4 eV-715.4 eV (FeO).

This last section reviews the works focus in validate the presence of boronic acid and glycated hemoglobin in the sample. *Mohapatra et al 2009,* working with the spectra the Fe(2p), found two binding energy at 710.0 eV and 725.0 eV which will be correspond to Fe_3O_4. *Chakraborty et al in 2018*, found a peak at 710 eV in the spectrum of Fe(2p), and they considered it to be the iron present in the blood dots (BD), in a divalent Fe (II) state, which confirm the precursor an iron-containing metalloprotein hemoglobin. The hemoglobin can be considered as biological Fenton catalyst, which degraded heme group. And they show that the spectrum of the hemoglobin had different peaks with correspond to binding energy, 285.0 eV assigned to the C(1s) core-level spectra, 400.0 eV assigned to the spectrum of N(1s), 532.0 eV assigned to the spectrum of O(1s) and 710.0 eV assigned to the spectrum of Fe (II).

The XPS detailed analyses the atoms of B(1s), C(1s), N(1s), O(1s) and Fe(2p) confirming the immobilization of APBA in our biosensor. This indicates the immobilization of HbA_{1c}, since this is done through the cis-diol bounds of the boronic acid to the glycosylated hemoglobin. We were also able to demonstrate the presence of hemoglobin, through the Fe(2p) atoms, which is an iron-containing oxygen-transport metalloprotein. The hemoglobin molecule contains 4 subunits of

globular protein attached to a heme group. The heme group contains an ion of Fe (II) inside a porphyrin ring, and this state facilitates the union of oxygen for transport. *Wang et al, 2018,* also, identified two peaks with the binding energy an theirs correspond bound, 283.0 eV (C-C bond) and 534.0 eV (C-O bond), and a third peak at 400 eV attributed to the C-N bonds that form hemoglobin.

4. 2. 4. Electrochemical characterization of PA-PPE-APBA-HbA1c.

Modified electrodes were used to demonstrate the immobilization of APBA, with different probes such as 5 mM potassium ferricyanide chloride, 5 mM hexamine ruthenium III chloride and 0.01 PBS through the CV tests. Studies were performed through CV with H_2O_2 y 0.01M PBS, and modified electrodes (PA-PPE-EDC/NHS-APBA and PA-PPE-EDC/NHS-APBA-HbA1c) to demonstrate the immobilization of HbA1c through APBA.

a. **Cyclic voltammetry (CV) analysis.** A pair of well-defined and nearly symmetric redox peaks can only be observed with a formal potential of -0.34 V to -0.65 V at the PA-PPE-APBA-HbA_{1c}, which result for redox process of the heme groups of HbA_{1c} captured on APBA, similar to reports *Kim & Shim, 2013*.

We compare the CV graphic for PA-PPE-APBA, which show an anionic probe-left side with increased current with 5 mM potassium ferricyanide chloride, and a cationic probe-right side with 5 mM hexamine-ruthenium III chloride which prove the APBA immobilization. Two different probes towards the same electrode, explain the electron transfer involved and interaction between electrodes (negative charge) and electrostatic interaction between electrode and probe molecules (specific potential for oxidation and reduction). The fig. 4.12.A show the CV for 5 mM potassium

ferricyanide chloride and fig. 4.12.B. show the CV for 5 mM hexamine ruthenium chloride over PA-PPE-APBA with different scan rate range 30 mV/s to 200 mV/s, probing the immobilization the APBA in the modified electrode.

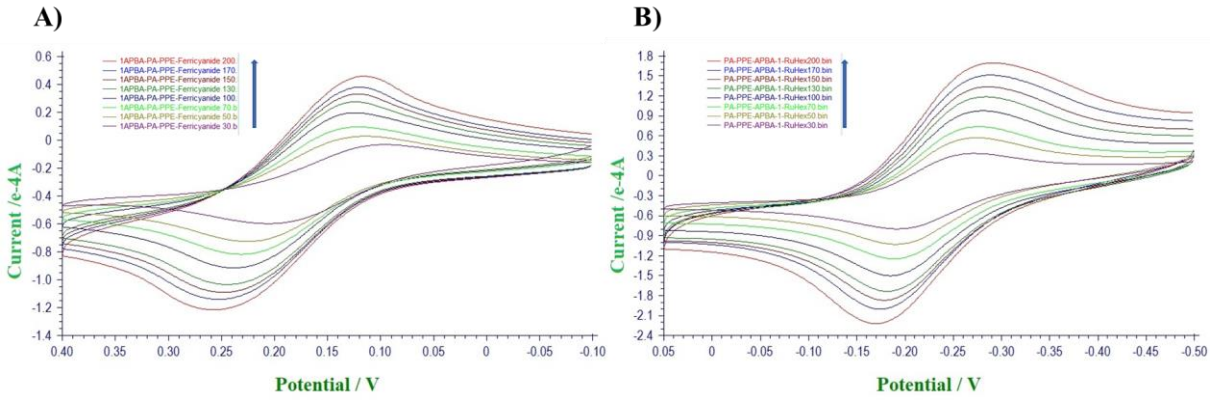

Figure 4.12. A. CV for PA-PPE-APBA with 5mM K-ferricyanide (anionic probe-left side) and B. 5mM ruthenium-hexamine chloride 5mM (cationic probe-right side) comparative.

The $HbA_{1}c$ was immobilized by PA-PPE-APBA through cis-diol interactions between the diol group of glucose of HbA_{1c} and the boronic acid group. Overall, the oxygen functionalities and edge plane-like sites formed at the PA-PPE play an important role in facilitating the electron transfer between the APBA-HbA_{1c} and electrode. The catalytic reduction peak of H_2O_2 by the immobilized HbA_{1c}, appeared around -0.31 V on the PA-PPE-APBA-HbA_{1c}, show in Fig. 4.13.A & 4.13.B, probe with 0.01 M PBS and H_2O_2 5 mM, at 0.100 V/s of scan rate, means that the catalytic process occurs and the reduction current of H_2O_2 increases when the concentration of H_2O_2 increases. The best results with different concentrations of HbA_{1c} was obtained in H_2O_2 of 5 mM. (SD: 0.0845, SE: 0.0378, R^2 of 0.997321).

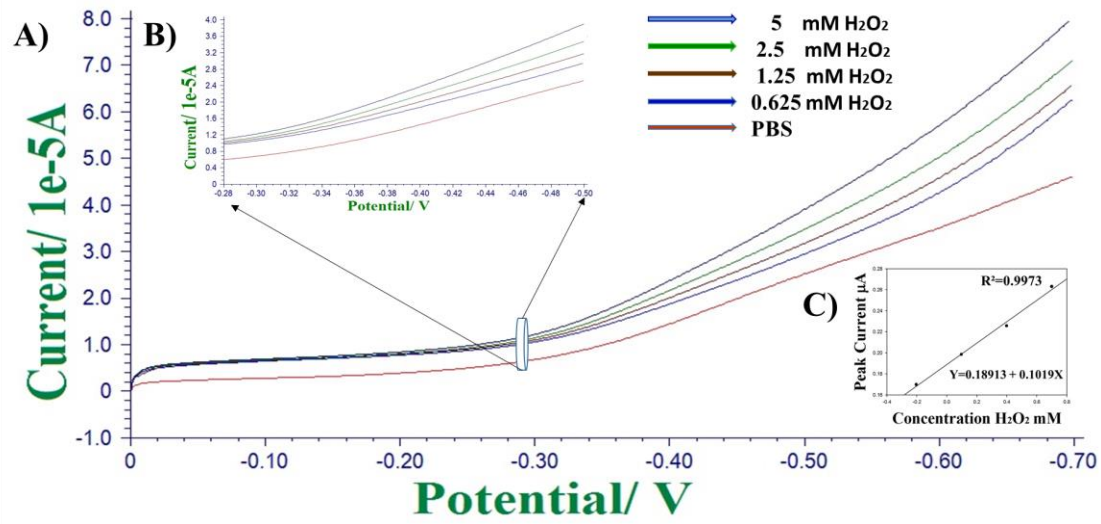

Figure 4.13. CV response of PA-PPE-HbA1c immobilized by APBA with different concentrations of H_2O_2.

We compare the catalytic reduction of Total Hemoglobin (HbT) and HbA_{1c} through (PA-PPE-APBA-HbT) and (PA-PPE-APBA-HbA_{1c}) electrodes, probes with 0.01 M of PBS and 5 mM H_2O_2 which was selected by showed the best activity. The peak in HbT is decreased compared to the HbA1c peak, with the two probes, because HbT do not have too much bounding groups and therefore show less reduction, see Fig. 4.14.A & 4.14.B.

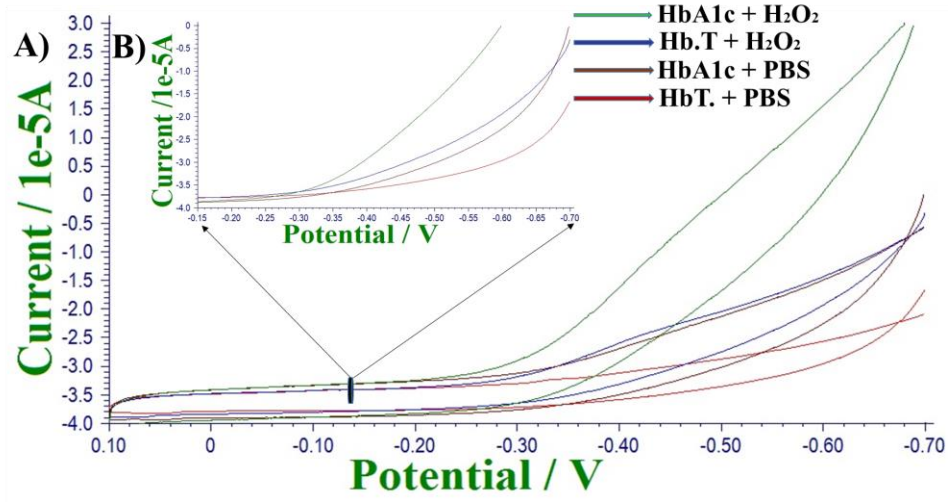

Figure 4.14. (A & B) CV response of PA-PPE-APBA-HbA1c and PA-PPE-APBA-HbT with 5mM H_2O_2 at a scan rate of 50 mV/s.

CV was analyzed for PA-PPE-APBA-HbA_{1c} at different scan rates ranged from 50 to 300 mV/s. We found a well-defined graphic for a redox process with an electroactive reduction and electroactive oxidation curves with two well-defined peaks, fig.4.15. A. The currents for the anodic and cathodic peaks have a good linearly relationship with the scan rate, see fig. 4.15.B. and the plot of logarithm between the log of peak current (i_p) versus log of scan rate ***(v),*** the relationship show a linear ***(log i_p (μA) = 0.7967 + 0.4629 log v***) proportionality suggested that the reaction, indicates a surface-diffusion controlled process, with a curve slopes of ***m= 0.4629*** as a transfer coefficient ***(a)*** (fig. 4.15.C) (SD: 0.1154, SE: 0.0483, R^2: 0.98854), it is thus expected that the PA-PPE-APBA-HbA_{1c} molecule does not extend gradually to an unfolded structure, and its behavior is very similar to voltammetric sensor developed by *Zhou et al, 2015*, based on phenylboronic acid-modified pyrroloquinolone (APBA-PPQ) and reduced graphene oxide.

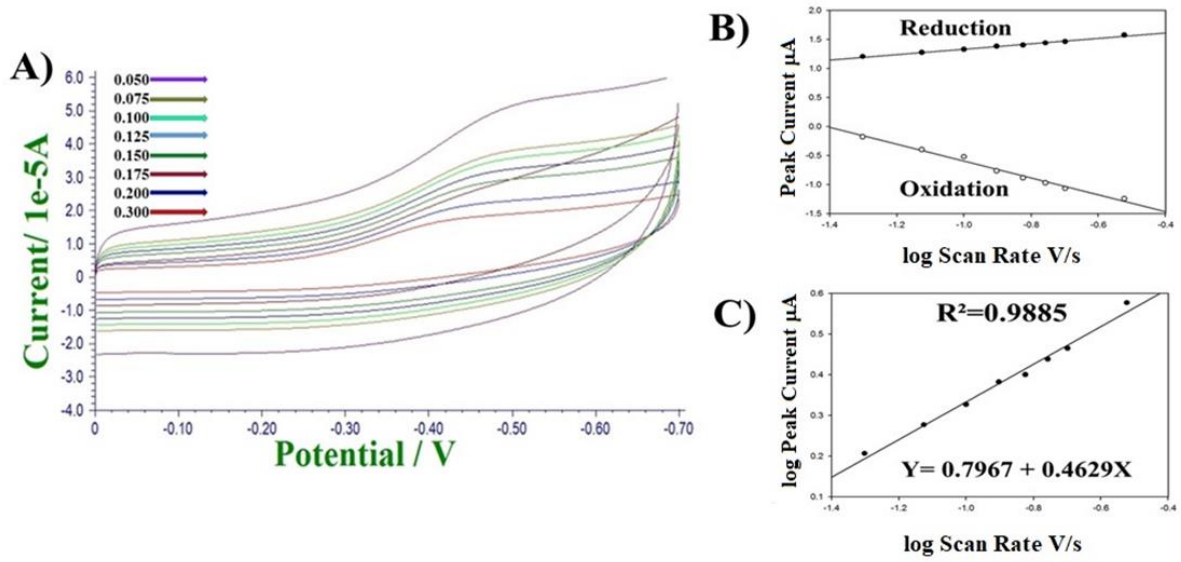

Figure 4.15. (A). CV response of PA-PPE immobilized with APBA-HbA_{1c} 3.125% in 0.01 M PBS at a scan rate of 50-300 mV/s, and (B), plots of anodic and cathodic peak current with scan rate, (C) show the plot of the log of scan rate (V/s) and log of peak current (μA), with linear relationship and slope of 0.4629.

The electron transfer constant, (K_s) for the PA-PPE-APBA-HbA1c biosensor was calculated with the Laviron equation ***($n\Delta Ep < 200$)*** *(Laviron, 1979):*

Equation 26: $K_s = (1-\alpha)\, nFv / RT$

Where a represent charge transfer coefficient (***$\alpha = 0.4629$***),

n is the transferred electrons number; ***F:*** Faraday constant 96,485.3321 $C.mol^{-1}$,

R is the Universal gas Constant, 8.1314 J mol^{-1} K^{-1},

T: Room temperature (298^o K), and

The ***$K_s = 4.277\ s^{-1}$.***

The surface average concentration (***Γ***) of electroactive APBA value, was calculated from the equation ***$\Gamma = Q/nFA$***, and ***Γ*** = 9.6416 e-9 mol/cm^2, which it is bigger than *Kim & Shim, 2013 (**Γ** =* 1.03 e-10 mol/cm^2), means that the higher heterogeneous direct electron transfer rate constant is directly influenced by the multilayer coverage of APBA. The ***(Γ)*** is bigger than Cobalt ferrite nanoparticles and chitosan film on the surface of glass carbon electrode biosensor to detect H_2O_2 based on direct electrochemistry of Hb (*Yang et al. 2011, **Γ**= 2.10e-11mol/cm^2).*

Different experiments of calibration conducted through CV on the PA-PPE-APBA-HbA_{1c} biosensor show good performance to identify glycated hemoglobin at different concentrations with a sensitivity of 208.9461 $\mu AmM^{-1}cm^{-2}$ (SE 0.2578) which, was calculated as the current density (current/area) and plotted against the concentration of HbA_{1c}.

b. **Chronoamperometry (CA) analysis**. We analyzed the CA response for the PA-PPE-APBA-HbA_{1c} because it is more sensitive and can reach lower and higher detection limits. The amperograms for the reduction of HbA_{1c} were recorded using the sensor probe in 0.01 M PBS (pH 7.4) and H_2O_2 5 mM containing different concentration of HbA_{1c}. Figure 4.16. shows the CA responses of HbA_{1c} reduction at different concentrations of HbA_{1c} at -0.55 V. As there is a

progressive increase in the concentration of HbA_{1c} immobilized, the current catalyst of HbA_{1c} concentration increases, therefore is an increase in the catalytic current of H_2O_2. HbA_{1c} specifically catalyzes the reduction of H_2O_2 (*Kim & Shim, 2013*). The figure 4.16.A and figure 4.16.B show the CA responses at different concentrations of HbA_{1c}, lower as 0.0015% through 6.25% higher and the fig. 4.16.C show the plot for log of peak current (1e-4A) and log of HbA_{1c}% concentrations. The analysis of plot fig. 4.8.C show (SD:0.2790; SE: 0.0659; and R^2: 0.9943) show that the biosensor-electrode PA-PPE-APBA-HbA_{1c} have high sensitivity, with a low detection limit as 4.54ng/5mL. The linearity of the glucose concentrations range for precision evaluations in the human range is between 30 mg/dL through 400 mg/dL and for HbA_{1c} 2.6 through 16.9% (*FDA, 2016).*

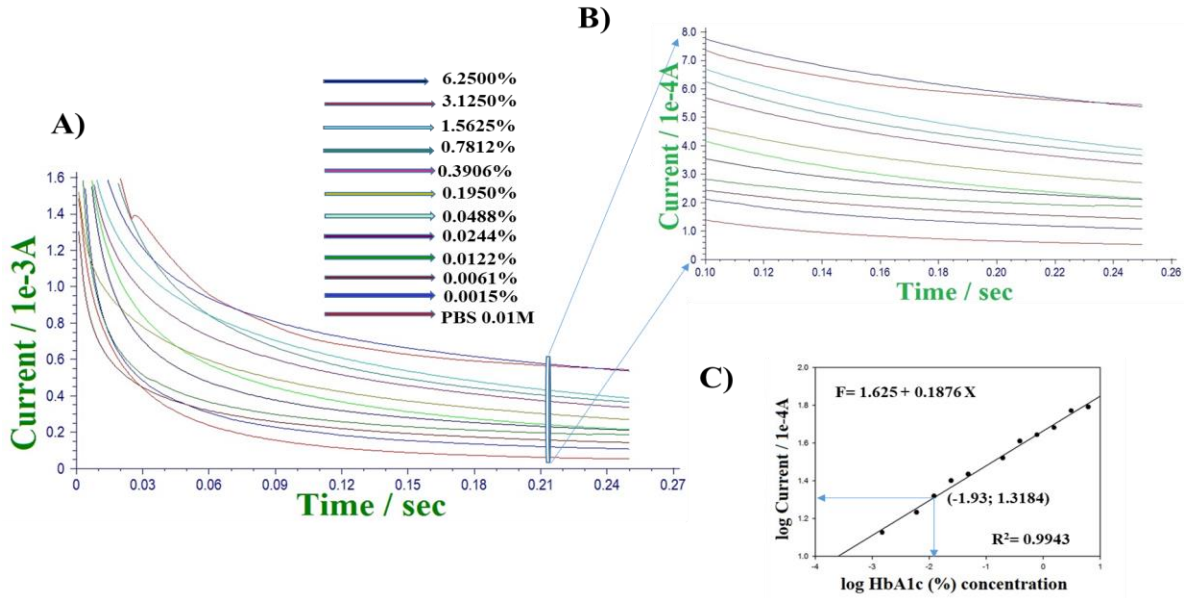

Figure 4.16. (A & B) Chronoamperometric (CA) response for PA-PPE-APBA-HbA_{1c} towards different concentrations of $HgbA_{1c}$. (C) Plot: Y= log of the peak current μA and X= log of the HbA_{1c} % concentration.

4. 2. 5. Discussion.

i. A well-defined redox peak, due to improved electrochemical conductivity through the pre-anodization and covalent immobilization techniques with cross-linking agents. The PA-PPE-APBA-HbA_{1c}. has a redox peak of -0.34 V to -0.65 V, which result for the redox process of the heme groups of $HgbA_{1c}$ captured on APBA *(Kim & Shim, 2013*).

ii. The immobilization of APBA and APBA-HbA_{1c} was demonstrated with different probes, in our modified electrodes.

iii. Through FT-IR we can demonstrate first the immobilization of APBA cofactor and subsequently the immobilization of APBA-HbA_{1c}, with their respective modifications and differences in their characterization. Likewise, we established the differences observed in the immobilization of total hemoglobin and glycated hemoglobin.

iv. The spectrum of B(1s), C(1s), N(1s) and O(1s) found in studies conducted through XPS, allows us to demonstrate first the presence of the APBA immobilized in our electrode PA-PPE-APBA and second the immobilization of glycosylated hemoglobin (HbA_{1c}), because it is attached to the APBA through the cis-diol bonds of the boronic acid. Also, we can demonstrate the presence of hemoglobin, due to the spectrum of the Fe(2p), which appears only when there is an iron-metalloprotein precursor the hemoglobin *(McIntyre & Zetaruk in 1977; Lin et al in 1997; Grosvenor et al in 2004; Biesinger et al in 2011; Mohapatraa et al 2009; Chakraborty et al in 2018; Wang et al in 2018).*

v. The PA-PPE-APBA-HbA_{1c} as the progressive increase in the concentration of immobilized $HgbA_{1c}$, the current catalyst of HbA_{1c} concentration increases, therefore is an increase in the catalytic current of H_2O_2. HbA_{1c} specifically catalyzed the reduction of H_2O_2 (*Kim & Shim, 2013*). Plot the log HbA_{1c} concentration % versus log current show a linear range between 0.0015%

through 6.25% with high sensitivity and detection limit range of 4.54 ng/5 mL. This relationship shows a linear proportionality suggested that the reaction, indicates a surface-diffusion controlled process, with a curve slopes of ***m= 0.4629*** as a transfer coefficient ***(a).***

vi. The electron transfer rate constant, (K_s) for the PA-PPE-APBA-HbA_{1c} electrode was calculated with the Laviron equation ($n\Delta E_p < 200$) and $K_s = 4.277\ s^{-1}$.

vii. The surface average concentration of electroactive APBA **(Γ)** value was calculated = 9.6416 e-9 mol/cm^2).

viii. Calibration experiments of the PA-PPE-APBA-HbA_{1c} biosensor showed good performance to identified glycated hemoglobin at different concentrations with a sensitivity of 208.9461 $\mu AmM^{-1}cm^{-2}$ (SE 0.2578) calculated as the current density (current/area) and plotted against the concentration.

ix. The biosensor shows high selectivity and specificity, toward glycated hemoglobin, when we compared the glycated hemoglobin (HbA_{1c}) and total hemoglobin (HbT), adjusted on different concentrations.

x. In order to review the reproducibility, different electrodes (PA-PPE-APBA-HbA_{1c}) were testing in 3 days and 90 days show an EP of 3.96% and 4.47% respectively, means the electrodes have good shelf life, reproducibility and stability.

xi. The validation for the electrodes (PA-PPE-APBA-HbA_{1c}) was do through the analytical recovery experiments, which was performed with different samples of whole blood and the percentage of recovery was calculated from the data (calculated value of HbA_{1c} /original concentration or spiked concentration) x 100. The values are 90%, 105%, 102%, 97%) with eAverage 98.5% for $HgbA_{1c}$ (see Fig. 4.17).

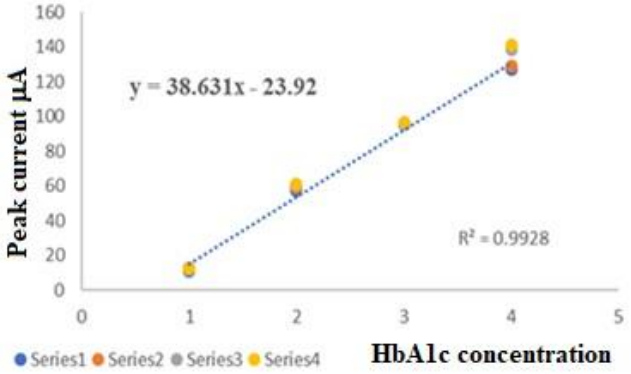

Figure 4. 17. Shows the plot graphic for percentage of recovery for the PA-PPE-APBA-HbA_{1c} for whole blood $HgbA_{1c}$ biosensor.

4. 3. Conclusions.

We can prove the electro catalytic proprieties of HbA1c, through CV and CA electro chemistries studies, show the interaction between HbA_{1c}, HPBA and the specific reaction of H_20_2 with HbA_{1c}. We can characterize the electrodes (PA-PPE-APBA and PA-PPE-APBA-HbA1c) through the FT-IR spectroscopy and XPS, showing the changes which occur when the APBA and the HbA_{1c} are immobilized in the electrode.

The biosensor shows high selectivity and specificity when we compared the glycated hemoglobin and total hemoglobin.

The novel pre-anodized paper printed electrode transducer to detects HbA_{1c} (PA-PPE-APBA-HbA_{1c}) shows high sensitivity (208.9461 µA mM^{-1} cm^{-2}) and low detection limit (4.54 ng/5mL), selectivity, stability, feasibility, portability and low costs.

Our biosensor offers new possibilities for the development of portable and customized equipment for better glucose control. Also, as a basis for the development of new applications in the medical-biological area.

OVERALL CONCLUSIONS

Our project allowed us to develop two biosensors, which can serve as the basis for building a diagnostic system for self-monitoring blood glucose (SMBG), blood glucose meter systems (BGMSs) and hemoglobin A_{1c}- point-of-care (HbA_{1c} POC), which meets the FDA requirements and recommendations.

Used individually, the biosensor for measuring glucose (PA-PPE-GOX-Glucose), provides the physician with accurate and quantitative measure of clinical glucose values in states of hypoglycemia and hyperglycemia. It also, serves as a system to monitor in the management of patients in these critical clinical states.

Glycolate hemoglobin measurement biosensor (PA-PPE-APBA-HbA_{1c}) will help physicians gain immediate knowledge of glucose behavior in diabetic and pre-diabetic patients, reducing subsequent medical visits to evaluate laboratory outcomes and provide timely and preventive management.

These biosensors have the potential for clinical acceptance due to their high sensitivity, high specificity, feasibility, low cost, and portability, as well as individualizing for management and monitoring in diabetic and prediabetic patients.

Can serve as a basis for building systems for people with disabilities.

REFERENCES

Adler, Amanda I.; Stratton, Irene M. et al. Association of systolic blood pressure with macro-vascular and micro-vascular complications of type 2 diabetes (UKPDS 36) prospective observational study. BMJ. 2000. 321:412-419.

Albery W. John and Knowles Jeremy R. Evolution of enzyme function and the development of catalytic efficiency. Biochemistry. 1976. Vol. 15 (25): 5631- 5640.

Albery, W. John. The application of the Marcus relation to reactions in solution. Ann. Rev. Phys. Chem. 1980. 31:227-263.

Alhazmi, Hassan A. FT-IR spectroscopy for the identification of binding sites and measurements of the binding interactions of important metal ions with bovine serum albumin. Scientia Pharmaceutica. 2019. 87.5(13 pp). doi:10.3390/scipharm87010005.

Ali, M.K.; Bullard, K.M et al. Achievement of goals in US diabetes care. 1999-2010. NEJM. 2013. 368(17):1613-1624.

Allen, David W.; Schroeder, W. A., and Balog, Joan. Observations on the chromatographic heterogeneity of normal adult and fetal human hemoglobin: A study of the effects of crystallization and chromatography on the heterogeneity and isoleucine content. J. Am. Chem. Soc. 1958. 80: 1628-1634.

American diabetes Association. Classification and diagnosis of diabetes: Standards of medical care in diabetes-2019. Diabetes Care. 2019. 42 (Suppl. 1): S13-S28.

American Diabetes Association. Executive summary: Standards of medical care in diabetes-2010. Diabetes Care. 2010. Vol.33. Sup.1: S4-10.

American Diabetes Association. Expert committee on the diagnosis and classification of diabetes mellitus. Follow-up report on the diagnosis of diabetes mellitus. Diabetes Care 2008. Vol. 31. Supp. 1: S55-60.

American Diabetes Association. Fast facts: data and statistics about diabetes. Revision 9/2015. **http://professional.diabetes.org/admin/UserFiles**

American Diabetes Association. Glycemic targets: Standards of medical care in diabetes-2018. Diabetes Care. 2018. 41 (suppl. 1): S55-S64. https://doi.org/10.2337/dc18-S006.

American Diabetes Association. Glycemic targets: Standards of medical care in diabetes-2019. Diabetes Care. 2019. 42(suppl. 1): S61-S70. https://doi.org/10.2337/dc19-S006.

American Diabetes Association. Standards of medical care in diabetes-2013. Diabetes Care. January2013, Vol.36: No. Supplement1:S11-S66. Doi: 10.2337/de13-S011.

Anderson, George W.; Zimmerman, Joan E. & Callahan, Francis M. The use of esters of N-hydroxysuccinimide in peptide synthesis1. J. Am. Chem. Soc. 1964. 86(9): 1839-1842.

Andes, Linda. J.; Cheng, Yiling.; Rolka, Deborah B, et al. Prevalence of prediabetes among adolescents and young adults in the United States, 2005-2016. JAMA Pediatrics. Dec.02, 2019. E1-E9.

Ang, Shu Hwang; Thevarajah, M. Alias, Yatimah and Khor, Sook Mei. Current aspects in hemoglobin A_{1c} detection a review. Clinica Chimica Acta. 2015. 439: 202-211.

Anson, Fred C. Innovations in the study of adsorbed reactants by chrono-coulometry. Analytical chemistry. 1966. 38(1): 54-57.

Aristov, N. and Habekost, A. Cyclic voltammetry. A versatile electrochemical method investigating electron transfer processes. World Journal of Chemical Education. 2015. 3(5): 115-119. doi: 10.12691/wjce-3-5-2.

Armstrong, Fraser A. and Lannon, Martin. Fast interfacial electron transfer between cytochrome c peroxidase and graphite electrodes promoted by aminoglycosides: Novel electroenzymic catalysis of H_20_2 reduction. American Chemical Society. 1987. Vol. 109 (23):7211-7212.

Baghayeri, Mehdi. Glucose sensing by a glassy carbon electrode modified with glucose oxidase and a magnetic polymeric nanocomposite. RSC Advances. 2015. 5:18267-18274.

Baghayeri, Mehdi; Veisi, Hojat and Ghanei-Motalagh, Masoud. Amperometric glucose biosensor based on immobilization of glucose oxidase on a magnetic glassy carbon electrode modified with a novel magnetic nanocomposite. Sensors and actuators B; Chemical. 2017. 249:321-330.

Banks, Craig E. and Compton, Richard G. Exploring the electrocatalytic site of carbon nanotubes for NADH detection: an edge plane pyrolytic graphite electrode study. Analyst. 2005. 130:1232-1239.

Banks, Craig E.; Davies, Trevor J.; Wildgoose, Gregory G. and Compton, Richard G. Electrocatalysis at graphite and carbon nanotube modified electrodes: edge-plane sites and tube ends are the reactive sites. Chem. Commun. 2005. 829–841.

Baranton, Steve and Belanger, Daniel. Electrochemical derivatization of carbon surface by reduction of in situ generated diazonium cations. J. Phys. Chem. B. 2005. Vol. 109. No. 51: 24410-24410.

Barbero, Cesar; Silber, Juana J.; Sereno, Leonides. Studies of surface-modified glassy carbon electrodes obtained by electrochemical treatment its effects on $Ru(bpy)^{2+}$ adsorption and the electron transfer rate of the Fe^{2+}/ Fe^{3+} couple. J. Electroanal. Chem. 1988. 248(2): 321-340.

Bard, Allen J. and Faulkner, Larry R. Electrochemical methods: Fundamentals and applications. 2nd ed.; John Wiley & Sons, Inc.: New Jersey. 2001.

Barker, G.C. and Jenkins, I.L. Square-wave polarography. Electrical methods. International Congress on analytical Chemistry. Nov. 1952. Vol. 77. 685-696.

Barre, Anais; Tintas, Mihaela-Liliana; Levacher, Vincent et al. An overview of the synthesis of highly versatile N-hydroxysuccinimide esters. Synthesis. 2017. 49. 472-483.

Barriet, David; Yam, Chi M.; Shmakova, Olga E. Jamison, Andrew C. and Lee, T. Randall. 4-mercaptophenylboronic acid SAMs on gold: Comparison with SAMs derived from thiophenol, 4-mercaptophenol, and 4-mercaptobenzoic acid. Langmuir. 2007. 23:8866-8875.

Barth, Andreas. Infrared spectroscopy of proteins, review. Biochimica et Biophysica Acta. 2007. 1767:1073-1101.

Beamson, G. and Briggs, D. High resolution XPS of organic polymers - The Scienta ESCA300 Database Wiley Interscience, 1992.

Bhattacharyya, Somnath; Cardinaud, C. and Turban, G. Spectroscopic determination of the structure of amorphous nitrogenated carbon films. J. Appl. Phys. 1998. Vol. 83. No. 8: 4491-4500.

Biesinger, Mark C.; Payne, Brad P.; Grosvenor, Andrew P.; Lau, Leo W.M.; Gerson Andrea R. and Smart, Roger St. C. Resolving surface chemical states in XPS analysis of first row transition metals, oxides and hydroxides: Cr, Mn, Fe, Co and Ni. Appl. Surf. Sci. 2011. 257: 2717-2730.

Bolt, Adrian W. Electrochemical methods for the determination of glucose. Current Separations. 1998. 17. 1:25-31.

Borai, A.; Livingstone, C.; Abdelaal, F et al. The relationship between glycosylated haemoglobin (HbA_{1c}) and measures of insulin resistance across a range of glucose tolerance. Scandinavian J. of Clinical and Laboratory Invest. 2011. 71:168–72.

Boulton AJ, Saudek CD. The need for standardization of glycated haemoglobin measurements. Diabetologia 2002;45: R19–21.

Bowling, Robert J.; Packard, Richard T. and McCreery, Richard L. Activation of highly ordered pyrolytic graphite for heterogeneous electron transfer: relationship between electrochemical performance and carbon microstructure. J. Am. Chem. Soc. 1989. 111(4): 1217–1223.

Boyd, K.J.; Marton, D.; Todorov, S.S.; Al-Bayati, A.H.; Kulik, J and Zuhr, R.A. Formation of C–N thin films by ion beam deposition. J. Vac. Sci. Technol. A13. 1995. 13. (4): 2110-2122.

Boyaci, Ismail H. Temiz, Havva T. Genis, Huseyin E. et al. Dispersive and FT-Raman spectroscopic methods in food analysis. Royal Society of Chemistry. Supplementary Data. 2015.

Brunauer, Stephen; Emmett, P.H. and Teller, Edward. Adsorption of gases in multimolecular layers. Journal of the American Chemical Society.1938. 60 (2): 309-319.

Bunn, H. F., D. N. Haney, K. H. Gabbay, and P. M. Gallop. Further identification of the nature and linkage of the carbohydrate in hemoglobin Al. Biochem. Biophys. Res. Commun. 1975; 67: 103-109.

Bunn, H. Franklin; Haney, David N.; Kamin, Steven et al. The biosynthesis of human hemoglobin A_{1c}. Slow glycosylation of hemoglobin in vivo. The Journal of Clinical Investigation. 1976. Vol.57. 1652-1659.

Bunn, H. Franklin; Gabbay, Kenneth H. and Gallop, Paul M. The glycosylation of hemoglobin: Relevance to diabetes mellitus. American Association for the Advancement of Science. 1978. Vol. 200. No. 4337: 21-27.

Cai, Chenxin and Chen, Jing. Direct electron transfer of glucose oxidase promoted by carbon nanotubes. Analytical Biochemistry. 2004. 332:75-83.

Cai, Zhihua and Martin, Charles. Electronically conductive polymer fibers with mesoscopic diameters show enhanced electronic conductivities. J. Am. Chem. Soc. 1989. Vol. 111: 4138-4139.

Carey. Robert I.; Folkers, John P. and Whitesides, George M. Self-assembled monolayers containing co-mercaptoalkylboronic acids adsorbed onto gold form a highly cross-linked, thermally stable borate glass surface. Langmuir. 1994. 10: 2228-2234.

Carnethon, M.R.; Biggs, M.L. et al. Diabetes and coronary heart disease as risk factors for mortality in older adults. The American Journal of Medicine. 2010. 123 (6):556e1-556e9.

Center for Disease Control and Prevention. After 20-year increase, new diabetes cases decline. May 28, 2019. Assessed Nov. 2019.

Centers for disease Control and Prevention (CDC). National diabetes statistics report, 2017. Estimates of diabetes and its burden in the United States. Assessed May 2018.

Centers for Disease Control and Prevention. Department of health and human services. National diabetes statistics report. 2014 National diabetes data fact sheet. Assessed December 2017.

Centers for Disease Control and Prevention. Diabetes report card 2012: National state profile of diabetes and its complications. August 2012. Pp.1-14. Assessed December 2017.

Centers for Disease Control and Prevention. National diabetes fact sheet, 2011. **http://www.cdc.gov/diabetes/pubs/pdf/ndfs_2011.pdf.Published2011.** Assessed Dec. 2017.

Chakraborty, Debayan; Sarkar, Saheli and Das, Prasanta Kumar. Blood dot: Hemoglobin derived carbon dot as hydrogen peroxide sensor and pro-drug activator. ACS Sustainable Chemistry and Engineering. 2018. 6:4661-4670.

Chan, H.S.O.; Ng, S.C.; Sim, W.S. Tan, K.L. and Tan, B.T. Preparation and characterization of electrically conducting copolymers of aniline and anthranilic acid: Evidence for self-doping by X-ray photoelectron spectroscopy. Macromolecules. 1992. 25(22):6029-6034.

Chawla, Aastha; Chawla, Rajeev and Jaggi, Shalini. Microvascular and macrovascular complications in diabetes mellitus: Distinct or continuum? Indian Journal of Endocrinology and Metabolism. 2016. Vol 20, Issue 4: 546-551.

Chawla, Sheetal and Pundir, Chandra Shekhar. An amperometric hemoglobin A_{1c} biosensor based on immobilization of fructosyl amino acid oxidase onto zinc oxide nanoparticles-polypyrrole film. Analytical Biochemistry. 2012. 430 (2):156-162.

Chen, J.; Zheng, X.; Miao, F.; Zhang, J.; Cui, X. and Zheng, W. Engineering graphene/carbon nanotube hybrid for direct electron transfer of glucose oxidase and glucose biosensor. J. Appl. Electrochem., 2012. 42:875-881.

Chen, Peihong and McCreery, Richard L. Control of electron transfer kinetics at glassy carbon electrodes by specific surface modification. Anal. Chem. 1996. 68(22): 3958-3965.

Chen, Ruopian and Spiro, Thomas G. Monitoring the allosteric transition and CO rebinding in hemoglobin with time resolved FTIR spectroscopy. Journal Phys. Chem. A. 2002. 106:3413-3419.

Chen, Xu; Jia, Jianbo et al... Organically modified sol-gel/chitosan composite based glucose biosensor. Electroanalysis. 2003. 15. No.7: 608-612.

Cholkar, Kishore; Ray, Animikh; Agrahari, Ibhuti et al. Transporters and receptors in the anterior segment of the eye. Ocular transporters and receptors. Their role in drug delivery. Woodhead Publishing Series in Biomedicine. 2013. 115-168. https://doi.org/10.1533/9781908818317.115.

Chou, Alison; Bocking, Till; Singh, Nagindar and Gooding, J. Justin. Demonstration of the importance of oxygenated species at the ends of carbon nanotubes for their favourable electrochemical properties. Chem. Commun. 2005. 842-844.

Chuang, Ya-Chun; Lan, Kung-Chieh et al. Detection of glycated hemoglobin (HbA_{1c}) based on impedance measurement with parallel electrodes integrated into a microfluid device. Sensors and Actuators B. 2012. 171-172: 1222-1230.

Compton, Richard G. & Banks, Craig E. Understanding voltammetry. Third Ed. 2018. World Scientific.

Conde, Joao; Ambrosone, A. Snaz, V. et al. Design of multifunctional gold nanoparticles for in vitro and in vivo gene silencing. ACS Nano. 2012. 6(9): 8316-8324.

Crocker, B.; Lewandrowski, EL.; Lewandrowski, N.; Gregory, K and Lewandrowski, K. Patient satisfaction with point-of-care laboratory testing: report of a quality improvement program in an ambulatory practice of an academic medical center. Clinica Chimica Acta. 2013. 424: 8-11.

Czupryniak, L. Barkai, S. Bolgarska, et al. Self-monitoring of blood glucose in diabetes: From evidence to clinical reality in central and eastern Europe. Recommendations from the international central-eastern European expert group. Diabetes Technology & Therapeutics. 2014. 16(7):460-475. DOI: 10.1089/dia.2013.030.

DCCT Research Group. The association between glycemic exposure and long-term diabetes complications in the diabetes control and complications trial. Diabetes 1995; 44 (8): 968–983.

D'Costa, E.J; Higgins, I.J. and Turner, A.P.F. Quinoprotein glucose dehydrogenase and its application in an amperometric glucose sensor. Biosensors. 1986. 2:71-87.

De Guibert, A.; Plichon, V. and Badoz-Lambling, J. Chronoamperometry study of lead sulfide oxidation in fused PbCl-KCl. Journal of the Electrochem. Society. 1979. 126(11):102-1905. DOI:10.1149/1.2128823.

Dekanski, Aleksandar; Stevanovic, Jasna.; Stevanovic, Rade et al. Glassy carbon electrodes I. Characterization and electrochemical activation. Carbon. 2001. 39(8): 1195-1205.

Delahay, Paul. Chronoamperometry and chronopotentiometry. In Treatise on analytical chemistry. 1963. Part I. SectionD-2. Chapter 44:2233-2267.

Delfino, I.; Portaccio, M.; Ventura B. Della et al. Enzyme distribution and secondary structure of sold-gel immobilized glucose oxidase by micro-attenuated total reflection FT-IR spectroscopy. Materials Science and engineering C. 2013. 33: 304-310.

Delfino.I.; Portaccio, M. et al. Enzyme distribution and secondary structure of sol-gel immobilized glucose oxidase by micro-attenuated total reflection FT-IR spectroscopy. Materials Science and Engineering C. 2013. 33: 304-310.

Dementjev, A.P.; de Graaf, A.; van de Sanden, M.C.M. et al. X-Ray photoelectron spectroscopy reference data for identification of the C N phase in carbon-nitrogen films. Diamond and related Materials. 2000. 9:1904-1907.

Deng, Dong and Yan, Nieng. GLUT, SGLT, and SWEET: Structural and mechanistic investigations of the glucose transporters. The Protein Science. 2016. Vol. 25:546-558.

Dervisevic, Muamer; Cevik, Emre and Senel, Mehmet. Development of glucose biosensor based on reconstitution of glucose oxidase onto polymeric redox mediator coated pencil graphite electrodes. Enzyme and Microbial Technology. 2014. 68:69-76.

Diao, Xiuhui; Chen, Hongyu et al. Magnetic carbon nanotubes for protein separation. Journal of Nanomaterials. 2012. Article ID 806019, 6 pages.

Dias, L.G.; Meirinho, S.G.; Veloso, A.C.A. et al. Electronic tongues and aptasensors. Bioinspired materials for medical applications. 2017. Chapter 13: 371- 402. http://dx.doi.org/10.1016/B978-0-08-100741-9.00013-9

Dong, Aichun and Caughey, Winslow. Infrared methods for study of hemoglobin reactions and structures. Methods of Enzymology. 1994. Vol.232: 13-175.

Dungchai, Wijitar; Chailapakul, Orawon and Henry, Charles S. Electrochemical detection for paper-based microfluidics. Analytical Chemistry. 2009. 81:5821-5826.

EAG laboratories. https://www.eag.com/resources/appnotes/xps-provides-chemical-bond-information/**.** Assessed in March 2020.

Eckermann, Amanda L.; Feld, Daniel J.; Shaw, Justine A. and Meade, Thomas J. Electrochemistry of redox-active self-assembled monolayers. Coord Chem. Rev. 2010. 254(15-16):1769-1802. Doi: 10.1016/j.ccr.2009.12.023.

Ekhlaspour, L.; Mondesir, D. Lautsch, N. et al. Comparative accuracy of 17 point-of care glucose meters. Journal of Diabetes and Technology. October 4, 2016. 1-9.

Eklund, John C.; Bond, Alan M.; Alden, John A. and Compton, Richard G. Perspectives in modern voltammetry: Basic concepts and mechanistic analysis. Advances in Physical Organic Chemistry. 1999. 32: 1-120.

Engstrom, Royce C. and Strasser, Vernon A. Characterization of electrochemically pretreated glassy carbon electrodes. Anal. Chem. 1984. 56 (2):136-141.

Erbach, Michael MD; Freckmann, Guido MD; Hinzmann, Rolf MD, PhD et al. Interferences and limitations in blood glucose self-testing: An overview of the current knowledge. Journal of Diabetes Science and Technology. 2016. Vol. 10(5) 1161–1168.

Evans, Dennis H.; O'Connell, Kathleen M.; Petersen, Ralph A. and Kelly, Michael J. Cyclic voltammetry. Journal of Chem. Educ., 1983. 60(4):290-293.

Evans, John F. and Kuwana, Theodore. Introduction of functional groups onto carbon electrodes via treatment with radio-frequency plasmas. Anal. Chem. 1979. 51(3): 358-65.

Fabre, Bruno and Hauquier, Fanny. Boronic acid-functionalized oxide-free silicon surfaces for the electrochemical sensing of dopamine. Langmuir. American chem. soc. 2017. 33(35): 8693-8699.

Falat, Ladislav and Cheng, Hung-Yuan. Electrocatalysis of ascorbate and NADH at a surface modified graphite-epoxy electrode. J. Electroanal. Chem. 1983. 157(2): 393-397

Fang, Lei; Li, Wei; Zhou, Yan and Liu, Chung-Chiun. A single-use, disposable iridium-modified electrochemical biosensor for fructosyl valine for the glycosylated hemoglobin detection. Sensors and Actuators B: Chemical. 2009. 137 (1): 235-238.

Faniran, J.A. and Shurvell, H.F. Infrared spectra of phenylboronic acid (normal and deuterated) and diphenyl phenylboronate. Canadian Journal of Chemistry. 1968. Vol.46: 2089-2095.

Fasold, H.; Klappenberger, J.; Meyer, C. and Remold, H. Bifunctional reagents for the crosslinking of proteins. Angew. Chem. Int. Ed. Engl. 1971. 10(11): 795-801.

FDA Executive Summary. Clinical chemistry and clinical toxicology devices Panel. July 22, 2016.

Fitzgibbons, James F.; Koler, Robert D. and Jones, Richard T. Red cell age-related changes of hemoglobins A_{1a+b} and A_{1c} in normal and diabetic subjects. The Journal of Clinical Investigation. 1976. 58:820-824.

Fong, Alex MD.; Serra, Allison E. MD.; Gabby, Lauryn; Wing, Deborah A. and Berkowitz, Kathleen M. Use of hemoglobin A_{1c} as an early predictor of gestational diabetes mellitus. Am. J. Obstet. Gynecol. 2014. 211:641. e1–7. doi: 10.1016/j.ajog.2014.06.016. Epub 2014 Jun 6.

Fourmond, Vincent; Thomas Lautier, Thomas; Baffert, Carole, et al. Correcting for electrocatalyst desorption and inactivation in chronoamperometry experiments. Anal. Chem. 2009. 81(8):2962-2968.

Freckmann, G.; Schmid, Ch.; Baumstark, A. et al. System accuracy evaluation of 43 blood glucose monitoring systems for self-monitoring of blood glucose according to DIN EN ISO 15197. Journal of Diabetes Science and Technology. 2012. Vol. 6. No. 5: 1060-1075.

Gallop, P.M., and Paz, M.A. Posttranslational protein modifications, with special attention to collagen and elastin. Physiological Reviews. 1975. 55 (3):418-487.

Gao, Yun-Fei; Yang, Tian; Yang, Xiao-Lu et al. Direct electrochemistry of glucose oxidase and glucose bio-sensing a hydroxyl fullerene modified glassy carbon electrode. Biosensors and Bioelectronics. 2014. 60:30-34.

Gebel, Erika. The start of something good: the discovery of HbA_{1c} and the American diabetes association Samuel Rahbar outstanding discovery award. Diabetes Care. 2012. 35 (12):2429–2431.

Gillery, Philippe. A history of HbA_{1c} through clinical chemistry and laboratory medicine. Clinical Chemistry and Laboratory Medicine. 2012.51(1):65–74.

Golczak, Sebastian; Kanciurzewska, Anna; Fahlman, Mats; Langer, Krzysztof and Langer, Jerzy J. Comparative XPS surface study of polyaniline thin films. Solid State Ionics. 2008. 179:2234–2239

Goldstein, David E. and DCCT Research Group. Feasibility of centralized measurements of glycated hemoglobin in the diabetes control and complications trial: a multicenter study. Clin Chem. 1987. 33 (12):2267-2271.

Goodall, I.; Colman, P. G.; Schneider, H. G.; Mclean, M. and Barker, G. Desirable performance standards for HbA_{1c} analysis–precision, accuracy and standardization: Consensus statement of the Australian association of clinical biochemists (AACB), the Australian diabetes society (ADS), the Royal college of pathologists of Australia (RCPA, Endocrine society of Australia (ESA), and the Australian diabetes educators association (ADEA). Clin Chem Lab Med. 2007. 45 (8):1083–97.

Goormaghtigh, Erik; Ruysschaert, Jean-Marie and Raussens, Vincent. Evaluation of the information content in infrared spectra for protein secondary structure determination. Biophysical Journal. 2006. Vol. 90:2946-2957.

Gould, Gwyn W. and Holman, Geoffrey D. The glucose transport family: structure, function and tissue-specific expression. Biochemistry Journal. 1993. 295:329-341.

Grabarek, Zenon and Gergely John. Zero-length crosslinking procedure with the use of active esters. Analytical Biochemistry. 1990. 185:131-135.

Gregg, S.J. and Sing, K.S.W. Adsorption, surface area and porosity. Academic Press. 1982.

Grosvenor, A.P.; Kobe, B.A.; Biesinger, M.C. & McIntyre, N.S. Investigation of multiplet splitting of Fe2p XPS spectra and bonding in iron compounds. Surf. Interf. Anal. 2004. 36: 1564-1574.

Gu, Li: Liang, Ying et al. A novel electrochemical sensor based on boronic acid-functionalized multi-walled carbon nanotubes for astragaloside IV determination using ARS as the current indicator. Analytical Methods. 2012. 4:492-495.

Guilbault, G.G. and Lubrano, G.J. An enzyme electrode for the amperometric determination of glucose. Analytical Chemistry Acta. 1973. 64:439:455.

Guiseppi-Elie, A; C. Lei and R.H. Baughman. Direct electron transfer of glucose oxidase on carbon nanotubes. Nanotechnology. 2002. 13 (5): 559-564.

Gunasekaran, S.; Uthra, D.; Sailatha, E. and Anita B. FTIR spectral study on jaundice blood samples before and after treatment. Asian Journal of Chemistry. 2010. Vol.22 No.1:51-56.

Guo, Chun Xian and Li, Chang Ming. Direct electron transfer of glucose oxide and biosensing of glucose on hollow sphere-nanostructured conducting polymer/metal oxide composite. Phys. Chem. Chem. Phys. 2010. 12: 12153-12159.

Guo, Yizhu and Guadalupe, Ana R. Direct electrochemistry of horseradish peroxidase adsorbed on glassy carbonelectrode from organic solutions. Chem. Commun. 1997. 1437-1438.

Haghighi, Nasibeh; Hallj, Rahman and Salimi, Abdollah. Immobilization of glucose oxidase onto a novel platform based on modified $Ti0_2$ and graphene oxide, direct electrochemistry, catalytic and photocatalytic activity. Materials science and Engineering C. 2017. 73:417-424.

Halámek, J.; Wollenberger, U.; Stöcklein, W.; Scheller, F.W. Development of a biosensor for glycated hemoglobin. Electrochim. Acta 2007, 53, 1127–1133.

Hanas, Ragnar MD. and John, Garry. Consensus statement on the worldwide standardization of the hemoglobin A_{1C} measurement. Diabetes Care. 2010. Vol. 33(8): 1903-1904.

Hanas, R. MD. and John, W.G. MD. Update on the worldwide standardization of the hemoglobin A_{1c} measurement. Pediatric diabetes. 2013. doi: 10.1111/pedi.12047

Harnisch, Falk and Freguia, Stefano. A basic tutorial on cyclic voltammetry for the investigation of electroactive microbial biofilms. Chem. Asian J. 2012. 00 10 pp. DOI: 10.1002/asia.201100740

Harper, Alice and Anderson, Mark R. Electrochemical glucose sensors-developments using electrostatic assembly and carbon nanotubes for biosensor construction. Sensors. 2010, 10: 8248-8274.

Hecht, H. J.; Kalisz, H. M.; Hendle, J.; Schmid, R. D.; Schomburg, D. Crystal structure of glucose oxidase from aspergillus Niger refined at 2-3 A resolution. J. Mol. Biol. 1993. 229(1):153-172.

Heineman, William R. & Kissinger, Peter T. Large-amplitude controlled-potential techniques. In laboratory techniques in electrochemical chemistry. Kissinger and Heineman Editors. 1984. Marcel Dekker, Inc.

Hendrickson, D. N.; Hollander, J. M. and Jolly, W. L. Core-electron binding energies for compounds of boron, carbon, and chromium. Inorganic Chemistry. 1970. 9. (3): 612-615.

Henrichs, Helmut R. HbA_{1c}-glycated hemoglobin and diabetes mellitus. 1st. ed. Bremen UNI-MED 2009.

Hermanson, Greg T. Zero-length crosslinkers in bioconjugate techniques. 3er Ed., 2013. Elsevier.

Hirst, Jennifer A.; McLellan, Julie H.; Price, Christopher P. et al. Performance of point-of-care HbA_{1c} test devices: implications for use in clinical practice- a systematic review and meta-analysis. Clin. Chem. Lab. Med. 2016. 55 (2):167-180. doi: 10.1515/cclm-2016-0303.

Hoare, D. G., and Koshland, D. E., Jr. A method for the quantitative modification and estimation of carboxylic acid groups in proteins. J. Biol. Chem. 1967. 242, 10: 2447-2453.

Holmquist, W.R. and Schroeder, W.A. A new N-terminal blocking group involving a Schiff base in hemoglobin A_{1c}. Biochemistry. 1966. Vol. 5 (8):2489-2503.

Holmquist, W.R. and Schroeder, W.A. The in vitro biosynthesis of hemoglobin A_{lc}*. Biochemistry. 1966. Vol. 5 (8):2504-2512.

Hu, Ing-Feng and Kuwana, Theodore. Oxidative mechanism of ascorbic acid at glassy carbon electrodes. Analytical Chemistry. 1986. 58(14): 3235-3239.

Hu, Ing-Feng; Karweik, Dale H. and Kuwana, Theodore. Activation and deactivation of glassy carbon electrodes. J. Electroanal. Chem. 1985. 188 (1): 59-72.

Hua, Liang; Wu, Xiaqin and Wang, Rong. Glucose sensor based on an electrochemical reduced graphene oxide-poly-(L-lysine) composite film modified GC electrode. Analyst. 2012. 137, 5716-5719.

Hui, Jianing; Cui, Jiewu, Xu, Guangqing et al. Direct electrochemistry of glucose oxidase based on Nafion-graphene-GOD modified gold electrode and application to glucose detection. Materials Letters. 2013. 108:88-91.

Huisman, THJ and Meyering, CA. Studies on the heterogeneity of hemoglobin: I. the heterogeneity of different human hemoglobin types in carboxymethylcellulose and in amberlite IRC-50 chromatography: qualitative aspects. Clinica Chimica Acta. 1960. 5:103-123.

IFCC Working Group HbA1c. Approved laboratories of the IFCC network laboratories for HbA_{1c}. http://www.ifcchba1c.net/network/approved. Assessed Nov. 2019.

Ilangovan, G. and Pillai, K.C. Electrochemical and XPS characterization of glassy carbon electrode surface effects on the preparation of a monomeric molybdate (VI)-modified electrode. Langmuir. 1997. 13(3): 566-575.

IUPAC Compendium of chemical terminology, 2nd edition, 1977.

Ivnitski, D.; Artyushkova, K.; Rincon,R.A.; Atanassov, P.; Luckarift, H.R. and Johnson, G.R. Entrapment of enzymes and carbon nanotubes in biologically synthesized silica: glucose oxidase-catalyzed direct electron transfer. Small. 2008. 4. No. 3:357-364.

Ivnitski, Dmitri; Brittany,Brancha; Atanassova, Plamen et al. Glucose oxidase anode for biofuel cell based on direct electron transfer. Electrochemixtry Communications. 2006. 8: 1204-1210.

Janegitz, Bruno C.; Pauliukaite, Rasa; Ghica, Mariana E. et al. Direct electron transfer of glucose oxidase at glassy carbon electrode modified with functionalized carbon nanotubes within a dihexadecylphosphate film. Sensors and Actuators B: Chemical. 2011. 158:411-417.

Jeppsson, JO.; Kobold, U.; Barr, J.; Finke, A. Hoelzel, W. et al. International federation of clinical chemistry and laboratory medicine. Approved IFCC reference method for the measurement of HbA_{1c} in human blood. Clin Chem Lab Med. 2002. 40:78-89.

Ji, Xiaobo; Banks, Craig E.; Crossley, Alison and Compton, Richard G. Oxygenated edge plane sites slow the electron transfer of the ferro/ferricyanide redox couple at graphite electrodes. Chem. Phys. Chem. 2006. 7:1337-1344.

Jia, Weiping. Standardizing HbA_{1c}-based diabetes diagnosis: opportunities and challenges. Expert Review of Molecular Diagnostics. 2016. Vol. 16 (3):343-355.

John, W. Garry; Mosca, Andrea; Weykamp, Cas and Goodall, Ian. HbA_{1c} standardization: history, science and politics. Clin. Biochem. Rev. 2007. Vol. 28: 163-168.

Juutilainen, Auni; Lehto, Seppo; Ronnemaa, Tapani et al. Similarity of the impact of type 1 and type 2 diabetes on cardiovascular mortality in middle-aged subjects. Diabetes Care. 2008. 31:714-719.

Kang, Xinhuang; Wang, Jun; Wu, Hong et al. Glucose oxidase-graphene-chitosan modified electrode for direct electrochemistry and glucose sensing. Biosensors and Bioelectronics. 2009. 25:901-905.

Katz, E; Heleg-Shabtai, V; Willner, N et al. Electrical contact of redox enzymes with electrodes: novel approaches for amperometric biosensors. Bioelectrochemistry and Bioenergetics. 1997. Vol. 42: 95-104.

Kavan, Ladislav. Electrochemical carbon. Chem. Rev. 1997. 97(8): 3061−3082.

Kepley, Larry J. & Bard. Allen J. Ellipsometric, Electrochemical, and elemental characterization of the surface phase produced on glassy carbon electrodes by electrochemical activation. Anal. Chem. 1988. 60(14): 1459-1467.

Kim, Dong-Min and Shim, Yoon-Bo. Disposable amperometric glycated hemoglobin sensor for the finger prick blood test. Analytical Chemistry. 2013. 85:6536-6543.

Kim, Shin Young; Park, Jeunghee; Choi, Hyun C.; Ahn, Jae P.; Hou, Jin Q. and Kang, Hong S. X-ray photoelectron spectroscopy and first principles calculation of BCN nanotubes. JACS. 2007. 129. (6):1705-1716.

Kissinger, Peter T. and Heineman, William R. Cyclic voltammetry. Journal of Chem. Edu. 1983. Vol. 60(9): 702-706.

Kneten, Kristin R. and McCreery, Richard L. Effects of redox system structure on electron-transfer kinetics at ordered graphite and glassy carbon electrodes. Anal. Chem. 1992. 64(21): 2518-2524.

Koenig, Ronald J.; Peterson, C. M.; Kilo, Charles; Cerami, Anthony and Williamson, Joseph R. Hemoglobin A_{1c} as an indicator of the degree of glucose intolerance in diabetes. Diabetes. 1976. 25(3):230-232.

Kong, Fen-Ying; Gu, Sai-Xi; Li, Wei-Wei et al. A paper disk equipped with graphene-polyaniline/Au nanoparticles/glucose oxidase biocomposite modified screen-printed electrode: toward whole blood glucose determination. Biosensors and Bioelectronics. 2014. 56:77-82.

Kovach, Paul M.; Deakin, Mark R. and Wightman, R. Mark. Electrochemistry at partially blocked carbon-fiber microcylinder electrodes. The Journal of Physical Chemistry. 1986. 90(19):4612-4617.

Krause, Matthew S. Jr. and Ramaley, Luois. Analytical applications of square wave voltammetry. Analytical Chemistry. 1969. Vol. 41 (11): 1365-1369.

Krimm, Samuel and Bandekar, J. Vibrational spectroscopy and conformation of peptides, polypeptides and proteins. Advances in Protein Chemistry. 1986. Vol.38:181-364.

Krishna, Siva Rama; Bhat, Navakanta and Amrutur, Bharadwaj. Detection of glycated hemoglobin using 3-aminophenylboronic acid modified graphene oxide. IEEE/NIH. LiSSA. 2011. Pp.1-4.

Kulys, J.; Tetianec, L. and Ziemys, A. Probing Aspergillus Niger glucose oxidase with pentacyanoferrate (III) aza-and thia-complexes. J. Inorg. Biochem. 2006. 100 (10):1614-1622.

Kunkel, G. R., Mehrabian, M., and Martinson, H. G. Contact-site cross-linking agents. Molecular and Cellular Biochemistry. 1981. 34: 3-13 1981.

Kurusu, F. Tsunoda, H. et al. The advantage of using carbon nanotubes compared with edge plane pyrolytic graphite as an electrode material for oxidase-based biosensors. Analyst. 2006. 131:1292-1298.

Kwon, Soon Sung; Kwon, Ja-Young; Park, Yong-Won; Kim, Young-Han and Lim, Jong-Baeck. HbA_{1c} for diagnosis and prognosis of gestational diabetes mellitus. Diabetes Res. Clin. Practice. 2015. 110:38–43.

Lakshminarayanan, Priya V.; Thghiani, Hossein and Pittman Jr, Charles U. Nitric acid oxidation of vapor grown carbon nanofibers. Carbon. 2004. 42: 2433-2442.

Lam, Mandy; Louie, Richard F.; Curtis, Corbin M. et al. Short-term thermal-humidity shock affects point-of-care glucose testing: Implications for health professionals and patients. Journal of Diabetes Science and Technology, 2014. Vol.8(1) 83-88.

Lan, Wen-Jie; Maxwell, E. Jane; Parolo, Claudio et al. Paper-based electroanalytical devices with an integrated, stable reference electrode. Lab on a Chip. 2013. 9 (13):4103-4108.

Laviron, E. General Expression of the linear potential sweep voltammogram in the case diffusionless electrochemical systems. J. Electroanal. Chem. 1979. 101:19-28.

Laxmibai National institute of physical education. Chronoamperometry. Advanced Analytical Chemistry. 2019.

Leca, Viviane MD; Ibrahim, Zouher MD; Lombard-Pontou, Elise MD et al. Point-of-care measurements of HbA_{1c}: simplicity does not mean laxity with controls. Diabetes Care. 2012. Vol. 35. (12); e85.

Leger, Christophe and Bertrand, Patrick. Direct electrochemistry of redox enzymes as a tool for mechanistic studies. Chem. Rev. 2008, 108(7): 2379–2438, DOI: 10.1021/ cr0680742.

Lenters-Westra, E. and Slingerland, RJ. Three of 7 hemoglobin A_{1c} point-of-care instruments do not meet generally accepted analytical performance criteria. Clinical Chemistry. 2014a: 60(8): 1062-1072.

Lenters-Westra, E. and Slingerland, RJ. Six of eight hemoglobin A_{1c} point-of-care instruments do not meet the general accepted analytical performance criteria. Clinical Chemistry. 2010: 56(1): 44-52.

Lenters-Westra, Erna; Schindhelm, Roger K.; Bilo, Henk J. and Slingerland, Robbert J. Haemoglobin A_{1c}: Historical overview and current concepts. Diabetes Research and Clinical Practice. 2013. 99:75-84.

Lenters-Westra, W.Berendina. Hemoglobin A1c; Standardisation, analytical performance and interpretation. University of Groningen, 2011.

Leroux, Fanny; Dementin, Sebastien; Burlat, Benedicte et al. Experimental approaches to kinetics of gas diffusion in hydrogenase. Proc. Natl. Acad. Sci. U.S.A. 2008, 105(32): 11188–11193, DOI: 10.1073/pnas.0803689105.

Li, Z.F.; Kang, E.T. Neoh, K.G. and Tan, K.L. Covalent immobilization of glucose oxidase on the surface of polyaniline films graft copolymerized with acrylic acid. Biomaterials. 1998. 19:45-53.

Liang, Wang and Zhuobin, Yuan. Direct electrochemistry of glucose oxidase at a gold electrode modified with single-wall carbon nanotubes. Sensors. 2003. 3:544-554.

Libby, W.F. Theory of electron exchange reactions in aqueous solution. J. Phys. Chem. 1952. Vol. 52 (7): 863-868.

Libertino, Sebania; Giannazzo, Filippo; Aiello, Venera; Scandurra, Antonino et al. XPS and AFM characterization of the enzyme glucose oxidase immobilized on SiO_2 surfaces. Langmuir. 2008. 24: 1965-1972.

Libertino, Sebania; Scandurra, Antonino; Aiello, Venera; Giannazzo, Filippo; Sinatra, Fulvia et al. Layer uniformity in glucose oxidase immobilization on SiO_2 surfaces. Applied Surface Science. 2007. 253. 23: 9116-9123.

Libertino, Sebania; Aiello, Venera; Scandurra, Antonino et al. Immobilization of the enzyme glucose oxidase on both bulk and porous SiO_2 surfaces. Sensors. 2008. 56-37-5648.

Lin, J.D.; Chang, J.B., Wu, C.Z. et al. Identification of insulin resistance in subjects with normal glucose tolerance. Annals Academy of Medicine. 2014. 43(2):113–119.

Lin, Tien-Chih; Seshadri, Gayatri and Kelber, Jeffry A. A consistent method for quantitative XPS peak analysis of thin oxide films on clean polycrystalline iron surfaces. Applied Surface Science. 1997. 119. Issues 1-2:83-92.

Little, Randie R.; Rohlfing, Curt and Sacks, David B. The NGSP: Over 20 years of improving HbA_{1c} measurement. Cli. Chem. 2019. 65 (7): 839-848.

Little, Randie R.; Rohlfing, Curt L. and Sacks, David B. Status of HbA_{1c} measurement and goals for improvement: from chaos to order for improving diabetes care. Clin. Chem. 2011. 57. (2):204-214.

Liu, Bingwen; Du, Dan; Hua, Xin et al. Paper-based electrochemical biosensors: From test strips to paper-based microfluidics. Electroanalysis. 2014. 26:1214-1223.

Liu, Guozhen; Paddon-Row, Michael and Gooding, J. Justin. A Molecular modified glassy carbon electrode for achieving direct electron transfer to native glucose oxidase. Electrochemistry Communications. 2007. 9:2218-2223.

Liu, Huiping.; Tao, Cheng-an; Hu, Zhihong; S. Zhang, Sida et al. Electrochemical glucose biosensor based on graphene composites: use of dopamine as reducing monomer and as site for covalent immobilization of enzyme. RSC Advances. 2014. DOI 10.1039/C4RA04975F

Liu, Jingquan; Chou, Alison Rahmat, Wibowo et al. Achieving direct electrical connection to glucose oxidase using aligned single walled carbon nanotube arrays. Electroanalysis. 2005. 17(1):38-46.

Liu, Jun-oh; Song, Seung-yeon; Ahn, Yeon-chan; Yoon, Hyun-chul; Lee, Jun-hwang and Choi, Yong-bok. Electrochemical measurement of glycosylated protein using boronic acid modified electrode. 2011.

Liu, Ying; Wang, Mingkui et al. The direct electron transfer of glucose oxidase and glucose biosensor based on carbon nanotubes/chitosan matrix. Biosensors and Bioelectronics. 2005. 21:984-988.

Liu, Yong; Yu, Dingshan; Zeng, Chao et al. Biocompatible graphene oxide-based glucose biosensors. Langmuir. 2010. 26 (9):6158-6160.

Liu, Yuxiang; Zhzng, Jin; Cheng, Yi et al. Effect of carbon nanotubes on direct electron transfer and electrocatalytic activity of immobilized glucose oxidase. ACS Omega. 2018. 3:667-676.

Lopez-Jaramillo, Patricio; Lopez-Lopez, Jose et al. The goal of blood pressure in the hypertensive patient with diabetes is defined: now the challenge is go from recommendations to practice. Diabetology & Metabolic Syndrome, 2014. 6:31(10 pp).

Lovric, M.; Komorsky-Lovric, S. and Bond, A.M. Theory of square-wave stripping voltammetry and chronoamperometry of immobilized reactants. J. Electroanalytic Chem. 1991. 319. 1-18.

Lyons, Timothy J. and Basu, Arpita. Biomarkers in diabetes: Hemoglobin A_{1c}, vascular and tissue markers. Translational Research. 2012. 159(4): 303-312.

Mabbott, Gary. An introduction to cyclic voltammetry. J. of Chem. Edu. 1983. 60(9):697-702.

MacDonald, Digby. Transient techniques in electrochemistry. 1977. Plenum Press. N.Y.

Malesevic, Alexander, et al. Synthesis of few-layer graphene via microwave plasma enhanced chemical vapour deposition. Nanotechnology. 2008. 19(30):305604.

Malesevic, Alexander; Vitchev, Roumen; Schouteden, Koen et al. Synthesis of few-layer graphene via microwave plasma enhanced chemical vapour deposition. Nanotechnology. 2008. 19. doi:10.1088/0957-4484/19/30/305604.

Mani, V.; Devadas, B. and Chen, S-M. Direct electrochemistry of glucose oxidase at electrochemically reduced graphene oxide-multiwalled carbon nanotubes hybrid material modified electrode for glucose biosensor. Biosensors and Bioelectronics. 2013. 41:309-315.

Mansson, Mats-Olle Larsson, Per-Olof and Mosbach, Klaus. Covalent binding of an NAD analogue to liver alcohol dehydrogenase resulting in an enzyme-coenzyme complex not requiring exogenous coenzyme for activity. Eur. J. Biocem. 1978. 86: 455-463.

Marcos, Juliana; Rios, Angel & Valcarcel, Miguel. Automatic determination of Michaelis-Menten constants by the variable flow-rate technique. Analytica Chimica Acta. 1993. 283:429-438

Marcus, R.A. Chemical and electrochemical electron-transfer theory. Ann. Rev. Phys. Chem. 1964. 15:155-196.

Marcus, R. A. and Sutin, Norman. Electron transfers in chemistry and biology. Biochima et Biophysica Acta. ReV. Bioenerg. 1985, 811(3):265-322.

Marcus, Rudolph A. Electron transfer reactions in chemistry. Theory and experiment. Reviews of Modern Physics. 1993. Vol. 65 (3):599-610.

Marcus, Rudolph A. Electron transfer reactions in chemistry. Theory and experiment. Pure and applied chemistry. 1997 IUPAC. 89 (1): 13-29.

Marcus, Rudolph A. Electron, proton and related transfers. Faraday discusses. Chem. Soc. 1982. 74:7-15.

Martinez, Andres W.; Phillips, Scott T. and Whitesides, George M. Diagnostics for the developing world: microfluidic paper-based analytical devices. Analytical Chem. 2010. Vol. 82. No.1:3-10.

Martin-Timon, Iciar; Sevillano-Collantes, Cristina et al. Type 2 diabetes and cardiovascular disease: Have all risk factors the same strength? World Journal of Diabetes. 2014. 5(4): 444-470.

Mauk A. Grant. Biological electron-transfer reactions. Essays in Biochemistry. 1999. Vol. 34:101-124.

McCreery, Richard L.; Cline, Kristin K.; McDermott, Christie. A. et al. Control of reactivity at carbon electrode surfaces. Colloids Surfaces A: Physicochem. Eng. Aspects. 1994. 93(Dec.5): 211-219.

McIntyre, N.S. and Zetaruk, D.G. X-ray photoelectron spectroscopic studies of iron oxides. Analytical Chemistry. 1977. Vol. 49. No 11: 1521-1529.

Mendez, Carlos E. MD.; Mok, Ki-Tae MD. Ata, Ashar et al. Increased glycemic variability is independently associated with length of stay and mortality in noncritically ill hospitalized patients. Diabetes Care. 2013. 36(12): 4091-4097.

Mirceski, Valentin; Gulaboski, Rubin; Lovric, Milivoj et al. Square-wave voltammetry: A review on the recent progress. Electroanalysis. 2013. 25 (11):2411-2422.

Mirceski, Valentin; Komorsky-Lovric and Lovric, Milijov. Square-wave voltammetry. Theory and application. 2007. Springer-Verlag. Berlin Heidelberg.

Mirceski, Valentin; Skrzypek, Slawomira and Stojanov, Leon. Square-wave voltammetry. ChemTexts. 2018. 4-17.

Mohapatra, S.; Panda, N. and Pramanik, P. Boronic acid functionalized superparamagnetic iron oxide nanoparticle as a novel tool for adsorption of sugar. Materials Science and Engineering C. 2009. 29: 2254-2260.

Moon, Jong-Min; Kim, Dong-Min; Kim, Moo-Hyun et al. A disposable amperometric dual sensor for the detection of hemoglobin and glycated hemoglobin in a finger prick blood sample. Biosensors and Bioelectronics. 2017. 91: 128–135

Moore, Thomas R. MD. aTrnd Griffing, George T. MD. Diabetes mellitus and pregnancy. Medscape. Jul.07, 2014.

Mott, Jenna R. Munson, Paul J. et al. Design, development, and characterization of an inexpensive portable cyclic voltammeter. Journal of Chem. Edu. 2014. 91(7):1028-1036.

Murphy, Brian M.; Antonio, Jennifer D.; Manning, Mark C. and Ai-Azzam, Wasfi. Use of the amide II infrared band of proteins for secondary structure determination and comparability of higher order structure. Current Pharmaceutical Biotechnology. 2014. 15:880-889.

Nakamizo, M. and Tamai, K. Raman spectra of the oxidized and polished surfaces of carbon. Carbon. 1984. 22(2): 197-198.

Nathan, David M.; Kuenen, Judith; Borg, Rikke; Zheng, Hui; Schoenfeld, David and Heine, Robert J. Translating the A1Cassay into estimated average glucose values. Diabetes Care. 2008. 31:1473–8.

Nathan, David M. The diabetes control and complications trial/epidemiology of diabetes interventions and complications study at 30 years: Overview. Diabetes Care. 2014. 37(1):9-16.

National glycohemoglobin standardization program (NGSP) (Internet)2019. Harmonizing HgA_{1c} testing. Assessed Nov. 2019.

Navale, Archana M. and Paranjape, Archana N. Glucose transporters: physiological and pathological roles. Biophys Rev. 2016. 8:5-9.

Newton, Marshall D. and Sutin, Norman. Electron transfer reactions in condensed phases. Ann. Rev. Phys. Chem. 1984. 35: 437-480.

Ni, Jing; Wu, Weidong; Ju, Xin; Yang, Xiangdong et al. Bonding structure of a-CNx: H films obtained in methane–nitrogen system and its influence on hardness. Thin Solid Films. 2008. 516:7422-7426.

Nicholson, R.S. & Shain, I. Theory of stationary electrode polarography. Single scan and cyclic methods applied to reversible, irreversible and kinetics systems. Anal. Chem.1964. 36(4): 706-723.

Nie, Zhihong; Nijhuis, Christian A.; Gong, Jinlong. et al. Electrochemical sensing in paper-based microfluidic devices. Lab on a Chip. 2010. 10:477-483.

Notsu, Hideo; Yagi, Ichizo; Tatsuma, Tetsu et al. Introduction of oxygen-containing functional groups onto diamond electrode surfaces by oxygen plasma and anodic polarization. Electrochemical and Solid-State Letter. 1999. 2(10): 522-524.

NGSP. International federation of clinical chemistry (IFCC) standardization of HbA_{1c}. Assessed Nov. 2019.

Önal, ZE.; Atasayan, V.; Akici, N.; Gurbuz, T. and Nuhoglu, C. The relationship between glycosylated haemoglobin (HbA_{1c}) levels and serum lipid profiles in insulin resistant children. HK J Paediatr. 2014. 19:22-27.

Ong, C.W. and Huang, H. X-ray photoemission spectroscopy of nonmetallic materials: Electronic structures of boron and BxOy. Journal of applied Physics. 2004. Vol. 95. No. 7:3527-3534.

Osteryoung, Janet G. and Osteryoung, Robert. Square wave voltammetry. Analytical Chemistry. 1985. Vol. 57. (1):101A-110A.

Osteryoung, Janet. Voltammetry for the future. Accounts of Chemical Research. 1993. Vol. 26(3): 77-83.

Paknikar, S.; Sarmah, R.; Sivaganeshan, L.; Welke, A.; Rizzo, A.; Larson, K. and Rendell, M. Long-term performance of point-of-care hemoglobin A_{1c} assays. J. Diabetes Sci. Technol. 2016. 10(3):1308-1315.

Palanisamy, S.; Cheemalapati, S. and Chen, S-M. Amperometric glucose biosensor based on glucose oxidase dispersed in multiwalled carbon nanotubes/graphene oxide hybrid biocomposite. Materials Science and Engineering C. 2014. 34:207-213.

Paneni, Francesco; Beckman, Joshua A. et al. Diabetes and vascular disease: pathophysiology, clinical consequences, and medical therapy: part I. European Heart Journal.2013. 34:2436-2446.

Park, Jin-Young; Chang, Byoung-Yong et al. Selective electrochemical sensing of glycated hemoglobin (HbA_{1c}) on thiophene-3-boronic acid self-assembled monolayer covered gold electrodes. Analytical Chemistry. 2008. 80:8035-8044.

Paul, Rajib; Voevodin, Andrey A.; Dimitry, Zemlyanov; Roy, Ajit K. and Fisher, Timothy S. Microwave-assisted surface synthesis of a boron–carbon–nitrogen foam and its desorption enthalpy. Advanced functional materials. 2012. 22:3682-3690.

Poolsup, N; Suksomboon, N. and Rattanasookchit, S. Meta-analysis of the benefits of self-monitoring of blood glucose on glycemic control in type 2 diabetes patients: an update. Diabetes Technologies & Therapeutics. 2009. Vol. 11(12):775-784.

Prasad, K. S; Chen, J.-C.; Ay, C. & Zen, J-M. Mediatorless catalytic oxidation of NADH at a disposable electrochemical sensor. Sensors and Actuators B. 2007. 123:715–719.

Prasad, K. Sudhakara; Chuang, Min-Chieh and Ho, Ja-An Annie. Synthesis, characterization, and electrochemical applications of carbon nanoparticles derived from castor oil soot. Talanta. 2012. 88:445-449.

Prasad, K. Sudhakara; Muthuraman. Govindan and Zen, Jyj-Myng. The role of oxygen functionalities and edge plane sites on screen-printed carbon electrodes for simultaneous determination of dopamine, uric acid and ascorbic acid. Electrochemistry Communications. 2008. 10:559-563.

Prasad, K. Sudhakara; Walgama, Charuska, and Krishnan, Sadogopan. Enhanced electroactivity and substrate affinity of microperoxidase-11 attached to pyrene-linkers p-p stacked on carbon nanostructures electrodes. RSC Advances. 2015. 5:11845-11849.

Prasad, K.S.; Walgma, C. and Krisnan, S. Enhanced electroactivity and substrate affinity of microperoxidase-11 attached to pyrene-linkers π-π stacked on carbon nanostructures electrodes. REC Advances. 2015. 5: 11845-11849.

Prasad, K.S.; Zen, J.M. et al Mediator less catalytic oxidation of NADH at a disposable electrochemical sensor. Sensors and Actuators B. 2007. 123:715-719.

Prasad, K.Sudhakara; Walgama, Charuska and Krishnan, Sadagopan. Enhanced electroactivity and substrate affinity of microperoxidase-11 attached to pyrene-linkers p-p stacked on carbon nanostructure electrodes. RSC Advances. 2015. 5:11845-11849.

Prasad, Sudhakara K.; Muthuraman, Govindan & Zen, Jyh-Myng. The role of oxygen functionalities and edge plane sites on screen-printed carbon electrodes for simultaneous determination of dopamine, uric acid and ascorbic acid. Electrochemistry Communications. 2008. 10: 559–563.

Price, C.P. Point of care testing in diabetes mellitus. Clinical Chemistry Lab. Medicine. 2003. 41:1213-1219.

Pundir, Chandra Shekhar and Chawla, Sheetal. Determination of glycated hemoglobin with special emphasis on biosensing methods. Analytical Biochemistry. 2014. 444: 47-56.

Rahbar, Samuel. An abnormal hemoglobin in red cells of diabetics. Clin. Chim. Acta. 1968. 22(2): 296-298.

Ray, Kenneth III and McCreery, Richard L. Spatially resolved Raman spectroscopy of carbon electrode surfaces: Observations of structural and chemical heterogeneity. Anal. Chem. 1997. 69(22): 4680-4687.

Razmi, Habib and Mohammad-Rezaei, Rahim. Graphene quatum dots as a new substrate for immobilization and direct electrochemistry of glucose oxidase: Application to sensitive glucose determination. Biosensors and Bioelectronics. 2013. 41: 498-504.

Research and Markets Releases Report: The world market for HbA_{1c} tests. Gale OneFile. Dec.2, 2019. Health and Medicine. https://link.gale.com/apps/doc/A607262333/HRCA?u=txshracd2603&sid=HRCA&xid=7db84c8b. Assessed Dec 4, 2019.

Rice, Ronald J. and McCreery, Richard L. Quantitative relationship between electron transfer rate and surface microstructure of laser-modified graphite electrodes. Anal. Chem. 1989. 61(15):1637–1641

Sehat, Ali A.; Khodadadi, Abbas A.; F. Shemirani, Farzaneh and Y. Mortazavi, Yadollah. Fast immobilization of glucose oxidase on graphene oxide for highly sensitive glucose biosensor fabrication. Int. J. Electrochem. Sci. 2014. 10(20145) 272-286.

Selvin, Elizabeth; Steffes, Michael W.; Zhu, Hong et al. Glycated hemoglobin, diabetes, and cardiovascular risk in nondiabetic adults. The New England Journal of Medicine. 2010. 362 (9):800-811.

Shaw, J.E.; Sicree, R.A. And Zimmet, P.Z. Global estimates of the prevalence of diabetes for 2010 and 2030. Diabetes Research and Clinical Practice. 2010. 87:4-14.

Sheikloleslam, Mohammadoli; Pritzker, Mark D. and Chen, Pu. Electrochemical biosensor for glycated hemoglobin (HbA_{1c}), Chapter 13 in Biosensor for health environment and biosecurity. Edited by Prof. Pier Andrea Serra. July 2011.

Sherwani, Shariq I.; Khan, Haseeb A.; Ekhzaimy, Aishah et al. Significance of HbA_{1c} test in diagnosis and prognosis of diabetic patients. Biomarker Insights. 2016. 11:95-104.

Shirale, D.J.; Gade, V.K.; Gaikwad, P.D.; Savale, P.A. et al. Studies of immobilized glucose oxidase on galvanostatically synthesized poly(N-methylpyrrole) film with PVS-$NaNO_3$ composite dopant. Int. J. Electrochemistry Sci. 2006. 1:62-70.

Skoog, Douglas; Holler, F. James and Crouch, Stanley R. Principles of instrumental analysis. Sixth Edition. Thomson Higher Education. 2007.

Song, Seung-Yeon and Yoon, Hyun C. Boronic-acid-modified thin film interface for specific binding of glycated hemoglobin (HbA_{1c}) and electrochemical biosensing. Sensors and Actuators B: Chemical. 2009. 140:233-239.

Sriswasdi, Sira. In-depth analysis of zero-length crosslinking for structural mass spectrometry. University of Pennsylvania, 2013.

Staros, J. V.; Wright, R.W. and Swingle, A. M. Enhancement by N-hydroxysulfosuccinimide of water-soluble carbodiimide-mediated coupling reactions. Anal. Biochem. 1986. 156: 220-222.

Staros, James. A-hydroxysulfosuccinimide active esters: Bis(A-hydroxysulfosuccinimide) esters of two dicarboxylic acids are hydrophilic, membrane-impermeant, protein cross-linkers1. Biochemistry. 1982. 21(17): 3950-3955.

Stokes, A. and Mehta, N. Mortality and excess risk in US adults with pre-diabetes and diabetes: a comparison of two rationally representative cohorts, 1998-2006. Population Health Metrics. 2013. 11:3. doi:10.1186/1478-7954-11-3.

Stollner, Daniela; Stocklein, Wlater; Scheller, Frieder and Warsinke, Axel. Membrane-immobilized haptoglobin as affinity matrix for a hemoglobin-A_{1c} immunosensor. Analytica Chimica Acta. 2002. 470 (2):111-119.

Stutts, Kenneth J.; Kovach, Paul M.; Kuhr, Werner G. and Wightman, R. Mark. Enhanced electrochemical reversibility at heat-treated glassy carbon electrodes. Analytical Chemistry. 1983. 55(9):1632-1634.

Takada, T.; Nakahara, M.; Kumagai, H. and Sanada, Y. Surface modification and characterization of carbon oxygen plasma. Carbon. 1996. 34(9): 1087-1091.

Takahashi, Shigehiro and Anzai, Jun-ichi. Phenylboronic acid monolayer-modified electrodes sensitive to sugars. Langmuir. 2005. 21(11):5102-5107.

Tang, Zuping MD; Du, Xiaogu et al. Effects of pH on glucose measurement with handheld glucose meters and a portable glucose analyzer for point-of-care testing. Archives of Pathology & Laboratory Medicine. 2000. Vol. 124. No. 4:577-582.

Tang, Zuping MD; Louie, Richard F.; Lee, Judith H. et al. Oxygen effects on glucose meter measurements with glucose dehydrogenase and oxidase-based test strips for point-of-care testing. Crit. Care Medicine, 2001. Vol. 29 No.5 1062-1070.

Tandon, Nikhil; Ali, Mohammed K. and Narayan, K.M. Venkat. Pharmacologic prevention of microvascular and macrovascular complications in diabetes mellitus implications of the results of recent clinical trials in type 2 diabetes. Am. J. Cardiovasc. Drugs. 2012. 12(1):7-22.

Technavio. Global blood glucose monitoring devices market 2017-2021. Feb. 2017.

Terse-Thakoor, T.; Komori, K.; Ramnani, P.; Lee, I. and Mulchandani, A. Electrochemically functionalized seamless three-dimensional graphene-carbon nanotube hybrid for direct electron transfer of glucose oxidase and bioelectrocatalysis. Langmuir. 2015. 31:13054-13061.

Thermo Fisher Scientific. Web assessed Dec. 2017

Thiyagarajan, N.; Chang, J-L.; Senthilkumar, K and Zen, J-M. Disposable electrochemical sensor: A mini review. Electrochemistry Communications. 2014. 38: 86-90.

UK prospective diabetes study (UKPDS) group. Intensive blood glucose control with sulphonylureas or insulin compared with conventional treatment and risk of complications in patients with type 2 diabetes (UKPDS 33). Lancet. 1998. 352 (9131): 837-853.

Umam, K. Saepudin, E and Ivandini, TA. Preparation of hemoglobin-modified boron-doped diamond for acrylamide biosensors. Int. symposium current progress in functional materials. 2017. 188:012006. doi:10.1088/1742-6596/755/1/011001

U.S. Department of health and human services. Food and Drug Administration. Center for devices and radiological health office of in vitro diagnostics and radiological. Health Division of chemistry and toxicology devices. Blood glucose monitoring test systems for prescription point-of-care use. October 11,2016.

U.S. Department of Health and Human Services. Food and Drug Administration. Center for devices and radiological health office of in vitro diagnostics and radiological. Health division of chemistry and toxicology devices. Self-monitoring blood glucose test systems for over-the-counter use. Draft guidance for industry and food and drug administration staff. Nov. 30, 2018.

U.S. Preventive Services Task Force. Screening for type 2 diabetes mellitus in adults. U.S. Preventive services task force recommendation statement. Annals of Internal Medicine. 2008. 148 (11). **http://www.uspreventiveservicestaskforce.org/uspst08/type2/type2rs.htm.**

Unnikrishnan, Binesh; Palanisamy, Selvakumar and Chen, Shen-Ming. A simple electrochemical approach to fabricate a glucose biosensor based on graphene-glucose oxidase biocomposite. Biosensors and Bioelectronics. 2013. 39:70-75.

Upadhyay P. K. A simple procedure for activating a glassy carbon electrode. J. Electroanal. Chem. 1989. 271(1-2):339–343.

Vedasri, Vedharathinam. Electroanalytical techniques. (Chronoamperometry/chronoculometry). Center for electrochemical engineering research. RUSS college of engineering and technology. Ohio University. July12, 2011.

Vijan, S. Type 2 DM. Annals of Internal Medicine. March. 2010. Mar. 2:150(5).

Wang, Jen-Yuan; Chou, Tse-Chuan et al. Using poly (3-aminophenylboronic acid) thin film with binding-induced ion flux blocking for amperometric detection of hemoglobin A_{1c}. Biosensors and Bioelectronics. 2015. 63:317-324.

Wang, Jianxiu; Li Meixian; Shi, Zujin et al. Direct electrochemistry of cytochrome C at a glassy carbon electrode modified with single wall carbon nanotubes. Analytical Chemistry. 2002. 74:1993-1997.

Wang, Joseph. Analytical Electrochemistry. Third edition. John Wiley & Sons Inc. New Jersey.2006.

Wang, Joseph. Electrochemical glucose biosensors. Chemical Rev.2008. 108:814-825.

Wang, Joseph; Musameh, Mustafa et al. Solubilization of carbon nanotubes by Nafion toward the preparation of amperometric biosensors. JACS. 2003. 125:2408-2409.

Wang, Qi; Kaminska, Izabela et al. Sensitive sugar detection using 4-aminophenylboronic acid modified graphene. Biosensors and Bioelectronics. 2013. 50:331-337.

Wang, Quan; Zhang, Ruirui; You, Guoxing; Hu, Jilin et al. Influence of polydopamine-mediated surface modification on oxygen-release capacity of haemoglobin-based oxygen carriers. Artificial cells, Nanomedicine and Biotechnology. 2018. Vol. 46. No. S2. S484-S492.

Wang, Ziyi; Liu Shuna et al. Detection of glucose based on direct electron transfer reaction of glucose oxidase immobilized on highly ordered polyaniline nanotubes. Analytical Chemistry 2009. Vol.81. (4):1638-1645.

Ward, Colin. Glucose transport. Diapedia. 2015. 5104085195. Rev. No.33. https://doi.org/10.14496/dia.5104085195.33 (Assessed in Nov. 2019).

Walsh, John; Roberts, Ruth; Vigersky, Robert A. and Schwartz, Frank. New criteria for assessing the accuracy of blood glucose monitors meeting, October 28, 2011. J. Diabetes Sci. Technol. 2012. 6:466-474.

Whitley, Heather P.; Yong, Ee V. and Rasinen, Casey. Selecting an A1C point-of-care instrument. Diabetes Spectrum. 2015: 28(3): 201-208.

WHO/IDF. Definition and diagnosis of DM and intermediate hyperglycemia. WHO. 2006. p21.

Willner, I.; Baron, R. and Willner, B. Integrated nanoparticle-biomolecule systems for biosensing and bioelectronics. Biosens. Bioelectron. 2007. 22 (9-10):1841-1852.

Wilson, R. and Turner, A.P.F. Glucose oxide: an ideal enzyme. Biosensors & Bioelectronics, 1992. 7:165-185.

Wise, Jacqui. Diabetes is rising in OECD countries, report warns. BMJ. June 2015. 350:h3293.

Woo, Taeha; Huh, Jin Young and Nikles, David E. Surface chemistry and dispersion of magnetic pigment for a solvent less process. IEEE Trans. Magn. 2001. Vol. 37 No. 4:1634-1636.

World health organization (WHO). Diabetes in 2018. Global report on diabetes. Assessed in May 2019.

World health organization consultation. Use of glycated haemoglobin (HbA_{1c}) in the diagnosis of diabetes mellitus. Diabetes Research and Clinical Practice. 2011. 93:299-309.

Wu, Ming-Sieng; Wen, Ten-Chin and Gopalan, A. Electrochemical copolymerization of diphenylamine and anthranilic acid with various feed ratios. Journal of The Electrochemical Society. 2001.148. (5): D65-D73.

Wu, Yunhua and S. Hu, Shengshui. Direct electrochemistry of glucose oxidase in a colloid Au-dihexadecylphosphate composite film and its application to develop a glucose biosensor. Bioelectrochemistry. 2007. 70: 335-341.

Xie, Ying-bo; Qiao, Wen-ming et al. Effect of the surface chemistry of activated carbon on its electrochemical properties in electric double layer capacitors. New Carbon Materials. 2010. 25(4):248-254.

Xu, Zhifeng; Ahsan Uddin, Khan Mohammed et al. Fluorescent boronic acid polymer grafted on silica particles for affinity separation of saccharides. ACS Applied Materials & Interfaces. 2014. 6: 1406-1414.

Yang, Ting-Hao; Hung, Chi-lung et al. An electrochemically pre-anodized scree-printed carbon electrode for achieving direct electron transfer to glucose oxidase. Electrochemistry Communications. 2008. 10: 1094-1097.

Yang, Ting-Hao; Hung, Chi-Lung; Ke, Jyh-Harng and Zen, Jyh-Myng. An electrochemically preanodized screen-printed carbon electrode for achieving direct electron transfer to glucose oxidase. Electrochemistry Communications. 2008. 10:1094-1097.

Yazdanpanah, Sara; Rabiee, Mohammad; Tahriri, Mohammadreza et al, Glycated hemoglobin-detection methods based on electrochemical biosensors. Trends in Analytical Chemistry. 2015. 72. 53-67.

Yoo, Eun-Hyung and Lee, Soo-Youn. Glucose biosensors: An overview of use in clinical practice. Sensors. 2010. 10:4568-4576. Doi:10.3390/s100504558

Zen, Jyh-Myng; Chung, Hsieh-Hsun; Ilangovan, G. and Kumar, A.S. Electrochemical impedance study and sensitive voltammetric determination of Pb (II) at electrochemically activated glassy carbon electrodes, Analyst. 2000. 125: 1139–1146.

Zhang, H.; Meng, Z.; Wang, Q. and J. Zheng, J. A novel glucose biosensor based on direct electrochemistry of glucose oxidase incorporated in biomediated gold nanoparticles-carbon nanotubes composite film. Sensors and Actuators B: Chemical. 2011. 158: 23-27.

Zhang, Honghua and Coury Louis A. Effects of high-intensity ultrasound glassy carbon electrodes. Anal Chem. 1993. 65(11):1552–1558.

Zhang, Jingdong and Oyama, Munetaka. A hydrogen peroxide sensor based on the peroxidase activity of hemoglobin immobilized on gold nanoparticles-modified ITO electrode. Electrochim. Acta 2004. 50((1): 85−90.

Zhang, Xuanping; Gregg, Eduard W.; Williamson, David F. et al. A1C level and future risk of diabetes: a systematic review. Diabetes Care, 2010: 33. (8):1665-1673.

Zhao, Hua-Zhang; Sun, Juan-Juan; Song, Juan and Yang, Qin-Zheng. Direct electron transfer and conformational change of glucose oxidase on carbon nanotube-based electrodes. Carbon, 2010. 48:1508-1514.

Zhou, Yanli; Dong, Hui et al. A novel potentiometric sensor based on a poly (anilneboronic acid)/graphene modified electrode for probing sialic acid through boronic acid-diol recognition. Biosensors and Bioelectronics. 2014. 60:231-236.

Zhou, Yanli; Dong, Hui et al. Fabrication of electrochemical interface based on boronic acid-modified pyrroloquinoline quinine/reduced graphene oxide composites for voltammetric determination of glycated hemoglobin. Biosensors and Bioelectronics. 2015. 64:442-448.

Zhou, Yanli; Dong, Hui, Liu, Lantao et al. Fabrication of electrochemical interface based on boronic acid-modified pyrroloquinoline quinine/reduced graphene oxide composites for voltammetric determination of glycated hemoglobin. Biosensors and Bioelectronics. 2015. 64: 442-448.

ABBREVIATIONS

A_{1c}DAG	A_{1c}-derived average glucose
AA	ascorbic acid
AACC	American association clinical chemistry
AAP	acetaminophen
ADA	American diabetes association
APBA	amino phenyl boronic acid
BET	Bernauer-Emmett-Teller
BGMS	blood glucose monitoring system
CA	chronoamperometry
CAGR	compound annual growth rate
CAP	college of American pathologists
CCP	cytochrome c-peroxidase
CDC	Center for disease control and prevention
CE	counter electrode
CMC	1-cyclohexyl-3-(2-morpholinoethyl) carboiimide
CNDO	complete neglected of differential overlap
CNTs	carbon nanotubes
CPRL	central primary reference laboratory
CV	cyclic voltammetry
CVD	cardiovascular disease
DCC	dicyclohexyl cardodiimide
DCCT	diabetes control and complications trial
DET	direct electron transfer
Dend-FPBA	dendrimer layer 4-formil-phenyl-boronic acid
DIC	diisopropyl carbodiimide
DOCA	deoxycholate
DPA	diphenylamine
EDC	1-ethyl-3-(3-dimethylaminopropyl) carbodiimide hydrochloride
EDIC	epidemiology of intervention and diabetes complications

FAD	flavin adenine dinucleotide, oxidized form
$FADH_2$	flavin adenine dinucleotide, reduced form
FAO	fructosyl amino acid oxidase
FBPA	4-formyl-phenyl-boronic acid
FcBA	ferrecene-boronic acid
FDA	The food and drug administration
FPG	fasting blood glucose
FTIR	Fourier transform infrared
FV	fructosyl valine
GC	glassy carbon
GCE	glassy carbon electrode
GDH	glucose dehydrogenase
GDH-PQQ	glucose-1-dehydrogenase-pyrroloquinoline quinone
GM	blood glucometer
GOX	glucose oxidase
HbA	hemoglobin A
HbF	fetal hemoglobin
HCGO	highly concentrated graphene oxide
HCT	hematocrit
HOPG	highly ordered pyrolytic carbon electrode
HPLC	high performance liquid chromatography
HRP	horseradish peroxidase
IFCC	international federation of clinical chemistry and laboratory medicine
IUPAC	international union of pure and applied chemistry
LA	lactic acid
MBA	4-mercaptobenzoic acid
MBG	mean blood glucose
MPBA	ω-mercapto-phenylboronic acid
MWCNTs	multi-walled carbon nanotubes
NGSP	National glycohemoglobin standardization program
NHS	N-hydrosuccinimide or 1-hydroxy-2-5-pyrrolidinedione

OECD	Organization of economic cooperation and development
OGTT	oral glucose tolerance test
PAPBA	poly (3-amino-phenil boronic acid)
PA-PPE	pre-anodized printer paper electrode
PBA-PQQ	phenyboronic acid-modified pyrroquinoline quinine
PDPA	poly(diphenylamine)
PG	plasma glucose
POC	point-of-care
PPE	printer paper electrode
PPQ-FAD	pyrroquinoline quinone-flavin adenine dinucleotide
RE	pseudo-reference electrode
RGO	reduced graphene oxide
SA	salicylic acid
SAM	self-assembled monolayer
SMBG	self-monitoring blood glucose
SPCE*	pre-anodized screen-printed carbon electrode
SRL	secondary reference laboratory
SWCNTs	single-walled carbon nanotubes
SWV	square-wave voltammetry
T3BA	thiophene-3-boronic acid
TBA	p-benzoic acid
TBO	toluidine blue O
UA	uric acid
UKPDS	United Kingdom prospective diabetes study
WE	working electrode
WHO	World health organization
XPS	X-ray photoelectron spectroscopy
ZnONPs/PPy	zinc oxide nanoparticles/polypyrrole

APPENDICES

Appendix 1.

1.1. Criteria for the diagnosis of diabetes (ADA, 2019)

*Fasting plasma glucose (FPG) ≥126 mg/dL (7.0 mmol/L). Fasting is defined as no caloric intake for at least 8 h.**

OR

*2-h Plasma glucose (PG) ≥200 mg/dL (11.1 mmol/L) during oral glucose tolerance test (OGTT). The test should be performed as described by the WHO, using a glucose load containing the equivalent of 75-g anhydrous glucose dissolved in water. **

OR

A1C ≥6.5% (48 mmol/mol).

*The test should be performed in a laboratory using a method that is NGSP certified and standardized to the DCCT assay. **

OR

In a patient with classic symptoms of hyperglycemia or hyperglycemic crisis, a random plasma glucose ≥200 mg/dL (11.1 mmol/L).

**In the absence of unequivocal hyperglycemia, diagnosis requires two abnormal test results from the same sample or in two separate test samples*

1. 2. Criteria defining prediabetes. *** (ADA, 2019)**

Fasting plasma glucose (FPG) 100 mg/dL (5.6 mmol/L) to 125 mg/dL (6.9 mmol/L) (IFG)

OR

2-h plasma glucose (PG) during 75-g oral glucose tolerance test (OGTT) 140 mg/dL (7.8 mmol/L) to 199 mg/dL (11.0 mmol/L) (IGT)

OR

A1C 5.7–6.4% (39–47 mmol/mol)

**For all three tests, risk is continuous, extending below the lower limit of the range and becoming disproportionately greater at the higher end of the range.*

1. 3. Criteria for testing for diabetes or prediabetes in asymptomatic adults

1. Testing should be considered in overweight or obese (BMI ≥25 kg/m2 or ≥23 kg/m2 in Asian Americans) adults who have one or more of the following risk factors:

- *First-degree relative with diabetes*
- *High-risk race/ethnicity (e.g., African American, Latino, Native American, Asian American, Pacific Islander)*
- *History of CVD*
- *Hypertension (≥140/90 mmHg or on therapy for hypertension)*
- *HDL cholesterol level <35 mg/dL (0.90 mmol/L) and/or a triglyceride level >250 mg/dL (2.82 mmol/L)*
- *Women with polycystic ovary syndrome*

- *Physical inactivity*
- *Other clinical conditions associated with insulin resistance (e.g., severe obesity, acanthosis nigricans)*

2. Patients with prediabetes (A1C ≥5.7% [39 mmol/mol], IGT, or IFG) should be tested yearly.
3. Women who were diagnosed with GDM should have lifelong testing at least every 3 years.
4. For all other patients, testing should begin at age 45 years.
5. If results are normal, testing should be repeated at a minimum of 3-year intervals, with consideration of more frequent testing depending on initial results and risk status.

Table. 1. 4. Glucose meters accuracy standards. (ADA, 2019, FDA, 2018)

Table 7.1—Comparison of ISO 15197 and FDA blood glucose meter accuracy standards

Setting	FDA[125,126]	ISO 15197-2013[127]
Home use	95% within 15% for all BG in the usable BG range† 99% within 20% for all BG in the usable BG range†	95% within 15% for BG ≥100 mg/dL 95% within 15 mg/dL for BG <100 mg/dL 99% in A or B region of Consensus Error Grid‡
Hospital use	95% within 12% for BG ≥75 mg/dL 95% within 12 mg/dL for BG <75 mg/dL 98% within 15% for BG ≥75 mg/dL 98% within 15 mg/dL for BG <75 mg/dL	

BG, blood glucose. To convert mg/dL to mmol/L, see http://www.endmemo.com/medical/unitconvert/Glucose.php. †The range of BG values for which the meter has been proven accurate and will provide readings (other than low, high, or error). ‡Values outside of the "clinically acceptable" A and B regions are considered "outlier" readings and may be dangerous to use for therapeutic decisions[128].

Appendix 2. HbA_{1c}.

2. 1. Discovery of HgA1c and its sequential utility in the medical clinic.

- *1958: Allen et al, demonstrated the heterogeneity of the human hemoglobin (Hb).*
- *1958: Huisman, T.H.J. and Meyering, C.A. Isolate three different hemoglobin fractions, including the isolation of Hemoglobin $A_{1c.}$*
- *1966: Holmquist, W.R. and Schroeder, W.A. identify five subtypes of hemoglobin A, including HbA_{1c}.*
- *1968: Bookchin, R.M. and Gallop, P.M. Identify the structure of HbA_{1c} as a glycoprotein,*
- *1968: Rahbar, S. discovers that HbA_{1c} percentage for this fraction is elevated in patients with diabetes.*
- *1976: Bunn, H.F. characterizes the biosynthesis in formation of HbA_{1c}*
- *1976: Koenig, R.J and Cerami, A. propose HbA_{1c} as an indicator for blood glucose levels in diabetes*
- *1977: measured of Total HbA1 introduced in routine clinical laboratories as a tool for monitoring diabetes.*
- *1995: Diabetes control and complications trial research group (DCCT), establishes significance of HbA_{1c} as a clinical marker in type-1 diabetes.*
- *1998: United Kingdom prospective diabetes study (UKPDS), sets the relationship between HbA_{1c} y frequency of microvascular complications in patients with type 2 diabetes.*
- *2007: NGSP recommendations for the standardization criteria of HbA_{1c} assays indicate average blood glucose.*
- *2010: WHO, ADA, validate HbA_{1c} as diagnostic test for diabetes and prediabetes*

Allen, David W.; Schroeder, W. A., and Balog, Joan. Observations on the chromatographic heterogeneity of normal adult and fetal human hemoglobin: A study of the effects of crystallization and chromatography on the heterogeneity and isoleucine content. J.Am.Chem. Soc. 1958. 80: 1628-1634.

Bunn, H. F., D. N. Haney, K. H. Gabbay, and P. M. Gallop. Further identification of the nature and linkage of the carbohydrate in hemoglobin Al. Biochem. Biophys. Res. Commun. 1975; 67: 103-109

Bunn, H.F., D.N. Haney, S. Kamin, K.H. Gabbay, and P.M. Gallop. 1976. The biosynthesis of human hemoglobin A1c. Slow glycosylation of hemoglobin in vivo. J. Clin. Invest. 1976; 57:1652–1659

DCCT Research Group. The association between glycemic exposure and long-term diabetes complications in the diabetes control and complications trial. Diabetes 1995; 44 (8): 968–983.

Gallop, P.M., and Paz, M.A. Posttranslational protein modifications, with special attention to collagen and elastin. Physiol. Rev. 1975. 55 (3):418-487.

Gebel, Erika. The start of something good: the discovery of HbA1c and the American diabetes association Samuel Rahbar outstanding discovery award. Diabetes Care. 2012. 35 (12):2429–2431.

Gillery, Philippe. A history of HbA_{1c} through clinical chemistry and laboratory medicine. Clinical Chemistry and Laboratory Medicine. 2012.51(1):65–74.

Holmquist, W.R. and Schroeder, W.A. The in vitro biosynthesis of hemoglobin A_{lc}*. Biochemistry. 1966. Vol. 5 (8):2504-2512.

Holmquist, W.R., and W.A. Schroeder.1966. A new N-terminal blocking group involving a Schiff base in hemoglobin A_{1c}. Biochemistry. 5:2489-2503.

Huisman, THJ and Meyering, CA. Studies on the heterogeneity of hemoglobin: I. the heterogeneity of different human hemoglobin types in carboxymethylcellulose and in Amberlite IRC-50 chromatography: qualitative aspects. Clinica Chimica Acta. 1960. 5:103– 2 3.

John, W. Garry; Mosca, Andrea; Weykamp, Cas and Goodall, Ian. HbA_{1c} standardization: history, science and politics. Clin. Biochem. Rev. 2007. Vol. 28 163-168.

Koenig, Ronald J, Peterson, Charles M.; Kilo, Charles; Cerami, Anthony and Williamson, Joseph R. Hemoglobin A_{1c} as an indicator of the degree of glucose intolerance in diabetes. Diabetes. 1976. 25(3):230-232.

Koenig, R.J, Peterson, C.M, Jones, R.L, Saudek, C.; Lehrman, M. and Cerami, A. Correlation of glucose regulation and hemoglobin A_{1c} in diabetes mellitus. N. Engl. J. Med. 1976; 295 (8): 417–20

Rahbar S. An abnormal hemoglobin in red cells of diabetics. Clinica Chimica Acta. 1968. 22(2):296-298.

UK Prospective Diabetes Study (UKPDS) group. Intensive blood glucose control with sulphonylureas or insulin compared with conventional treatment and risk of complications in patients with type 2 diabetes (UKPDS 33). Lancet. 1998. 352 (9131): 837-853.

2. 2. The relationship between HbA1c results from the NGSP network (%HbA1c) and the IFCC network (mmol/mol) and calculations:

Type of Patient	NGSP Value	IFCC Value
Non-diabetic (normal)	<5.7 %	<39 mmol/mol
Diabetic	6.5% or higher	48 mmol/mol or higher
High risk developing diabetes	5.7% – 6.4%	39-46 mmol/mol

NGSP – National glycohemoglobin standardization program
IFCC – International federation of clinical chemistry
HgbA1c (IFCC) SI units mmol/mol = {[HgbA1c (NGSP) unit in % x 10.93] – 23.50}
(IFCC)A1c (mmol/mol) = [(NGSP)A1c (%) – 2.15] x 10.929

NSGP (%) = 0.09148 x IFCC (mmol HbA1c / mmol Hb) = 2.512

The equation to calculate eAG (in mg/dL) from hemoglobin A1c (in %) is as follows:

eAG (mg/dL) = [28.7 x (NGSP)A1c (%)] – 46.7 or eAG (mg/dL) = (28.7 x HbA1c%) – 46.7

Table A1.2 Relationships between NGSP, IFCC and eAG.

HbA1c		eAG	
%	mmol/mol	mmol/L	mg/dL
5	31	5.4	97
6	42	7	126
7	*53*	*8.6*	*154*
8	64	10.2	183
9	75	11.8	212
10	86	13.4	240
11	97	14.9	269
12	108	16.5	298
13	119	18.1	326
14	130	19.7	355
15	140	21.3	384
16	151	22.9	413
17	162	24.5	441
18	173	26.1	470
19	184	27.7	499

Diabetes UK. Assessed May 2020.

Hanas, Ragnar MD. And John, Garry. 2010 consensus statement on the worldwide standardization of the hemoglobin A1C measurement. Diabetes Care. 2010. Vol. 33 (8): 1903-1904.

Hanas, R. MD and John, W.G. MD. 2013 Update on the worldwide standardization of the hemoglobin A_{1c} measurement. Pediatric diabetes. 2013. doi: 10.1111/pedi.12047

NGSP. International federation of clinical chemistry (IFCC) standardization of HbA_{1c}. (Assessed November 2019).

Nathan David M.; Kuenen, Judith; Borg, Rikke; Zheng, Hui; Schoenfeld, David and Heine, Robert J. Translating the A1Cassay into estimated average glucose values. Diabetes Care. 2008. 31:1473–8.

2. 3. Recommendations for HbA1c testing (ADA, 2018 & 2019).

- Perform the A_{1C} test at least two times a year in patients who are meeting treatment goals (and who have stable glycemic control). E
- Perform the A_{1C} test quarterly in patients whose therapy has changed or who are not meeting glycemic goals. E
- Point-of-care testing for A_{1C} provides the opportunity for more timely treatment changes. E

American Diabetes Association. Glycemic targets: Standards of medical care in diabetes-2018. Diabetes Care. 2018. 42 (suppl. 1): S61-S70. https://doi.org/10.2337/dc18-S006.

American Diabetes Association. Glycemic targets: Standards of medical care in diabetes-2019. Diabetes Care. 2019. 42(suppl. 1): S61-S70. https://doi.org/10.2337/dc19-S006.

2. 4. The following prerequisites for the introduction of an HbA_{1c}-POC instrument should be met to ensure optimal POC testing: (Lenters-Westra et al, 2012)

(1) HbA_{1c}-POC instruments should fall under responsibility of the central laboratory and (2) acceptable analytical performance (ideally: no bias, coefficient of variation < 3.0% (based on IFCC numbers), < 2.0% (based on DCCT numbers)). Validation of the POC instrument by central laboratory.
(2) connectivity to the central Laboratory for data management.
(3) education and training for users should be done by experienced POC coordinators (e-learning).
(4) only accredited users should be allowed to use the instrument.
(5) internal and external quality control should be coordinated by a POC coordinator.
(6) ordering and control of reagent/cartridges should also be done by a POC coordinator (check of new lot number).
(7) once a year the patients HbA_{1c} should be analyzed with the central laboratory method.

Lenters-Westra, Erna; Schindhelm, Roger K; Bilo, Henk J. and Slingerland, Robbert J. Haemoglobin A_{1c}: Historical overview and current concepts. Diabetes research and clinical Practice. 2013. 99: 75-84.

Appendix 3. HbA_{1c}.

Table 1
Comparison of analytical properties of amperometric FV and HbA1c biosensors.

Sample number	Type of biosensor	Support of immobilization	Working voltage (V)	Response time (s)	Optimal pH	Optimal temperature (°C)	Linear range (mM)	Detection limit (mM)	Sensitivity ($\mu A\ mM^{-1}\ cm^{-2}$)	CV (%)	Reference
1	Amperometric	FAO/membrane/ Pt electrode	0.6	ND	7.0–7.5	30–45	0.05–1.8	0.05	0.42	ND	[17]
2	Amperometric	PVI polymer onto carbon paste electrode	0.1	ND	ND	ND	20–700	20	0.135	ND	[18]
3	Amperometric	PB film/ electrode	−0.05	ND	ND	ND	0.1–0.3	0.1	0.42	ND	[19]
4	Amperometric	FAO/PVA–SbQ on oxygen electrode	0.6	ND	7.0	25	0.2–10.0	0.2	0.0046	ND	[20]
5	Amperometric	FAO/iridium modified carbon electrode	0.25	120	7.0	25	0.2–2.0	0.2	21.5	ND	[21]
6	Nonenzymatic	Glassy carbon microparticle carbon paste/ ITO	1.0	40	7.4	35	0–1.0	0.05	5.26	ND	[22]
7	Amperometric	FAO/core–shell MNPs/Au electrode	0.25	4	7.5	35	0.1–2.0	0.1	35.72	2.58–5.63	[12]
8	Nonenzymatic	FcBA/GCPE	0.1	10	7.4	25	0.5–4.0	0.5	5.9	ND	[23]
9	Amperometric	ZnONPs/PPy/Au electrode	0.27	2	7.0	35	0.1–3.0	0.05	38.42	1.58–2.07	[10]
10	Amperometric	Haptoglobin/ CDI-activated cellulose membranes	0.6	ND	ND	ND	0.78×10^{-5} to 3.9×10^{-5}	ND	ND	0.9–3.3	[25]
11	Amperometric	FcBA/ZrO_2NPs/ PGE	0.299	1800	8.0	22	6.8–14.0%	ND	ND	12.7	[26]
12	Amperometric	APBA/GO/GCE	0.2	ND	8.0	ND	ND	ND	ND	ND	[27]

Note. PVI, polyvinylimidazole; PB, Prussian blue; PVA–SbQ, poly(vinylalcohol)-Stylbazole; ITO, indium tin oxide; MNPs, magnetic bionanoparticles; Au, gold; ZnONPs, zinc oxide nanoparticles; CDI, 1,1′-carbonyldiimidazole; ZrO_2NPs, zirconium dioxide nanoparticles; PGE, pyrolytic graphite electrode; GO, graphene oxide; GCE, glassy carbon electrode; ND, not detected.

Pundir, Chandra S and Chawla, Sheetal. Determination of glycated hemoglobin with special emphasis on biosensing methods. Analytical Biochemistry. 2014. 444:47-56. Permission received to publish tables.

Table 1
Point-of-care A1c devices.[a]

Point-of-care instruments for A1c tests	Manufacturer	Types of methods/assay time (min)	Detection range and coefficient variants (CV)
In2it*	Bio-rad, California	Affinity separation/10 min	HbA1c (10 μL whole blood): 4% to 14% (20 mmol/mol to 130 mmol/mol), CV 2.4–3.9% [56]
DCA vantage*	Siemens Medical Solutions Diagnostics, New York	Immunoassays/6 min	HbA1c (1 μL whole blood): 2.5% to 14% (4 mmol/mol to 130 mmol/mol) [57], CV <3% [49]
Afinion*	Axis-Shield, Norway	Affinity separation/3 min	HbA1c (1.5 μL whole blood): 4% to 15% (20 mmol/mol to 140 mmol/mol), CV <3% [58]
Nyocard	Axis-Shield, Norway	Affinity separation/3 min	HbA1c (5 μL whole blood): 4% to 15% (20 mmol/mol to 140 mmol/mol)[58], CV <5% [60]
GDX/Micromat II*	Bio-Rad, California	Affinity separation/5 min	HbA1c (10 μL whole blood): 4% to 15% (20 mmol/mol to 140 mmol/mol), CV 2.93–4.65% [61]
Clover	Infopia, Korea	Affinity separation/5 min	HbA1c (4 μL whole blood): 4% to 14% (20 mmol/mol to 130 mmol/mol), CV <3% [62]
InnovaStar	DiaSys, Germany	Agglutination/7 min	HbA1c: 4% to 15% (20 mmol/mol to 140 mmol/mol), CV <3% [63]
A1CNow+*	Metrika, Bayer, California	Immunoassay/5 min	Accurate between 7% and 8.5% (53 mmol/mol to 69 mmol/mol) [55]
Quo-test	Quotient Diagnostics, UK	Affinity separation/4 min	HbA1c: 4% to 15% (20 mmol/mol to 140 mmol/mol), CV <3% [64]

[a] Point-of-care (POC) devices play very significant role in aiding the patience compliance of self-monitoring and also allow the practitioners to perform routine checking in situ on patients who are not convenient in moving around for blood testing. POC analyzers which are in par with laboratory machineries in HbA1c testing provide a more practical way for better clinical monitoring in order to perform better personalized treatments (*CLIA-waived POC technologies [53]).

Ang, Shu Hwang; Thevarajah, M. Alias, Yatimah and Khor, Sook Mei. Current aspects in hemoglobin A_{1c} detection A review. Clinica Chimica Acta. 2015. 439: 202-211. Permission received to publish tables

Table S1. A partial list of the electrochemical Hb_{A1c} sensors.

Electrode	Method	Sensing Target	Key species (redox mediator, enzyme)	Linear range
AuNPs/GCE	impedance (R_{ct} change)	Hb_{A1c}	$Ru(NH_3)_6^{3+}/Ru(NH_3)_6^{2+}$	0–23.3%
T3BA[1]/Au	impedance (R_{ct} change)	Hb_{A1c}	$Fe(CN)_6^{3-}/Fe(CN)_6^{4-}$	4–12%
T3BA/Au	impedance (capacitance change)	Hb_{A1c}	no redox mediator or enzyme	10–100 ng/μl
PPy[2]–AuNPs/Au	potentiometric	Hb_{A1c}	Ppy, Hb_{A1c} antibody	4–18 μg/ml
GCE	potentiometric	Hb_{A1c}	alizarin red s (ARS)	5.0–50 μg/ml
FAO/ZnONPs/Ppy/Au	amperometric (CV)	Fructosyl valine	$Fe(CN)_6^{3-}/Fe(CN)_6^{4-}$, FAO	0.1–3.0 mM
PVI-FAO[3]/CPE[4]	amperometric	Fructosyl valine	m-PMS[5], FAO	20 μM–0.7 mM
PVA-FAO/Pt	amperometric (FIA)	Fructosyl valine	FAO	0.2–10 mM
FAO/FeNPs/Au	amperometric (CV)	Fructosyl valine	$Fe(CN)_6^{3-}/Fe(CN)_6^{4-}$, FAO	0.1–2.0 mM
GCE	amperometric	Fructosyl valine	FcBA[6]	0.1–4.0 mM
platinum	amperometric	Hb_{A1c}	glucose oxidase horseradish peroxidase Anti-Hb antibody	5–20%
ZrO_2/DDAB[7]/PGE[8]	amperometric	Hb_{A1c}	FcBA	6.8–14.0%
Si/Au-Cys-$FPBA_2$[9]	amperometric	Hb_{A1c}	ferrocenemethanol, glucose oxidase	4.5–15.0%
APBA/pTTBA[10]/AuNPs/SPCE	amperometric	Hb_{A1c}	H_2O_2	0.1–1.5%
PAPBA/SPCE	amperometric	Hb_{A1c}	PAPBA on the eletrode	0.975–156 μM

[1]T3BA: thiophene-3-boronic acid; [2]PPy: polypyrrole; [3]FAO:fructosylamine oxidases; [4]CPE: carbon paste electrode; [5]m–PMS: 1-methoxyphenazinemethosulphate; [6]FcBA: Ferrocene boronic acid; [7]DDAB: didodecyldimethylammonium bromide ; [8]PGE: pyrolytic graphite

Wang, Jen-Yuan; Chou, Tse-Chuan et al. Using poly (3-aminophenylboronic acid) thin film with binding-induced ion flux blocking for amperometric detection of hemoglobin A_{1c}. Biosensors and Bioelectronics, 2015. 63:317-324. Permission received to publish tables.

Table 2
HbA1c biosensors.[a]

Compound detected	Characteristics	Types of biosensors	Detection range/limits	Sensitivity	Limitations
Fructrosyl valine (FV)	-Detect: End product from decomposition of glycated hexapeptides -Biological recognition element: Enzyme fructosyl amine oxidase (FAO)	Electrochemical (amperometric) with magnetic nanoparticles	-Detection range: 0 to 2 mM FV -Detection limit: 0.1 mM for FV (Chawla et al., 2011) [74]	Not available	-Lack of reproducibility and stability
		Electrochemical (amperometric) with zinc oxide nanoparticles–polypyrrole film	-Detection range: 0.1 to 3 mM FV -Detection limit: 50 uM FV (Chawla et al., 2012) [73]	38.42 μA/mM	
		Disposable iridium-modified electrochemical biosensor (amperometric)	-Detection range: 0 to 2 mM of FV -Detection limit: Not available (Fang et al., 2008) [72]	21.5 μA/mM cm^2	
Glycated hemoglobin (HbA1c)	-Detect: HbA1c -Biological recognition element: Anti-HbA1c antibody	Electrochemical (potentiometric) immunosensors with mixed SAMs wrapped nano-spheres array	-Detection range: 50 to 170.5 ng/mL HbA1c -Detection limit: Not available (Xue et al., 2010) [67]	94.73 μV/(ng/mL)	-Reproducibility is of concern
	-Detect: Fc-IgG-HbA1c immunocomplexes -Biological recognition element: anti-HbA1c antibody	On-chip electrochemical flow immunoassay	-Detection range: up to 500 μg/mL -Detection limit: Not available (Tanaka et al., 2007) [75]	Not available	-Laborious pretreatment
	-Detect: HbA1c -Biological recognition element: Anti-HbA1c antibody Boronic acid-based HbA1c Biosensors	Sandwich immunoassays on polydimethylsiloxane-based antibody microarrays	-Detection range: 10–100 ng/mL -Detection limit: 3.58 ng/mL (Chen et al., 2012) [68]	4–5 orders of magnitude higher	-Long incubation time (2 h)
	Detect: HbA1c -Biological recognition element: Ferroceneboronic acid	Electrochemical (piezosensor) immunoassay	-Detection range: 0 to 20% -Detection limit: >5% (standard deviation 20%) (Halamek et al., 2007) [76]	Not available	-Low sensitivity -Low specificity
	-Detect: HbA1c -Biological recognition element: Ferroceneboronic-acid labeled anti-HbA1c antibody	Electrochemical (piezosensor) immunoassay	-Detection range: 4 to 13% -Detection limit: Not available (Halamek et al., 2007) [66]	Sensitivity was increased at three fold compared to without antibodies (Halamek et al., 2007)	-Low sensitivity
	-Detect: Wide range of glycoproteins, for example HbA1c -Biological recognition element: Boronic-acid	Disposable biochip	Not available (Son et al., 2006) [77]	Not available	-Laborious pretreatment on sample matrix. -High sample volume was required (50 μL)
	-Detect: Wide range of glycoproteins, for example HbA1c -Biological recognition element: Boronic-acid -Coupled with GOx (glucose oxidase) backfilling assay	Electrochemical	-Detection range: 2.5 to 15% HbA1c -Detection limit: Not available (Song et al., 2009) [70]	Not available	-Lack of specificity to HbA1c
	-Detect: Glycoproteins -Biological recognition element: Self-assembled monolayer (SAM) thiophene-3-boronic acid	Affinity biosensors with impedance measurement	-Detection range: 1 to 100 ng/μL -Detection limit: 1 ng/μL of HbA1c (Hsieh et al., 2013) [71]	Not available	-Lack of stability
	-Detect: HbA1c -Biological recognition element: phenylboronic acid	SPR (surface plasmon resonance) biosensor	-Detection range:0.43 to 3.49 μg/mL -Detection limit: 0.01 μg/mL (Liu et al., 2008) [69]	Not available	-Expensive instrumentation

[a] The table shows examples of fabricated HbA1c biosensors. HbA1c biosensors can be grouped under two main groups: the Fructrosyl valine (FV) and HbA1c biosensors. The FV biosensors measure the end product from the decomposition of glycated hexapeptides (after proteolysis of HbA1c), while the HbA1c biosensors measure concentrations of HbA1c directly. The HbA1c biosensors typically involve immunoglobulins as the biological recognition elements, and some of them utilize the biomimetic ability of boronic acid to selectively measure HbA1c.

Yazdanpanah, Sara; Rabiee, Mohammad; Tahriri, Mohammadreza et al, Glycated hemoglobin-detection methods based on electrochemical biosensors. Trends in Analytical Chemistry. 2015. 72. 53-67. Permission received to publish tables.

Table 2. Comparison of HbA1c biosensors based on boronic acid derivatives.

Type of Boronic Acid	Modified Element/Electrode/ Label or Redox Indictor	Detection Method	Dynamic Range [a] (μg/mL or %)	Limit of Detection (μg/mL)	Reference
FcBA	ZrO_2 NPs/PGE	Amperometric	6.8–14%	ND	[24]
	DOCA-4-aminothiophenol monolayer/Au	Voltammetric	0–20%	ND	[25]
T3BA	Au/HCF	Impedimetric	0.1–1	ND	[27]
	Au/IgG-FITC	Impedimetric	10–100	1	[28]
	Au/anti-HbA1c-IgG-FITC	Impedimetric	10–100	ND	[29]
APBA	glutaraldehyde-SAM Cys/IDAs/HCF	Impedimetric	0.10–8.36%	0.024%	[26]
	GO/GCE/HCF	Impedimetric	10.32–61.92	ND	[30]
	glutaraldehyde-ESMs/Screen printed Pt/HCF	Impedimetric	2.3–14%	0.19–0.21%	[31,32]
	pTTBA-Au NPs/SPE	Impedimetric/ Amperometric	0.5–6.0%/0.1–1.5%	0.052%	[33]
	PBA-ARS/GCE/HCF	Potentiometric	5.0–50	ND	[34]
	PAPBA NPs-thin film/SPCE/PAPBA	Amperometric	63–10062 (0.975–156 μM)	ND	[35]
	PQQ-ERGO/GCE/PQQ	Voltammetric	9.4–65.8	1.25	[36]
	SAM DTBA/Au	SPR	0.43–3.49	0.1	[37]
FPBA	SAM cystamine/ Au-Si/FcM & GOx	Voltammetric	4.5–15%	ND	[38]
	poly(amidoamine) G4 dendrimer/Au/FcM & GOx	Voltammetric	2.5–15%	ND	[39]

[a] μg/mL for HbA1c concentration only, % for the concentration ratio of HbA1c to HbA.

Lin, Hua and Yi, Jun. Current status of HbA_{1c} biosensors. Sensors. 2017. 17. (8). 1798. 1-18. https://doi.org/10.3390/s17081798. Permission received to publish tables.

Table 3. Comparison of HbA1c immunosensors based on recognition methods.

Types	Modified Element/Electrode/ Label or Redox Indictor	Detection Method	Dymamic Range (μg/mL)	Reference
Immobilized Hbs	DOCA/Au/FcBA	Voltammetric	ND	[40]
	Hp/cellulose membrane or microtiter/TMB & anti IgG-GOx	Amperometric	0–25% (7.8–39 nM)	[41]
Competitive inhibition	GPP/microtiter plate/ TMB & anti IgG-GOx	Photometric	1.5–10 (1 nM)	[42]
	Oligo(phenylethynylene) MW-FDMA-GPP/GC/FDMA	Amperometric	4.5–15.1%	[43]
	Au NPs -FDMA-GPP/GCE/FDMA	Amperometric	4.6–15.1%	[44]
	Au NPs-GPP/GCE/$Ru(NH_3)_6^{3+/2+}$	Impedimetric	0–23.3%	[45]
Immobilized anti-HbA1c Antibody	SAM 3-MPA/Au/HCF	Voltammetric	7.5–20	[46]
	Ppy-Au NPs /Au/PPy	Potentiometric	4–18	[47]
	SAM 1,6-hexanedithiol Au NPs/Au/HCF	Potentiometric	4–24	[48]
	mixed SAMs/Au/HCF	Potentiometric	ND	[49]
	mixed SAMs wrapped nano-spheres array/Au/HCF	Potentiometric	0.050–0.1705	[49–52]
	seed mediated growth nano-gold/Au/HCF	Potentiometric	0.00167–0.07214	[52]
	Protein A/laser ablated Au electrode/anti HbA1c-QDs	Optic-electrochemical	ND	[53]

Lin, Hua and Yi, Jun. Current status of HbA_{1c} biosensors. Sensors. 2017. 17. (8). 1798. 1-18. https://doi.org/10.3390/s17081798. Permission received to publish tables.

Table 5. HbA1c biosensors for whole blood sample measurement.

Biosensors			Detection Method	Dynamic Range (μg/mL)		Ref.
HbA1c/HbA0	Electrode	Label/Redox Indictor	HbA1c/HbA0	HbA1c	HbA0	
ESMs-APBA/Hp-ESMs	SPCE	HCF	Impedimetric	2.3–14%	5000–200,000	[32]
APBA-PQQ-ERGO/none	GC	PQQ	Voltammetric/ Photometric	9.4–65.8	92.5	[36]
DOCA-4-aminothiophenol monolayer/none	Au	FcBA or anti-HbA1c Ab	Voltammetric/ Piezoelectric	0–20%	ND	[25,40]
mixed SAMs wrapped nano-spheres array-anti-HbA1c/ anti-HbA0 Ab	FET	HCF	Potentiometric	0.05–0.1705	0.167–0.570	[51]
ABPA-mercaptoundecanoic acid/none	Au	ND	Piezoelectric/ Photometric	3–11% 50–2000	10–90	[69]
m-APBA agarose beads/none	IDAs	HCF	Electrochemical	ND	ND	[70]
APBA-column/none	GC	Ferrocene/FC-Ab	Amperometric	4–12.6%	0–500	[71]
APBA/sol-gel film	RVC/SPE	ND	Amperometric	200–12,000	20,000–200,000	[72]
carboxy-EG6-undecanethiol -APBA/11-amino -1-undecanethiol	Au	Luminol/H_2O_2	Chemiluminescence	2.5–17% 2–80	50–200	[73]
MWCNT-pTTBA-TBO & aptamer/TBO	SPCE	TBO	Amperometric	0.387–484	6.45–645	[74]

Lin, Hua and Yi, Jun. Current status of HbA_{1c} biosensors. Sensors. 2017. 17. (8). 1798. 1-18. https://doi.org/10.3390/s17081798. Permission received to publish tables.

VITA

Gilberto Henao-Pabon, Dr. Med (lagaleria02@hotmail.com) was born in Jamundi, Valle, Colombia. Dr. Henao-Pabon went to the Jose Manuel Saavedra Galindo high school, in Cali Colombia. In 1977 he obtained a Master's in Education (Chemistry-Biology) at the Universidad del Valle, Cali, Colombia.
From 1979 to 1983 he attended, and graduated as Doctor in Medicine, the school of medicine of the Universidad Autonoma of Guadalajara, Jalisco Mexico.
From 1984- Feb.1986. Critical care medicine, he practiced as resident. Physician at the general hospital of Zoquipan, Jalisco, Mexico. This was followed by a one year of training in general surgery and two years training on critical care medicine at the American British hospital, Mexico DF, Mexico.
From the year 1990 to the present Dr. Henao-Pabon has been an attending physician at the social security hospital No 35 of Ciudad Juarez, Mexico.
Since 2014, Dr. Henao-Pabon has been a graduate PhD student in biomedical engineering at the college of engineering, UTEP, El Paso TX.

Dr. Henao-Pabon teaching experience is as follows: Basic and I level of teaching education Autonoma University of Guadalajara, Guadalajara Mexico. Assistant professor at high school and college, Universidad Autonoma de Guadalajara, Guadalajara, Mexico. Continuing education for medical residents in the intensive care medicine unit of the general hospital No 35 IMSS. Ciudad Juarez, Mexico.

Dr. Henao-Pabon research experience is as follows: Student research associate in the neurophysiological department at the Universidad del Valle, Colombia on monoclonal antibodies during his master's degree.
Research associate in Texas Tech University, health sciences center school of medicine, department of surgery, El Paso Tx. "Malignant hyperthermia gene mapping", with Dr. Charles Williams.
Electrochemistry research with Dr. James Li and Dr. Sudhakara Prasad, for chronic metabolic diseases as diabetes and comorbidities diseases, with electrochemistry detection of glucose and $HgbA_{1c}$ through new and novel biosensors.

Cancer and Nutrition, in Nutritional Support. Lopes-Habib, Gabriel. Editor.

Manual de la enfermera en la unidad de medicina critica. Lopez-Habib, G. & Henao-Pabon, Gilberto. Hospital general de occidente, 1985. Guadalajara, Mexico.

Tratamiento quirurgico del cancer gastrico. Solis, Jorge & Henao-Pabon, Gilberto. Memory of ABC Hospital X Congress, Mexico City. Mexico.

El cirujano ante la neoplasia inesperada. Cervantes-Castro, Jorge & Henao-Pabon, Gilberto. Añ̃o IX, Vol. VIII, No 8 pp 25-28.

Embolismo de la arteria renal: Tratamiento Quirurgico. Cervantes-Castro, Jorge & Henao-Pabon, Gilberto. ABC hospital. Añ̃o 87, Vol. 32, No3. Pp 68-70.